Chondrogenesis of Stem/Progenitor Cells by Chemotaxis Using Novel Cell Homing Systems

Avital Mendelson

Submitted in partial fulfillment of the
requirements for the degree of
Doctor of Philosophy
in the Graduate School of Arts and Sciences

COLUMBIA UNIVERSITY

2012

©2012

Avital Mendelson

All rights reserved.

ABSTRACT

Chondrogenesis of Stem/Progenitor Cells by Chemotaxis Using Novel Cell Homing Systems

Avital Mendelson

The predominant approach for cartilage tissue engineering involves cell transplantation with or without cytokine delivery, biomaterial scaffolds, bioreactors, applied mechanical stimulation and altered oxygen tension. Despite its scientific merit, cell delivery faces drawbacks including scarce cell availability, donor site trauma, possible immune rejection and potential tumorigenesis. Tissue regeneration by cell homing is a novel concept and may offer the advantage of accelerated clinical translation. Promising results have been shown using a cell homing approach to engineer a number of tissue types including dental pulp, vascular tissue and bone. Various stem/progenitor cell populations are present in tissues adjacent to an articular cartilage defect including subsets of cells that have the ability to differentiate into cartilage-like tissue. Furthermore, several factors have been elucidated that stimulate stem/progenitor cell homing and selected cytokines have been discovered to be potent at inducing chondrogenic differentiation of stem/progenitor cells.

Cell homing is an exciting area of regenerative medicine but many critical questions remain such as cell origin, homing distance, and effective chemotactic cues. In addition to currently studied cell homing cues, other cytokines present during inflammation that are not typically known for their homing abilities might be helpful in recruiting additional cells to the scaffold and improving the quality of cartilage tissue formation. The effect of concurrently

exposing a cell population to multiple cytokine signals, similar to conditions that cells experience *in vivo*, has not been fully investigated. Determining which cytokine or groups of cytokines that induce high levels of chemotaxis would be critical for designing effective bioactive scaffolds for cell recruitment and chondrogenesis.

This thesis develops novel systems to characterize stem/progenitor cell migration and uses the knowledge gained from these systems to develop new methods for inducing chondrogenesis by cytotactic homing. First, the concept of stem/progenitor cell homing for cartilage tissue regeneration is reviewed (Chapter 1). Next, a system was developed for the *in vitro* recruitment and chondrogenesis of Adipose Stem Cells (ASCs), Mesenchymal Stem Cells (MSCs) and Synovium Stem Cells (SSCs), all of which are natively located adjacent to a full-thickness articular cartilage defect (Chapter 2). Using microfluidic principles, novel assay systems were designed and built to characterize the process of stem cell migration in the presence of single and competing cytokine signals (Chapter 3). An in-depth study was conducted investigating the process of stem/progenitor cell migration in the presence of competing cytokine signals (Chapter 4). Lastly, the knowledge gained through extensive chemokine testing using these novel assay systems was used to develop a bioactive scaffold to induce cell homing and chondrogenesis for rhinoplasty augmentation in a rat model (Chapter 5).

The novel migration devices developed herein offer a rare opportunity for screening of cell homing efficacy, potentially applicable to any stem cell population including embryonic, iPS, skeletal, muscular, neural, cardiac and adipose. A number of basic biological concepts have been examined by studies using these devices such as cell motility behavior and optimal migratory distances. The competitive cytotactic assay system provided new insight into stem cell behavior in response to gradients of multiple cytotactic cues, thus mimicking native *in vivo* conditions. By determining combinations of cytokines effective at maximizing cell homing, novel

approaches for cartilage tissue engineering without the need for cell delivery, were developed for rhinoplasty augmentation. These systems for inducing chondrogenesis by chemotactic homing were shown to be an effective alternative to cell transplantation for cartilage tissue regeneration therapies.

Table of Contents

List of Tables…….. iv

List of Figures……v

Acknowledgements……..x

Related Publications…… xii

Chapter 1. Background…….……... 1

1.1 Introduction……1

1.2 Cell-Based Cartilage Tissue Engineering Approaches……... 1

1.3 Acellular Cartilage Tissue Engineering Approaches……5

1.4 Comparison of Tissue Regeneration by Cell Homing and Cell Delivery……..…7

1.5 Stem Cell Homing……. 9

1.6 Cell Migration…… 14

1.7 Existing Cell Migration Systems……..15

1.8 Current Approaches for Rhinoplasty Augmentation…… 18

1.9 Summary and Specific Aims……20

Chapter 2. The Development of an *In Vitro* System for the Recruitment and Chondrogenesis of ASCs, MSCs and SSCs……..……24

2.1 Introduction……24

2.2 Methods……..… 26

2.3 Results…… 31

2.4 Discussion…….. 40

Chapter 3. The development of novel microfluidic devices to characterize the process of homing stem/progenitor cells…...…….……..…… 44

3.1 Introduction……44

3.2 Methods…… 46

3.3 Results…… 54

3.4 Discussion…….. 67

Chapter 4. An Investigation of the homing behavior of stem/progenitor cells due to competing cytokine signals..……..……70

4.1 Introduction……70

4.2 Methods…… 72

4.3 Results…… 75

4.4 Discussion…….. 89

4.5 Future Studies……91

Chapter 5. In Vivo Chondrogenesis by Cell Homing for Rhinoplasty Augmentation 94

5.1 Introduction……94

5.2 Methods…… 95

5.3 Results…… 100

5.4 Discussion…….. 119

5.4 Future Studies…….…… 121

Chapter 6. Conclusions and Discussion..……...124

6.1 Global Conclusions……... 124

6.2 Accomplishment of Specific Aims……...124

6.3 Future Directions……... 129

6.4 Impact to the Field……132

References……...……138

Appendix…….. 149

A.1 Equine Blood-derived Biologics…….……..…….. 149

List of Tables

Table 1.1 Comparison of cell transplantation and cell homing for cartilage regeneration...8

Table 4.1 Cytokine selection for cell migration assays……. 74

Table 5.1 Experimental design for pilot in vivo study…… 98

Table 5.2 Experimental design for second round of *in vivo* experiments……...108

Table 6.1 Bioactive scaffold design for tissue regeneration by cell homing…….. 132

List of Figures

Figure 1.1 General approach to cell based tissue engineering.……..……2

Figure 1.2 Cell types near a cartilage defect expressing CXCR4...……..……..…… 10

Figure 1.3 Cell migration process……..……..…….. 14

Figure 1.4 Current migration devices…….. 16

Figure 1.5 Current grafts for rhinoplasty augmentation…… 19

Figure 2.1 Gelatin microspheres cross-linked with various levels of glutaraldehyde……...31

Figure 2.2 Experimental schematic and tissue morphology…… 31

Figure 2.3 Release kinetics of SDF1β and TGFβ3……33

Figure 2.4 Chemokine mediated recruitment of adipose, mesenchymal and synovium stem cells…..…… 34

Figure 2.5 Quantification of ASC, MSC and SSC recruitment…….……34

Figure 2.6 Tissue formation upon cytokine-induced cell recruitment…….. 35

Figure 2.7 Chondrogenic differentiation of chemokine-recruited cells……36

Figure 2.8 Gene expression of aggrecan and type II collagen…… 37

Figure 2.9 Immunohistochemistry staining of aggrecan……..……38

Figure 2.10 Immunohistochemistry staining of type II collagen…….. 39

Figure 2.11 Mitogenic effect of SDF1β and TGFβ3…….. 40

Figure 3.1 Mask designs of microfluidic migration devices…… 47

Figure 3.2 Fabricated microfluidic devices after plasma bonding……...48

Figure 3.3 Experimental setup to determine optimal glass coating for cell adhesion……50

Figure 3.4 MSC morphology on various coatings for glass substrates……..56

Figure 3.5 Experimental schematics and device characterization……57

Figure 3.6 ASC migration toward a gradient of 400ng SDF1β…… 58

Figure 3.7 MSC polarization and cytoskeleton rearrangement in the direction of increasing PDGFBB concentration……59

Figure 3.8 Effect of MSC alignment on channels with varying distances between the cell source and the PDGFBB source…… 60

Figure 3.9 Effect of MSC alignment in response to various cytokine signals..…….. 61

Figure 3.10 Equine MSC migration in response to equine biologics derived from bone marrow and whole blood sources…… 62

Figure 3.11 Serum Free MSC Migration in response to various chemotactic cues..……. 64

Figure 3.12 Effect of MSC migration in channels with varying distances between

the cell source and the PDGF source…….. 66

Figure 4.1 Competition device design schematic…….. 73

Figure 4.2 Diffusion profiles from the center chamber towards the peripheral chambers...77

Figure 4.3 Gradients converge from peripheral wells to the center chamber…….. 78

Figure 4.4 Representative time-lapse images of induced cell migration…….. 80

Figure 4.5 Competitive cell migration from the final round of cytotactic cues that were selected as the most robust from the first three groups……..…….. 81

Figure 4.6 Quantification of migrated cells in competition assay…..…..…… 83

Figure 4.7 Quantification of cell migration distance in competition assay.…… 84

Figure 4.8 Distribution of migration distances for final round……..…….……85

Figure 4.9 Quantification of Migration Index (MI) in competition assay...…….. 86

Figure 4.10 PDGFBB effects on cell migration in a non-competition setting…….88

Figure 4.11 Stem cell niche migration behavior…… 92

Figure 5.1 Surgical methods used for scaffold implantation..…….. 98

Figure 5.2 Profile pictures of rats immediately after implantation……..…….….. 99

Figure 5.3 PLGA scaffold degradation profile……...…..…… 100

Figure 5.4 SEM images of PLGA scaffold degradation over time…..…….. 101

Figure 5.5 Cross-section of 30% PLGA after 17 days of degradation…….. 102

Figure 5.6 Calcium release profile from alginate cross-linked with solutions of

50mM, 100mM and 200mM $CaCl_2$..…… 104

Figure 5.7 Schematics and gross images of rhinoplasty augmentation scaffolds

before implantation…….. 105

Figure 5.8 Gross images of harvested scaffolds from pilot study…..…… 105

Figure 5.9 Pilot study histological results…….……..106

Figure 5.10 Profile pictures of rhinoplasty augmentation before and immediately after

surgery……...110

Figure 5.11 Gross images of rhinoplasty harvests for groups 4-11…..……..112

Figure 5.12 Ectopically engineered tissue does not disturb underlying bone...…… 113

Figure 5.13 Hematoxylin & Eosin (H & E) staining of harvested tissue from second

round of *in vivo* experiments.……. 114

Figure 5.14 Toluidine Blue staining of harvested tissue from second round of *in vivo*

experiments.……..……... 115

Figure 5.15 Aggrecan immunohistochemical staining of harvested tissue from second

round of *in vivo* experiments…..…….…… 117

Figure 5.16 Modified Verhoeff Elastic-Van Gieson staining for elastic cartilage

of harvested tissue from second round of *in vivo* experiments…… 118

Figure 5.17 Cell Isolation to investigate potential stem/progenitor cell sources for

rhinoplasty augmentation by cell homing……..…….. 122

Acknowledgements

I would like to sincerely thank my research advisor, Dr. Jeremy Mao, for introducing me to the concept of tissue regeneration by stem cell homing, for training me to think critically, and offering continuous support throughout my doctoral studies. He very kindly provided me with access to state-of-the-art research facilities and generous resources that allowed me the freedom to fully explore all of my research curiosities. His eagerness to discuss new ideas, patience to work together on numerous manuscript revisions, and willingness to share his insight into the field were very much appreciated.

I would also like to thank my dissertation committee, Dr. Gordana Vunjak-Novakovic, Dr. Samuel Sia, Dr. Clark Hung, Dr. Jeffrey Ahn and Dr. Lance Kam for taking the time to provide me with their valuable feedback, which helped to significantly improve the quality of my thesis. In particular, I would like to acknowledge Dr. Sia for helping me to pursue my passion for microfluidic research by graciously providing me with unlimited access to his research facilities and putting me in contact with microfabrication experts in his laboratory. Additionally, I am extremely grateful for the guidance that I received from Dr. Jeffrey Ahn on my *in vivo* experiments. He provided me with unparalleled insight into current rhinoplasty procedures and challenges by allowing me to observe clinical procedures in his operating room. His willingness to take time off from his busy schedule to work directly with me on my animal surgeries and dissections were a major factor in my project's successful outcome.

I am very appreciative of the valuable guidance that I received from the members of both my laboratory and the laboratories of my collaborators. In particular, I would like to thank Dr. Yukkee Cheung, Dr. Midred Embree, Dr. Kimi Kong and Dr. Wenli Zhao for helping to troubleshoot my experiments, providing me with suggestions and sharing their research

protocols. The valuable advice that I received from them along the way was instrumental in my research success. I am very appreciative of our lab manager Fen Guo for her continuous and timely assistance in ordering reagents for my studies, which helped to ensure that my experiments were always able to move forward. Additionally, the numerous High School, Master's, Dental and Veterinary students that dedicated their time and energy to furthering my research projects were a critical factor in my research progress. Lastly, I would like to specially thank my mother Leah, my father Yitzhak, Karen, Adam and Asaff who have indirectly helped me through their continuous positive support and encouragement.

Related Publications

Peer Reviewed Publications

Chapter 1:

- Nie H, Lee CH, Lu C, **Mendelson A**, Chen M, Embree M, Kong K, Zhou H, Wang S, Cho S, and Mao JJ. Musculoskeletal Tissue Engineering by Endogenous Stem/Progenitor Cells. *Cell and Tissue Research*. Accepted. 2011.
- **Mendelson A**, Lee CH, Mao JJ. Cartilage Regeneration With and Without Cell Transplantation. *Stem Cell Bioengineering and Tissue Engineering Microenvironment*. Hackensack, NJ: World Scientific Publishing, 339-350. 2011.

Chapter 2:

- **Mendelson A**, Frank E, Allred C, Jones E, Chen M, Zhao W, Mao JJ. Chondrogenesis by chemotactic homing of synovium, bone marrow, and adipose stem cells in vitro. *FASEB J*, 25(10):3496-504. Oct 2011.
- Lee CH, Cook JL, **Mendelson A**, Moioli EK, Yao H, Mao JJ. Regeneration of the articular surface of the rabbit synovial joint by cell homing: a proof of concept study. *Lancet*, 376(9739):440-8. Aug 7, 2010.

Chapters 3 and 4:

- **Mendelson A**, Cheung Y, Paluch K, Chen M, Kong K, Sia SK, Mao JJ. Competitive Recruitment of Stem Cells by Multiple Cytotactic Cues. Submitted. 2012.

Invention Disclosures

Chapter 1:

- **Avital Mendelson** and Jeremy J. Mao. Homing of stem cells by competitive actions of multiple cytokines. U.S. Provisional Patent Application, 2009.

Chapters 3 and 4:

- **Avital Mendelson** and Jeremy J. Mao. Cartilage regeneration by cell homing and without cell transplantation. U.S. Provisional Patent Application, 2008.

Conference Presentations

Chapter 2:

- **Mendelson A**, Frank ED, Allred CM, Guo QF, Mao JJ. Cartilage Regeneration Without Cell Transplantation: Stem Cell Homing and Concurrent Chondrogenesis In Vitro. *Orthopedic Research Society*, 55th Annual Meeting, March 2009.

Chapters 3 and 4:

- **Mendelson A**, Cheung Y, Frank ED, Sybo BH, Knapp BR, Maneevese RV, Sia SK, Mao JJ. Homing of stem cells by competitive actions of multiple cytokines. *International Society for Stem Cell Research*, 8th Annual Meeting, June 2010.

Chapter 1. Background

1.1 Introduction

The majority of approaches for cartilage tissue engineering involve cell transplantation with or without cytokine delivery, biomaterial scaffolding, bioreactor culture and applied mechanical stimulation [1, 2]. Cells that have been delivered for cartilage regeneration include, but are not limited to, chondrocytes, mesenchymal stem cells, and adipose stem cells. However, cell delivery faces critical drawbacks including scarce cell availability, donor site trauma, possible immune rejection and potential tumorigenesis [3]. Tissue regeneration by cell homing is a novel concept and aims to recruit various local stem cell populations to a bioactive biomaterial scaffold placed in the cartilage defect site with the help of specific chemotactic cytokines that subsequently induce chondrogenic differentiation of the cells to promote tissue regeneration. This approach to tissue engineering may offer advantages over cell transplantation of lower cost and accelerated clinical translation. In the following sections of this chapter, we will explore existing techniques for cell delivery based and cell homing based cartilage tissue engineering and compare the benefits and limitations of both methods. Subsequently, we will discuss the process of cell migration, stem cell homing and existing *in vitro* systems for assaying cell migration. We will then discuss current rhinoplasty augmentation surgical methods and the potential for advancement using cell homing based cartilage tissue engineering. Lastly, we will discuss the specific aims of this dissertation.

1.2 Cell-Based Cartilage Tissue Engineering Approaches

Due to the ordered structure of cartilage, a scaffold is frequently used to define the shape of the tissue, provide an attachment site for cells, and guide tissue formation [4]. The conventional approach behind cell-based cartilage tissue engineering strategies is to fabricate a

biodegradable scaffold, seed it with progenitor cells or differentiated cells, and culture it *in vitro* or *in vivo*, either alone or in combination with cytokines, a bioreactor, mechanical stimulation or oxygen tension (**Figure 1.1**).

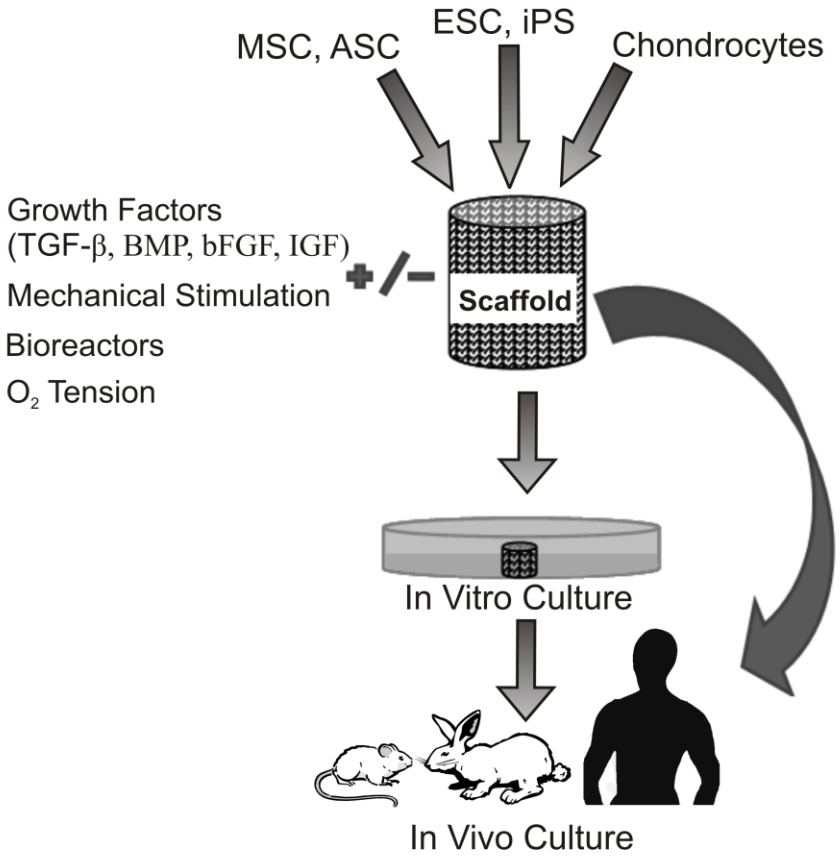

Figure 1.1. General approach to cell based tissue engineering.

The most common growth factors used in promoting cartilage regeneration include transforming growth factor β1 and β3 (TGF-β1 and TGF-β3), bone morphogenic protein (BMP), basic fibroblast growth factor (bFGF), and insulin–like growth factor (IGF) [5].

Langer and Vacanti published one of the seminal papers showing that cartilage-like tissue could be formed by seeding an anatomically shaped scaffold with cells and culturing it subcutaneously [6]. Although Langer and Vacanti initially proposed to use fully differentiated cells such as chondrocytes, the scientific community soon realized that fully differentiated cells are not only scarce as an autologous cell source, but are also difficult to expand *ex vivo*. Subsequently, an interest arose in using bone marrow stem/stromal cells [7] as well as human embryonic stem cells [8] as cell sources for cartilage repair. Additionally, one of the stated motivations for the recent discovery of induced pluripotent stem cells (iPS) is to transplant them for regenerative therapies [9, 10].

Several elegant approaches have been described for the delivery of cells in cartilage regeneration. For example, an osteochondral construct was fabricated by press–coating a high density pellet of chondrogenically induced human mesenchymal progenitor cells (hMPCs) onto one face of the construct, and osteogenically induced hMPCs onto the opposing face of the construct. After 10 weeks in culture, the construct formed cartilage–like and bone–like layers [11]. In addition to *in vitro* culture, many researchers have investigated the possibility of regenerating cartilage *in vivo*. In one such study, a bioceramic scaffold was fabricated from β-tricalcium phosphate (β-TCP) powder, seeded with autologous chondrocytes or left unseeded as a control and implanted in sheep for up to 24 weeks. Following explantation, the cell seeded constructs were fully covered with tissue, whereas the acellular constructs were not [12]. An alternative approach used swine chondrocyte seeded fibrin glue infused polytetrafluoroethylene (ePTFE) membrane to support engineered cartilage. Constructs were implanted subcutaneously in nude mice for 12 weeks. New cartilage tissue was formed with lacunae structures similar to native tissue and tightly bonded to the ePTFE scaffold material [13]. Another osteochondral construct was fabricated from medical grade polycaprolactone (mPCL) to serve as the bone region and fibrin glue for the cartilage portion. The entire construct was seeded with bone

marrow derived mesenchymal stem cells (bMSCs) and implanted in adult white rabbits. However, at six months post–operation, only two of the six implanted constructs showed mature cartilage formation [14].

Additionally, gene therapy has been combined with cell delivery approaches for cartilage regeneration. Periosteal derived rabbit MSCs were modified to overexpress the BMP 7 gene, seeded onto polyglycolic acid scaffolds and implanted *in situ* into a rabbit osteochondral defect model. Constructs harvested after 8 and 12 weeks had an enhanced cartilage regenerative ability as compared to the empty defect and empty vector transduced, cell–seeded control groups [15]. Recently, high density chondrocyte culture has been attempted to eliminate the need for a scaffold in cartilage regeneration, since highly confluent chondrocytes generate chondral tissue without the presence of synthetic scaffolds [16].

Many of these aforementioned studies used adult stem cells. However, when cultured *in vitro*, adult stem cells have a reduced ability to expand and differentiate into numerous cell types as compared to *in vivo* culture. Embryonic stem cells (ESCs), on the other hand, are more capable of multipotency *in vitro*, but are limited in use because of their controversial nature. Recently, it was discovered that mouse embryonic or adult fibroblast cells can be reprogrammed to become ESC–like pluripotent stem cells by inducing the following genes: Oct3/4, Sox 2, c-Myc, and Klf4. However, the process of somatic cell nuclear transfer (SCNT), used to create IPS cells, has been linked to premature aging, respiratory conditions as well as organ abnormalities. Furthermore, SCNT could potentially form tumors *in vivo,* thus hindering its clinical use [17].

Most of the previous work in cartilage regeneration has focused on the repair of small, localized cartilage or osteochondral defects by bioengineered plugs [18, 19]. A number of studies have shown that composite cartilage–bone tissue can be regenerated in surgically

created focal defects [4, 20-23]. However, commercial approaches to replace focal cartilage defects with processed tissues or cells in patients are only marginally successful. Current clinical treatment methods for focal osteoarthritis, such as abrasion arthroplasty or autologous chondrocyte implantation, have limitations including the loss of chondrocyte phenotype, poor integration and guarded functional outcome [4, 24]. Clinically, focal cartilage defects deteriorate into more severe arthritis that warrants total joint arthroplasty [25-27]. Accordingly, biological replacement of the entire synovial joint has been advocated [18, 27-29]. Initial attempts to regenerate an entire human synovial joint with anatomic dimensions *in vivo* were conducted ectopically and contained stratified layers of cartilage and bone formed from several cell sources, such as a single population of bone marrow–derived mesenchymal stem cells (MSCs) [29-31] or differentiated chondrocytes and osteoblasts [32, 33]. In summary, cell seeding is a meritorious scientific approach for cartilage regeneration. The seeded stem cells or chondrocytes are capable of generating cartilage tissue. However, cell delivery approaches encounter critical barriers including scarce cell availability, donor site morbidity, potential pathogen transmission or immune rejection, risk for tumor formation, long-term storage and regulatory approval. Therefore, alternative cartilage regeneration without cell seeding must be examined.

1.3 Acellular Cartilage Tissue Engineering Approaches

To date, there have been few attempts to regenerate cartilage without cell transplantation. Of these efforts, the general approach is to implant acellular, biomaterial based scaffolds into the defect site alone or in combination with growth factors or chemoattractants. In one study, a two–layered osteochondral scaffold was fabricated from basal porous β-tricalcium phosphate (β-TCP) to serve as the bone layer and a collagen type I/II fibrous layer to act as the

cartilage layer. Scaffolds were implanted in Göttinger minipigs alone or in combination with a mixture of growth factors containing BMP 2, 3, 4, 6, 7, TGF β1, β2, β3, FGF-1, osteocalcin and osteonectin. After 12 weeks, the group with the growth factors was able to regenerate a thicker layer of cartilage. However, after 56 weeks, there was no difference in the cartilage formed between the growth factor group and the scaffold alone group, which could be attributed to a complete resorption of growth factors by 52 weeks [34].

A composite of interconnected porous hydroxyapatite was used to harbor recombinant human BMP-2 that was infused in poly-D, L-lactic acid/polyethylene glycol. Control groups included scaffolds without BMP-2 and a second group of scaffolds lacking both BMP-2 and hydroxyapatite. Scaffolds were implanted in rabbits for up to six weeks. Follow–up analysis revealed that the control groups had a rough fibrous surface, whereas the experimental group formed a smooth surface, with a less visible junction between the native and repaired cartilage. However, histological evaluation revealed an irregular morphology in the junction between the host and engineered cartilage [35].

In another study, scaffolds were fabricated from polyglycolic acid and hydroxyapatite and infused with human serum to act as a chemoattractant. Scaffolds were implanted into full thickness defects in sheep for up to three months, after which time, new tissue formation in the defect site was observed. Human serum acted as a chemo-attractant because it contains various growth factors and chemokines. However, since serum constituents vary from one individual to another, this could potentially make it difficult to ensure consistent results between individuals if the therapy was to be used clinically [36].

Another study investigated the role of implanting acellular PLGA scaffolds in combination with continuous passive motion (CPM) on the regeneration of osteochondral defects in rabbits. After creating full-thickness osteochondral defects, the defect was either left empty or filled with

a PLGA scaffold and the rabbits were subjected to immobilization, intermittent passive motion or continuous passive motion. After 12 weeks of implantation, the PLGA scaffolds that were subjected to CPM showed the best osteochondral regeneration, with type II collagen expression, osteocyte maturation and trabecular bone formation. However, the PLGA scaffolds that were subjected to immobilization or intermittent passive motion were only able to regenerate fibrocartilage tissue. The cell source involved in the regeneration was not fully investigated and the regenerated tissue was irregular in morphology compared to native articular cartilage surfaces. Nevertheless, this study demonstrates the potential for tissue regeneration without cell transplantation as an osteochondral defect therapy [37].

These approaches using acellular scaffolds were successful in filling in critical sized defects with cartilage-like tissue. However, some drawbacks of these techniques include irregular tissue morphology, regenerated cartilage that was not level with the host cartilage, and inconsistent results between samples. Furthermore, using a cocktail of growth factors could potentially cause negative cross–talk between factors and significantly increase the cost of the product, limiting its clinical appeal.

1.4 Comparison of Tissue Regeneration by Cell Homing and Cell Delivery

While cell transplantation approaches for regenerating cartilage have been able to produce remarkable cartilage–like tissue, there are many limitations associated with this approach in comparison to cell homing (**Table 1.1**). When the cell source is autologous, two surgical procedures are required, one to obtain the autologous cells and a second to transplant the cell seeded scaffold *in vivo*. If allogeneic cells or cell homing is used, the procedure can be accomplished with only one surgery. Fewer surgeries could mean a faster recovery time.

However, transplanting allogeneic cells poses a risk for patient rejection. Furthermore, for both allogeneic and autologous cells, once they are harvested from the body, they must be manipulated and cultured *in vitro* prior to re-transplantation. For cell transplantation procedures to be clinically used, the tissue biopsies must be sent to a lab for digestion and expansion.

Table 1.1: Comparison of cell transplantation and cell homing for cartilage regeneration

	Cell transplantation		**Cell homing**
	Autologous cells	***Allogeneic cells***	
# of surgeries	**2**	**1**	**1**
***Ex vivo* cell manipulation**	**Yes**	**Yes**	**No**
Cell shipping and storage	**Yes**	**Yes**	**No**
Off-the-shelf product	**Difficult**	**Difficult**	**Possible**
Potential immunorejection	**No**	**Possible**	**No**
Pathogen contamination	**Possible**	**Possible**	**No**
Costs of therapy	**High**	**High**	**Not as high**

These limitations make it difficult to turn cell transplantation into an off-the-shelf product. The required manipulation of cells *ex-vivo* creates a potential risk for inadvertently contaminating the harvested cells. Furthermore, the procedure of obtaining cells from a harvested piece of tissue is time consuming and could delay patient treatment time. Lastly, cell manipulation requires specific culture medium, tissue digestion enzymes, culturing facilities and trained personnel. Cell delivery based approaches for cartilage regeneration to date have provided researchers with a model to characterize cell density, scaffold type, growth factor delivery and the

involvement of mechanical stress. The process of differentiating progenitor cells into cartilage–like tissue has been thoroughly studied. Cytokine cocktails and delivery systems have been investigated. Mechanical stimulation systems and bioreactors have been designed to enhance the mechanical and biochemical properties of the engineered cartilage. Biomaterials have been designed to maximize cell attachment and extracellular matrix production. Despite the generous knowledge base generated from cell–seeded cartilage regeneration approaches, these studies have also demonstrated that complexity can be a barrier for clinical use. Perhaps a reduction approach could be used to regenerate cartilage by involving fewer, instead of more, factors. Recent investigations into cell homing may offer new approaches to cartilage regeneration. Cell homing approaches have several key advantages over cell transplantation including lower cost, minimized risk for immunorejection and pathogen transmission and ease of clinical implementation. However, cartilage regeneration by cell homing is a concept that warrants rigorous investigation. Future regenerative approaches can potentially be designed to guide a patient's own cells into regenerating articular cartilage that may function as native articular cartilage.

1.5 Stem Cell Homing

Cell homing is defined by the hematopoietic community as the active migration of stem cells across the endothelium *in vivo*. Broadly, cell homing can be thought of as the directed cell migration to a target tissue. Multiple steps are involved in cell homing, including communication with the vascular endothelium and migration across the endothelial wall and into the target tissue [38]. A number of factors have been shown to promote progenitor cell homing such as stromal derived factor-1 (SDF-1), stem cell factor (SCF), insulin-like growth factor-1 (IGF-1), and granulocyte colony stimulating factor (G-CSF) [39-41]. Of these factors, the major factor used

clinically is G-CSF. This factor is used to promote stem cell migration from the bone marrow to the peripheral blood in patients recovering from chemotherapy. Subsequently, these cells can be isolated and used for transplantation. Recently, SDF-1 has been gaining substantial interest as a cell homing factor in experimental studies. It was first discovered as a chemotactic factor for T cells and monocytes as well as a growth factor for B-cell progenitors [42, 43]. Furthermore, it was found to be a co-receptor for human immunodeficiency virus entry [44].

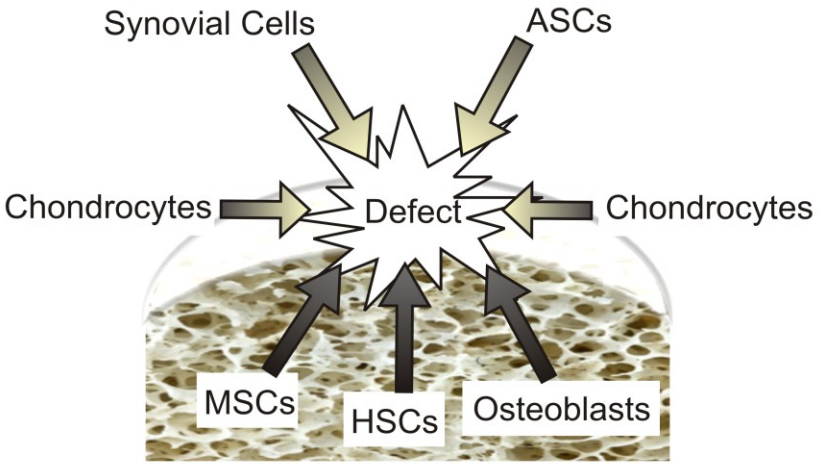

Figure 1.2. Cell types near a cartilage defect expressing CXCR4.

It was later discovered to be a chemoattractant successful in homing human CD34+ stem cells within three hours following exposure [45].

Expression levels of CXCR4, the receptor for SDF-1, are critical for cell homing. Many different cell types express this receptor, including embryonic stem cells, cord blood CD34+ cells, MSCs, adipose-derived stem cells (ASCs), synovial cells, chondrocytes, osteoblasts, and hematopoietic stem cells (HSCs) [46-49]. Cord blood CD34+ cells express stronger levels of

CXCR4 than adult CD34+ cells [50]. **Figure 1.2** shows various cells that express CXCR4 and are therefore potentially relevant to cell homing based cartilage regeneration.

Limited quantities of MSCs can be found circulating in the blood. To overcome this limitation, venapuncture has been used to yield additional MSCs, but this carries the risk of contamination from connective tissue cells [28]. Recently, chemically modified, systemically infused mesenchymal stem cells were found to accumulate in bone marrow [29]. However, this approach still requires *ex vivo* cell manipulation which also carries the potential for cell contamination. MSCs that have been accessed from the peripheral blood by cell sorting methods can differentiate into a number of cell lineages including chondrocytes [30]. After injury, the number of circulating MSCs in the peripheral blood has been shown to increase when compared to non-injured animals [31].

Significant levels of the CXCR4 receptor can be found in CD34+ cells circulating in the body or in the bone marrow [32]. The ability of CD34+ cells to respond to SDF-1 is greater in bone marrow as compared to cells found in the peripheral blood [23]. However, multiple studies have shown that the receptor is downregulated when MSCs are grown in tissue culture dishes *in vitro* [29]. Furthermore, CXCR4 expression level decreases with increasing passage number. Human MSCs cultured for more than two passages display a decreased expression level of CXCR4 [27]. This led to the investigation of potential methods to increase the CXCR4 expression *in vitro*. One method of upregulating the CXCR4 expression is by treating MSCs with stem cell factor (SCF), Interleukin-6 (IL-6), Flt-3 ligand, hepatocyte growth factor (HGF) or Interleukin-3 (Il-3) during *in vitro* culture [51]. Hypoxic conditions also upregulate SDF-1 expression levels *in vivo* [23]. Furthermore, cells cultured as 3-dimensional spheroids can upregulate CXCR4 expression. However, when the cells from the spheroids are returned to a monolayer culture, CXCR4 expression is once again reduced [27].

The role of CXCR4 expression levels during hMSC chondrogenic differentiation *in vitro* was studied by seeding hMSCs onto a hyaluronic acid scaffold and culturing in medium containing TGF-β1. CXCR4 receptor expression was downregulated in the engineered cartilage. This was consistent with native cartilage, which does not express CXCR4. MSC CXCR4 expression level is downregulated during chondrogenic differentiation, likely to prevent migration and adherence to other tissue types [52]. However, in patients with osteoarthritis and rheumatoid arthritis, SDF-1 produced by the synovium causes synovial fluid cytokine levels to be much higher than normal.

In addition to cytokines, other factors have been found to regulate progenitor cell migration. Ionic calcium levels are naturally elevated in the bone marrow. Calcium levels have been shown to regulate both embryonic and adult progenitor cell migration by modulating the CXCR4 surface receptor expression levels *in vivo*. Exposing MSCs to increased calcium levels *in vitro* for as little as four hours led to a significant homing effect *in vivo* [53].

A few tissue engineering studies have been carried out using SDF-1 to enhance tissue formation. A micropump cytokine delivery system fabricated from PCL was designed to deliver a constant supply of SDF-1. The system contained three parts: a top layer which when fit onto the bottom layer formed a closed system and a middle layer containing a pump and tubing for cytokine delivery. The middle layer was connected to a reservoir filled with cytokines and attached microneedles for controlled cytokine delivery. Following implantation of the scaffold system subcutaneously in rats, an automatic syringe pump was attached to the scaffold pump to deliver cytokines. Initially VEGF was injected to induce vascularization, followed by SDF-1 for MSC recruitment and finally BMP-6 to promote osteogenic differentiation. After 30 days, harvested constructs showed the presence of vascularization and tissue ingrowth. However, mature, mineralized bone tissue formation was not achieved. Furthermore, the current scaffold

design was very large in size, measuring 6 × 16 × 20 mm, which could potentially hinder the use of this device in a clinical setting [54].

In a different study, mRNA transfection was used to overexpress the CXCR4 receptor in human bone marrow-derived MSCs. The scaffold was made from porous mineralized type I collagen with and without agarose containing SDF-1, and subcutaneously implanted in NOD/SCID mice. The following conditions were tested: bMSCs transfected with CXCR4, empty vector transduced bMSCs, and cell free-agarose. After seven days, scaffolds were harvested and evaluated. Scaffolds containing CXCR4 upregulated cells were able to migrate up to 500 μm into the scaffold, whereas the empty vector control groups displayed cell migration only up to 220 μm. However, there was no observable difference in cell migration in scaffolds that did not have agarose containing SDF-1 [55].

Recently, a study was conducted to determine if locally delivered SDF1 in ultrapurified alginate gel (UPAL) could promote the regeneration of osteochondral defects in a rabbit model. Full thickness defects (4.5mm diameter by 3mm depth) were created in the patellar groove of the distal femur in 15 week old white rabbits and animals were harvested after 3 hours, 1 week, 2 weeks, 4 weeks and 16 weeks. Four groups were tested: defect alone, UPAL + 10μg/mL bovine serum albumin (vehicle control), UPAL + 10μg/mL SDF1 and UPAL + 250μg/mL antagonist of CXCR4 (AMD3100). At one week post implantation, the cell number in the SDF1 group was significantly higher in the defect site compared to all other groups, leading to the speculation that SDF1 enhanced the migration of cells to the defect site. After 16 weeks, the defect alone group resulted in only fibrous tissue formation containing fissures. The AMD3100 and vehicle groups displayed a hypocellular fibrocartilage-like tissue, containing large amounts of type I collagen and weak staining for type II collagen. In contrast, the SDF1 group formed a smooth cartilage surface containing GAG matrix and type II collagen in addition to regenerating

the subchondral bone and tide mark. However, many topics remain for further investigation such as the cell sources used in the regeneration and the heterogeneity of the regenerated tissue [56].

1.6 Cell Migration

Cell motility is a general term for the process in which cells adhering to a substrate reorganize their cytoskeleton to direct their motion in response to environmental factors [57]. Investigating cell migration behavior *in vitro* may offer insight into the cell homing behavior of cells *in vivo*. Cells follow a number of distinct steps that lead to motility (**Figure 1.3**).

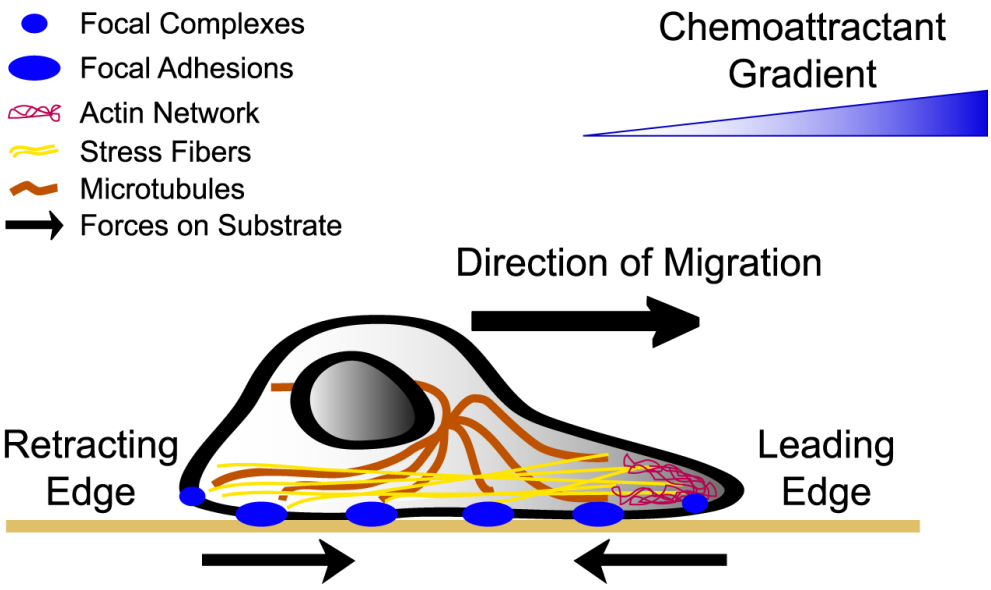

Figure 1.3. Cell migration process. Inspired by [58].

Initially, cytoskeleton actin filaments polymerize to form adhesive complexes at the front of the cell (leading edge) causing the plasma membrane to protrude. Adhesive complexes are formed

from natural focal complex regions of the plasma membrane containing densely arranged integrin receptors, actin filaments, and proteins, which expand into larger focal adhesions as the cell migrates. These large adhesive complexes provide the cell body with points of traction for movement. A net displacement of the cell is caused by the release of adhesive complexes located at the rear end of the cell. It was discovered that stationary cells contain focal adhesions that actively move, whereas migrating cells contain focal adhesions that remain fixed in place. The ability for migrating cells to fix their adhesions in place was later attributed to molecular clutches, which are thought to stabilize focal adhesions to allow for cell traction and contractility. Transmembrane adhesion receptors serve as connectors between the cell's extracellular matrix and internal cytoplasmic actin filaments, causing a vast number of adherent cells to experience tension when attached to a substrate. For fibroblasts, the stiffer the substrate, the more organized the actin filaments and the higher the cell tension. Migrating cells contain strong transient forces at the leading edge and weaker but more stable forces at the rear of the cell [58].

1.7 Existing Cell Migration Systems

Common migration assays include the Boyden chamber, Zigmond Chamber, Dunn Chamber, scratch assay and under agarose assay (**Figure 1.4**). The Boyden assay works by seeding cells on a membrane covered transwell and allowing them to migrate through the membrane towards an increasing cytokine concentration in the lower portion of the chamber [59]. However, the gradients generated are not defined and only one cytokine gradient can be

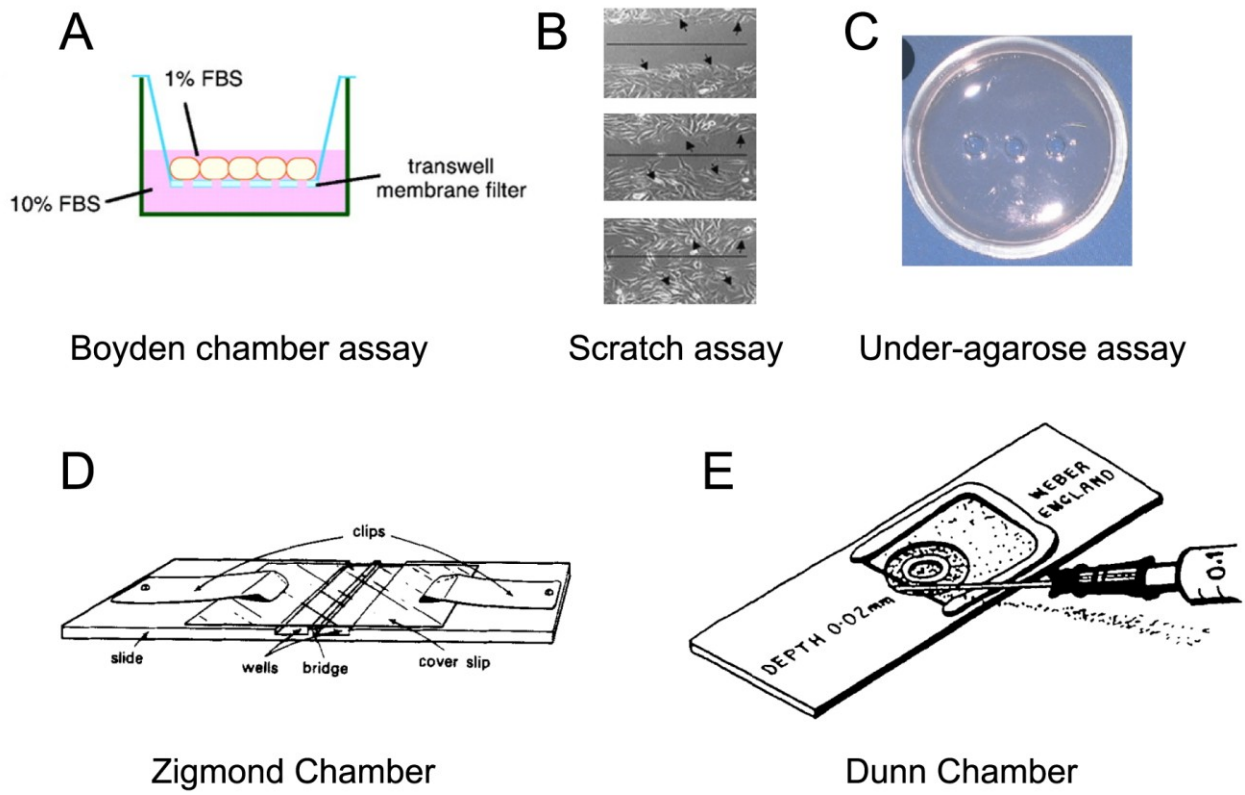

Figure 1.4. Current migration devices. (A) Boyden chamber or transwell assay, (B) Scratch or wound healing assay, (C) Under-agarose assay, (D) Zigmond chamber and (E) Dunn Chamber [60-64].

formed at a time. Thus, to study the effect of multiple cytokines, many experiments would have to be conducted sequentially. Furthermore, cell migration patterns cannot be monitored in real-time and only end-point data can be collected. Because live-cell imaging cannot be conducted, the effects of chemotaxis cannot be distinguished from chemokinesis.

The Zigmond chamber functions by creating a cytokine gradient over a thin bridge separating the cytokine chamber from the control solution chamber [64]. Cells are cultured on a coverglass and inverted to form the top surface of the bridge separating two rectangular chambers for cytokine or control solutions. However, the Zigmond gradient is subject to instability due to thermal effects, mechanical creep, and inconsistent fluid volumes between chambers [65]. This led to the development of the Dunn chamber, which functions identically to

the Zigmond chamber but promotes a stable long-term gradient due to a revised geometrical design consisting of two concentric ring-shaped chambers [63]. While these systems are amenable to live-cell imaging, both the Zigmond and the Dunn chambers only allow for the study of one chemotactic factor on one cell type at a time. Additionally, these systems have poor reproducibility, leading to large variation between experiments [66].

The scratch assay works by manually creating a gap with a pipette tip in a confluent monolayer of cells, and monitoring the cell movement from the edge of the gap to fill the open space [61]. However, this system does not allow for cytokine gradients to be formed, thus limiting the migration studies to those of chemokinesis. Furthermore, the assay takes a long time to complete compared to other methods. A day is required to form a confluent cell monolayer and up to 18 hours are required for the cells to repopulate the open space. Additionally, a large number of cells are required for this method [61].

The original under agarose assay for cell migration [67] was conducted by polymerizing a layer of agarose hydrogel in a 60mm tissue culture dish and punching out three holes in the gel 2.4mm in diameter and 2.4mm apart. Cells were seeded in the inner well, the chemoattractant of interest was placed in one of the outer wells and a control non-chemotactic solution was placed in the other outer well. One important characteristic of agarose is that it does not adhere to glass surfaces. Thus, as the cytokine diffuses throughout the agarose, cells can migrate underneath the agarose towards an increasing concentration of cytokine. However, for multiple migration assays to be conducted in the same dish, multiple sets of 3 holes must be punched, potentially allowing for cross-contamination of cytokine gradients through the porous hydrogel. In addition, allowing the cells to migrate in all directions makes it difficult to monitor the cell motility patterns over time.

Several newly designed microfluidic devices can test the effects of two opposing chemotactic signals, but do not appear to test competitive recruitment of a given cell population

in response to multiple cytotactic cues in one single system [67-70]. A hydrogel-based microfluidic device was developed that can allow long-term chemical concentration gradients to be created and used as a stimulus for promoting cell migration. However, hydrogels are largely aqueous, and could be subject to evaporation or degradation over time. Since this device is not enclosed from environmental factors, it is conceivable that device parameters could vary over time [70]. An alternative platform was developed that allows endothelial cells to migrate from an intact cell layer into a 3D type I collagen scaffold in response to a chemical gradient. While this unique device attempts to simulate 3D cell migration behavior occurring *in vivo*, to test the chemotactic effects of a single factor on multiple cell types, a co-culture would have to be conducted, making it difficult to isolate the chemotactic effects of individual cell populations within the co-culture [69]. Despite the limitations of these devices, microfluidic platforms contain a number of advantages over existing cell migration assays, including low cost, high reproducibility and minimal volume of required reagents.

1.8 Current Approaches for Rhinoplasty Augmentation

To test the concept of cell homing for cartilage regeneration in a small animal model, we chose to use the rhinoplasty augmentation model. One of the major reasons for choosing not to use an *in situ* synovial joint model is due to the fact that in rats the tibial growth plate never fuses after the animal reaches maturity, allowing for the animal to self-heal and form new cartilage as the animal ages [71]. Thus, a less biased model for cartilage formation in a small animal would be an ectopic model. Current rhinoplasty augmentation procedures utilize a biological or synthetic ectopic structure to maintain an aesthetic shape, but have limitations, which will be discussed in the next section. Cartilage formation by cell homing could potentially serve as an alternative approach for rhinoplasty augmentation.

Many rhinoplasty augmentation procedures to date rely on autologous sources of cartilage such as the nasal septum, outer ear or rib. Rib cartilage is less desirable because the mechanical properties vary from those of native nasal cartilage [72]. To create a tip graft for nasal augmentation, small pieces of harvested cartilage are stacked and sutured together. The graft is shaped such that the projecting end is wider than the proximal end and is sutured in place at the caudal margin of the medial crura. However, obtaining a sufficient amount of cartilage is invasive, time consuming and results in donor site morbidity [73, 74]. Another graft method involves the use of autologous fascia wrapped around diced autologous cartilage. Although this method requires a smaller source of autologous cartilage, harvesting autologous fascia increases the invasiveness of the procedure and obtaining a large enough volume of fascia is often challenging [73]. Allogeneic sources of cartilage circumvent the issue of donor site morbidity, but are difficult to obtain and require the patient to take long-term immunosuppressant medication to avoid graft rejection [72].

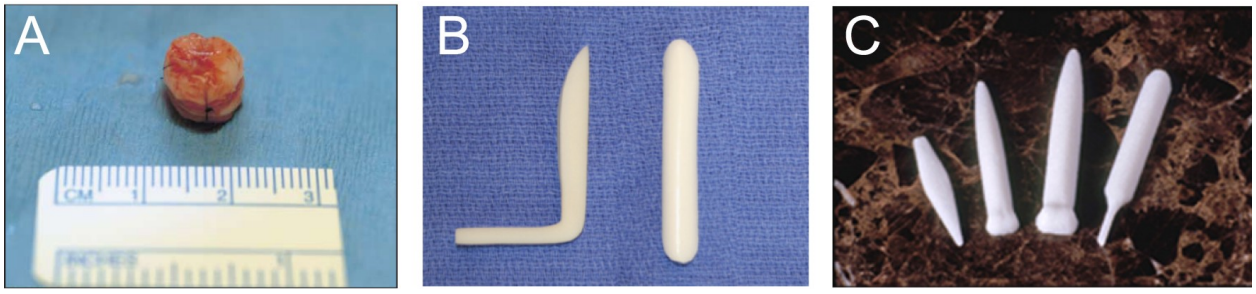

Figure 1.5 Current grafts for rhinoplasty augmentation. (A) Autologous stacked cartilage, (B) Silicone grafts and (C) Medpor high density polyethylene grafts [75-77].

As an alternative to harvesting autologous cartilage, a number of acellular biomaterial implants are commercially available [75]. Medical grade silicone rubber known as Silastic has

been used widely for nasal augmentation for over 40 years. Silicone is nonporous, can be shaped by the surgeon, and does not undergo enzymatic degradation. However, because the graft is nonporous, it does not integrate well with the surrounding tissue, and shifting of the implant position may result in chronic inflammation or graft extrusion. High-density polyethylene, known as Medpor, has also been extensively used for rhinoplasty implants. The material is flexible, easily carved and is porous to allow tissue ingrowth and implant fixation. However, because of its high stiffness, the resulting augmentation is often unnatural in appearance and feel. Lastly, polytetrafluoroethylene, most commonly known as Gore-Tex, is a polymer with a 30μm pore size that promotes limited tissue ingrowth, but can be easily contoured and layered. While short-term studies reveal mainly positive outcomes, long-term studies suggest that Gore-Tex implants may be susceptible to infection and extrusion.

Nasal cartilage is elastic and differs in morphology and mechanical properties from the hyaline nature of articular cartilage. The stiffness of human nasal cartilages is much lower than articular cartilages; nasal septal, columellar, L-strut and allar have a stiffness of 0.8, 0.56, 0.59 and 0.49 respectively. The extracellular matrix of nasal cartilage consists of collagen fibers, proteoglycans and elastic fibers. Thus, tissue engineered constructs for rhinoplasty applications must be flexible in addition to mechanically stable. To date, the studies for nasal cartilage tissue engineering are limited in number and all involve cell transplantation. The potential of cell homing as a treatment method for rhinoplasty augmentation has yet to be investigated [72].

1.9 Summary and Specific Aims

Cell homing approaches have several key advantages over cell transplantation, including lower cost, minimized risk for immunorejection, decreased chance for pathogen

transmission, ease of clinical implementation and may offer new approaches for cartilage regeneration. Future regenerative approaches can potentially be designed to guide a patient's own cells into regenerating articular cartilage that may function as native articular cartilage. However, cartilage regeneration by cell homing is a concept that warrants rigorous investigation.

A significant roadblock that effects the development of tissue engineered cartilage by cell homing for osteoarthritis treatment is a limited understanding of the chemotactic behavior of stem/progenitor cell populations residing in the tissues near the synovial joint and potent cytokines for inducing the migration of these cells. Critical questions remain such as homing distance and effective biomaterial scaffolds to promote chondrogenic differentiation of the homed cells. In addition to currently studied cell homing cues, other cytokines present during inflammation that are not typically known for their homing abilities might be helpful in recruiting additional cells to the scaffold and improving the quality of cartilage tissue formation. The effect of concurrently exposing a cell population to multiple cytokine signals, similar to conditions that cells experience *in vivo*, has not been fully investigated. Determining which cytokine or groups of cytokines that induce high levels of stem/progenitor cell chemotaxis would be critical for designing effective bioactive scaffolds for cell recruitment and chondrogenesis.

The goal of this research was to develop a method of inducing chondrogenesis by chemotactic homing and demonstrate the feasibility with *in vitro* experiments (**Aim 1**). Using microfluidic principles, novel assay systems were designed and built to characterize the process of stem cell homing in the presence of single and competing cytokine signals (**Aims 2 and 3**). Lastly, the knowledge gained through extensive chemokine testing in Aims 2 and 3 was used to develop a bioactive scaffold to induce cell homing and cartilage formation in a small animal model (**Aim 4**).

The following specific aims were proposed:

1. **To develop a system for the recruitment and chondrogenesis of ASCs, MSCs and SSCs, all of which are natively located adjacent to a full-thickness articular cartilage defect.** We aimed to fabricate gelatin microspheres to slowly release TGFβ3 and/or SDF1β over time and characterize their release profile. Additionally, we aimed to develop a bioactive scaffold incorporating the slow releasing microspheres on top of a porous collagen sponge for *in situ* cell recruitment of stem/progenitor cells and chondrogenesis.

2. **To develop novel microfluidic devices to characterize the process of homing stem/progenitor cells.** We aimed to design microfluidic devices that allow efficient migration assays to be conducted and monitored with time-lapse microscopy. We aimed to design devices with both fixed and variable distances between the cell source and cytokine source. We aimed to characterize cytokine diffusion through the device using fluorescent dextran with varying molecular weights.

3. **To investigate the homing behavior of stem/progenitor cells due to competing cytokine signals, mimicking *in vivo* microenvironments.** We aimed to develop a novel microfluidic chemotaxis assay system that allows one population of MSCs to be simultaneously exposed to 6 different cytokines, mimicking *in vivo* conditions. We aimed to quantify the number of migrated cells and migration distances to determine which cytokine or group of cytokines induce chemotaxis.

4. **To apply the knowledge gained in specific aims 1-3 to develop a bioactive cell homing scaffold to promote chondrogenesis for rhinoplasty augmentation.** We aimed to develop and characterize a PLGA based scaffold incorporating the gelatin

microspheres designed in Aim 1. We aimed to test the principle of *in situ* chondrogenesis by cell homing by implanting scaffolds slowly releasing cytokines in the subcutaneous nasal dorsum of Sprague Dawley rats and analyzing cell homing efficacy and chondrogenesis at various timepoints.

The following hypotheses were proposed in correspondence to these specific aims:

1. SDF1 would promote migration of ASCs, MSCs and SSCs into the scaffold and TGFβ3 would induce chondrogenic differentiation of the cells.

2. Cytokine concentration gradients would be formed in agarose filled microfluidic channels which would induce migration of stem/progenitor cells towards cytokines that are chemotactic.

3. Multiple cytokine concentration gradients could be separately formed but simultaneously exposed to a single population of stem/progenitor cells and would promote selective cell migration towards cytokines that are chemotactic.

4. PLGA would provide a rigid substrate for cell attachment, SDF1 would promote migration of local stem cells around the nasal dorsum into the scaffold and TGFβ3 would induce chondrogenic differentiation of the cells.

Chapter 2: The Development of an *In Vitro* System for the Recruitment and Chondrogenesis of ASCs, MSCs and SSCs.

2.1 Introduction

Articular cartilage is recalcitrant to regeneration, owing largely to the scarcity of native stem/progenitor cells [18]. Despite the presence of stem/progenitor cells in postnatal articular cartilage [8], it is difficult to conceive that they would serve as sources of transplanted cells for articular cartilage regeneration. Accordingly, chondrocytes or stem/progenitor cells from bone marrow, adipose, synovium and other sources have been investigated as cartilage-regenerating cells [78]. The most prevalent model for articular cartilage regeneration has been focal defects that are filled with cartilage-forming cells with or without biomaterial scaffolds [1]. Despite its scientific merit, cell transplantation for cartilage regeneration is associated with complicated, costly and multi-step procedures including donor site trauma, potential contamination, and possible immune rejection for allogeneic or xenogeneic cells [79]. Long-term *ex vivo* manipulation of cells, including stem/progenitor cells, may lead to tumorigenesis [80-82]. Culture and expansion of adult stem cells not only is time consuming, but also limited to finite passages [83]. Furthermore, culture of chondrocytes in a monolayer can lead to de-differentiation, and decreased proteoglycan and type II collagen production [84].

Tissue regeneration by cell homing is substantially under-investigated in comparison to regeneration by cell transplantation. We recently showed that transforming growth factor beta-3 (TGFβ3) acts as a cell homing cue that not only recruited endogenous cells, but also prompted the regeneration of articular cartilage with structural and mechanical properties on par with native articular cartilage in a rabbit model [85]. However, the sources of endogenous cells that regenerate articular cartilage remain elusive in cell homing models. Several stem/progenitor cell populations exist in tissues adjacent to articular cartilage defects including bone marrow,

adipose, synovium, periosteum and skeletal muscle [86]. Stem/progenitor cells have been isolated from these tissues, including mesenchymal stem cells (MSCs), adipose stem cells (ASCs) and synovium stem cells (SSCs) [86]. However, whether ASCs, MSCs and SSCs serve as effective cell sources for *in situ* cell homing to regenerate articular cartilage has not been adequately investigated.

In a cell homing approach for articular cartilage regeneration, one or more bioactive cues may be required for cell recruitment. Stromal derived factor-1 (SDF1) has gained significant interest as a cell homing factor in experimental studies. SDF1 binds to the CXCR4 receptor present on membrane surfaces of multiple cell types including embryonic stem cells, cord blood CD34+ cells, MSCs, ASCs, chondrocytes, osteoblasts and SSCs [46-49, 87, 88]. Importantly, SDF1 promotes cell migration within hours following receptor binding [23] and has been shown to improve the migration distance of MSCs in a biomaterial scaffold [54]. For the present study, we hypothesized that the recruitment of cartilage-forming cells may need to be supplemented by factors to induce chondrogenesis. Accordingly, we incorporated TGFβ3 which has been shown to play a pivotal role in the chondrogenic differentiation of ASCs, MSCs and SSCs [89]. The objective of the present study was to devise a strategy for both the recruitment and chondrogenesis of ASCs, MSCs, and SSCs, all of which are adjacent to a full-thickness articular cartilage defect. A bioactive scaffold was devised with control-released TGFβ3 and/or SDF1β from gelatin microspheres into an underlying porous collagen sponge cube for *in situ* cell recruitment and chondrogenesis. In this work we show that the recruited cells expressed marked gene and protein expression of aggrecan and type II collagen, two main macromolecules in articular cartilage. Thus, these findings suggest that *in situ* cell homing for cartilage regeneration with bioactive scaffolds can be an alternative or complementary approach to the current method of cartilage regeneration by cell transplantation.

2.2 Methods

Design and Characterization of Gelatin Microspheres.

Gelatin microspheres (Sigma, St. Louis, MO) were fabricated by water-in-oil emulsion and washed with acetone to remove residual oil (**Figure 2.1A**), similar to previously published approaches [90, 91]. Four batches of microspheres were prepared, chemically cross-linked with varying levels of glutaraldehyde (0%, 0.25%, 0.5% and 0.75% w/v) and washed with 0.75% w/v glycine containing tween to block residual aldehyde groups on unreacted glutaraldehyde. Microspheres were visualized by light microscopy to ensure shape uniformity. Following lyophilization, gelatin microspheres were sterilized using ethylene oxide.

A separate experiment was conducted to determine the optimal glutaraldehyde cross-linking concentration based on the microsphere degradation profiles. Dehydrated microsphere aliquots (30 mg) from each of the four batches were rehydrated in 30-μL phosphate-buffered saline (PBS) and placed in 12-well culture plates with 2mL of PBS + 1% Antibiotics/Antimicrotics (AB/AM) for 30 days. Microsphere structural changes were observed by light microscopy.

Design and Fabrication of the Bioactive Scaffold.

Microsphere aliquots (30 mg) made with 0.5% w/v glutaraldehyde were rehydrated in 30-μL phosphate-buffered saline (PBS) containing 100-ng recombinant human TGFβ3 (Cell BioSciences, Santa Clara, CA), 100-ng recombinant human SDF1β (R&D Systems, Minneapolis, MN) or PBS. At pH 7.4, the positively charged TGFβ3 and SDF1β were electrostatically bound to the negatively charged gelatin microspheres. Growth factor concentrations were based on their efficacy in previous work [40, 54, 92]. Calcium alginate (2% w/v, FMC BioPolymer, Philadelphia, PA) was mixed with 30 mg (dry wt) of microspheres, deposited over a type I and III collagen sponge [93] (Helistat, Integra LifeSciences, Plainsboro,

NJ) and cross-linked with calcium chloride. The total dimensions of the bi-layered bioscaffold were 6×6×4 mm^3.

Isolation of Primary Human ASCs, MSCs and SSCs.

Human bone marrow MSCs (AllCells, Emeryville, CA), human ASCs, and human SSCs were isolated from fresh adult donor samples using previously established methods [94-98]. MSCs were purified from bone marrow using the RosetteSep® Human Mesenchymal Stem Cell Enrichment Cocktail (Stem Cell Technologies, Vancouver, Canada) following the manufacturer's recommended protocol. Briefly, the bone marrow sample was mixed with the RosetteSep® Human Mesenchymal Stem Cell Enrichment Cocktail containing antibodies directed against cell surface antigens on hematopoietic cells and glycophorin A on red blood cells. Following 20-min incubation, the bone marrow mixture was diluted with PBS containing 2% FBS and 1mM EDTA. The diluted sample was subsequently placed on top of Ficoll-Paque™ and centrifuged to form a density gradient. The enriched MSCs were collected from the Ficoll-Paque™ interface, washed with PBS containing 2% FBS and 1mM EDTA and plated. To ensure multi-lineage potential, MSCs were differentiated into osteoblasts, chondrocytes and adipocytes for quality-control (data not shown). Ethical approval for isolating SSCs was obtained from Leeds Teaching Hospitals NHS Trust Ethics Committee. Synovial membranes were isolated aseptically, finely minced, washed in PBS and digested in 0.25% collagenase (Stem Cell Technologies, Vancouver, Canada). After incubation in a rotator at 37°C for 5 hrs, the collagenase solution was filtered through a 70-μm filter (BD, Oxford, UK). The liquid fraction containing the cells was centrifuged and plated [95, 98]. Synovium cells were subjected to extended phenotyping [86], [99] and were shown to differentiate into osteoblasts, chondrocytes and adipocytes [100]. ASCs were isolated from subcutaneous liposuction aspirates and digested with 0.25-mg collagenase (200 units/mg) per ml of Krebs-Ringer-Bicarbonate solution (Sigma, St Louis, MO) at 37°C for 40

min. Following centrifugation, the stromal-vascular fraction was isolated and plated, per our previously described protocol [101].

In Vitro Chondrogenesis by Cell Homing.

ASCs and MSCs were cultured with Dulbecco's Modified Eagle Medium (DMEM, Gibco, Carlsbad, CA), 10% FBS (Gibco, Carlsbad, CA) and 5% AB/AM. SSCs were cultured using Mesencult® (Stemcell Technologies, Vancouver, Canada). ASCs, MSCs and SSCs were expanded to passage 3 and seeded in 6-well plates with 100,000 cells per well. Four conditions were tested: cytokine free, TGFβ3 alone, SDF1β alone, and combined TGFβ3 and SDF1β. SDF1β was selected because it promotes the migration of multiple cell types [54]. TGFβ3 was investigated for its ability to induce chondrogenesis [102-105]. The combined SDF1β and TGFβ3 condition consisted of 15-mg SDF1β microspheres and 15-mg TGFβ3 microspheres (100-ng TGFβ3 or SDF1β/15mg microspheres). All scaffolds were placed in culture wells and incubated at 37°C and 5% CO_2 with medium changed every 3 days. Scaffolds were harvested after 3 hrs (n=6), 1 wk (n=6), 3 wks (n=6) and 6 wks (n=6), and cut vertically with one part used for real-time PCR and the other for histology and immunohistochemistry.

TGFβ3 and SDF1β Release Kinetics.

In a separate experiment, 30-mg of microspheres (dry wt%) made with 0.05% w/v glutaraldehyde containing either 100-ng SDF1β or 100ng TGFβ3 were placed in separate wells containing PBS and 1% BSA (n=3). As the gelatin microsphere matrix degraded, the encapsulated growth factor was presumed to be released. To ascertain this, samples of PBS were collected after 0, 1, 2, 4, 9, 12, 18, 24, 29, 34, 38 and 42 days, and replaced with fresh PBS containing 1% BSA. Total released SDF1β or TGFβ3 from microspheres per time point was determined by ELISA.

Cytokine Effects on Cell Proliferation.

Cell metabolic activity was measured to determine the potential contribution of cell proliferation upon SDF1β and/or TGFβ3 delivery to the overall cellularity in the collagen sponge. An MTS (3-(4,5-dimethylthiazol-2-yl)-5-(3-carboxymethoxyphenyl)-2-(4-sulfophenyl)-2H-tetrazolium) assay was conducted with the CellTiter 96 Aqueous Non-Radioactive Cell Proliferation Assay Kit (Promega, Madison, WI). Multiple plates were seeded with 4,000 cells each and treated with SDF1β or TGFβ3 (concentrations: 1, 10 or 100 ng) supplemented basal medium, with cytokine-free basal medium as a control. The absorbance was assessed at 490 nm after 0, 24, 48 and 96 hrs using a standard curve.

Histology and Quantification of Cell Migration.

Scaffolds were fixed in 10% buffered formalin, dehydrated, embedded in paraffin and sectioned at 5-μm thickness. Sections from the top, middle, and bottom of each scaffold were stained with 4',6-diamidino-2-phenylindole (DAPI; Vectorshield, Burlingame, CA) to visualize cell nuclei and subsequently quantified to derive the numbers of cells that were recruited into the collagen sponges. Additional sections were stained with hematoxylin and eosin (H&E) and 0.1% toluidine blue (Sigma, St. Louis, MO) to assess cartilage matrix formation and sulfated polysaccharides. For aggrecan immunohistochemistry, sections were digested with pepsin (0.6% w/v), 3% hydrogen peroxide in PBS, blocked with 3% normal horse serum (v/v) and then incubated with primary antibody (1:300) for 90 min at room temperature. A biotinylated secondary anti-mouse antibody (1:200) was used to detect immunoreactivity. For collagen type II immunohistochemistry, sections were digested with Pepsin (0.6 % w/v), 3% hydrogen peroxide in PBS, blocked with 10% normal goat serum (v/v) and then incubated with primary antibody (1:80) for 90 min at room temperature. Envision system labeled polymer-HRP (DAKO,

Carpinteria, CA) was used to detect immunoreactivity. Slides were counterstained with hematoxylin. Normal healthy human articular cartilage served as a positive control.

Quantitative RT-PCR.

Scaffolds were homogenized using a Powergen 125 (Fisher, Pittsburgh, PA) and total RNA was isolated using TRIzol (Invitrogen, Carlsbad, CA), following the manufacturer's protocol. Briefly, 0.2-mL chloroform was added to the homogenized scaffold and centrifuged. The aqueous, RNA containing phase was separated and mixed with 0.5-mL isopropyl alcohol and 20-µg glycogen. Following 10-min incubation, samples were centrifuged to form a pellet, washed with 75% ethanol and resuspended in dH_20. Complementary DNA (cDNA) was synthesized using the iScript cDNA Synthesis Kit (Bio-Rad, Hercules, CA). RT-PCR was performed using the TaqMan Assay Protocol (Applied Biosystems, Carlsbad, CA): hold for 2 min at 50°C, hold for 10 min at 95°C, and 50 cycles of melt for 15 s at 95°C and anneal/extend for 1 min at 60°C. All reactions were run in triplicate. Primers from Applied Biosystems were Hs00202971_m1 for Aggrecan, Hs01060344_g1 for Type II collagen and Hs99999901_s1 for 18s. Aggrecan and collagen type II expression was normalized to 18s and subsequently normalized to the negative control.

Statistical Analysis.

For each condition, the results were pooled from two independent sets of experiments with each experiment performed in at least triplicate. Upon confirmation of a normal data distribution, a one-way ANOVA with *post hoc* LSD test was used to detect significant differences using a value of $p \leq 0.05$.

2.3 Results

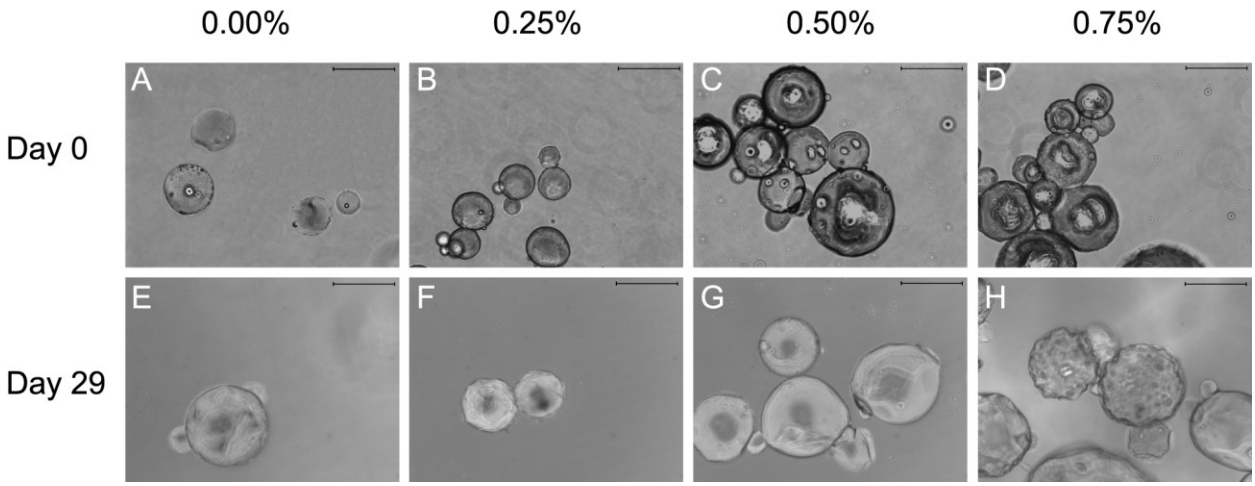

Figure 2.1. Gelatin microspheres cross-linked with various levels of glutaraldehyde (GA). (A) Day 0, 0% GA (B) Day 0, 0.25% GA (C) Day 0, 0.5% GA (D) Day 0, 0.75% GA (E) Day 29, 0% GA (F) Day 29, 0.25% GA (G) Day 29, 0.5% (H) Day 29, 0.75% GA.

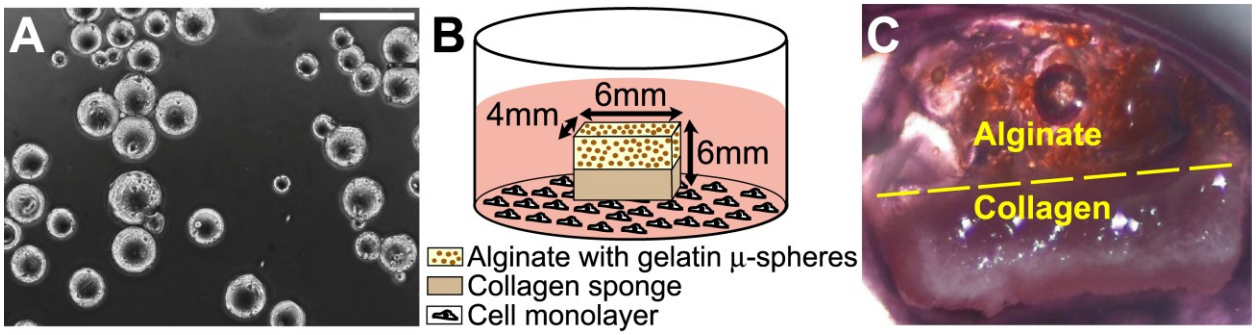

Figure 2.2. Experimental schematic and tissue morphology. (A) Light microscopy of microspheres with an average diameter of 70.8±21.5 μm. Scale: 200 μm. (B) Bilayered scaffold with an alginate layer containing gelatin microspheres overlaying a collagen sponge cube. Overall scaffold dimensions were 6x6x4 mm^3. Scaffolds were placed in the culture of adipose, mesenchymal and synovium stem cells (ASCs, MSCs, and SSCs). (C) Gross scaffold morphology following 3-wk culture. Glistening white tissue can be seen in the scaffold's collagen region.

Effect of Glutaraldehyde Cross-Linking on Microsphere Degradation.

While all four batches of microspheres could be fabricated, the batches cross-linked with 0% and 0.25% glutaraldehyde were technically more challenging (**Figure 2.1A & B**). The batch made without any glutaraldehyde was structurally instable and in some cases, disintegrated into a powder after lyophilization. The batch made with 0.25% glutaraldehyde encountered significant static attraction with polystyrene labware, which ultimately decreased the batch yield. Furthermore, the batches made with 0.5% and 0.75% glutaraldehyde (**Figure 2.1C & D**) appeared to be slightly larger in diameter than the batches made with 0% and 0.25% glutaraldehyde. In terms of degradation, the batches made with 0% and with 0.5% glutaraldehyde appeared to experience a thinning of bulk structure but maintained a smooth shaped outer wall. On the other hand, the batches of microspheres made with 0.25% and 0.75% glutaraldehyde experienced a drastic change in surface smoothness and were covered with many crater-like structures. Thus, because of fabrication ease and maintenance of surface smoothness during degradation, for all experiments described in this thesis other than this initial characterization experiment, microspheres used were cross-linked with 0.5% glutaraldehyde.

Cytokine Release Kinetics From Gelatin Microspheres.

The average diameter of the gelatin microspheres with a 0.5% (w/v) glutaraldehyde concentration was 70.8±21.5μm (**Figure 2.2A**). Microencapsulated SDF1β or TGFβ3 were control-released over the tested 42 days and displayed similar release patterns but at different amplitudes (**Figure 2.3**). By 42 days, a total of 42.3% SDF1β and 60.8% TGFβ3 was released, primarily as a function of their different molecular weights.

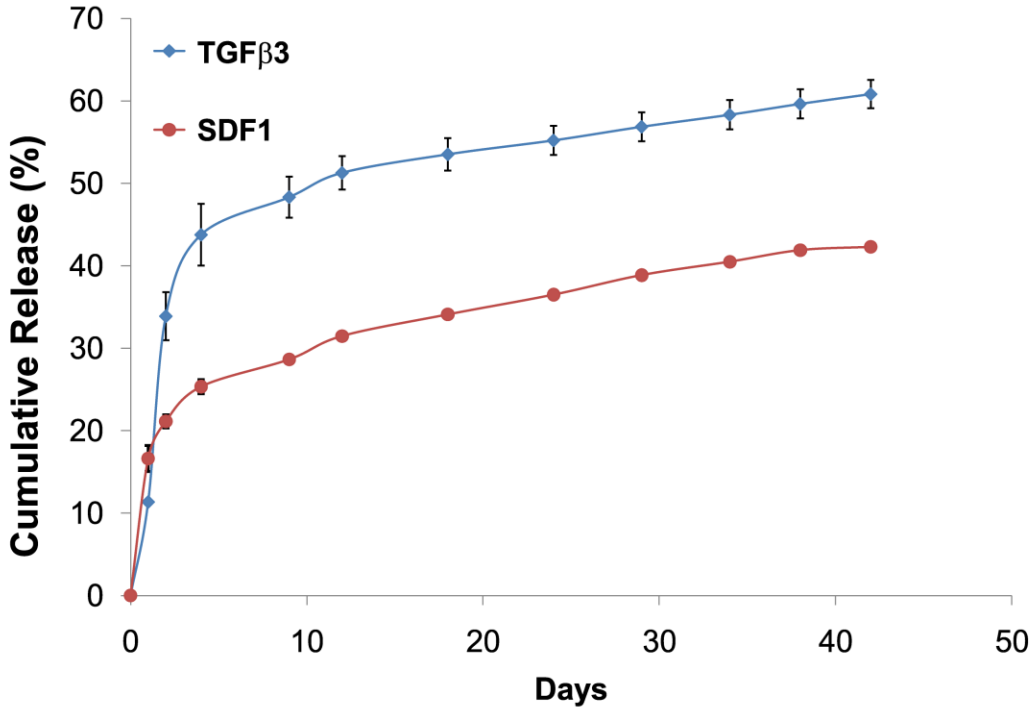

Figure 2.3. Release kinetics of SDF1β and TGFβ3. Fluid samples of gelatin microspheres encapsulating SDF1β or TGFβ3 were analyzed with ELISA (n=3). After 42 days, 42.3% SDF1β and 60.8% TGFβ3 were released.

Chemotaxis of Stem/Progenitor Cells by Control-Released TGFβ3 and/or SDF1β.

Scaffolds with control-released TGFβ3 and/or SDF1β were cultured over primary human ASCs, MSCs or SSCs (**Figure 2.2B**). A uniform layer of glistening white tissue was formed by the recruited cells in the collagen sponge cube as early as 3 wks (**Figure 2.2C**). DAPI staining (inverted for demonstration) revealed the nuclei of the cells that had migrated into the collagen sponge cubes from the underlying and adjacent ASCs, MSCs or SSCs (**Figure 2.4A-L**). Sections from the top, middle, and bottom of the scaffolds were DAPI-stained and pooled to calculate quantitative data (**Figure 2.5**). A general increase in cellularity was observed in the tested scaffold at 6 wks regardless of cell type or cytokines (**Figure 2.5**). TGFβ3 recruited

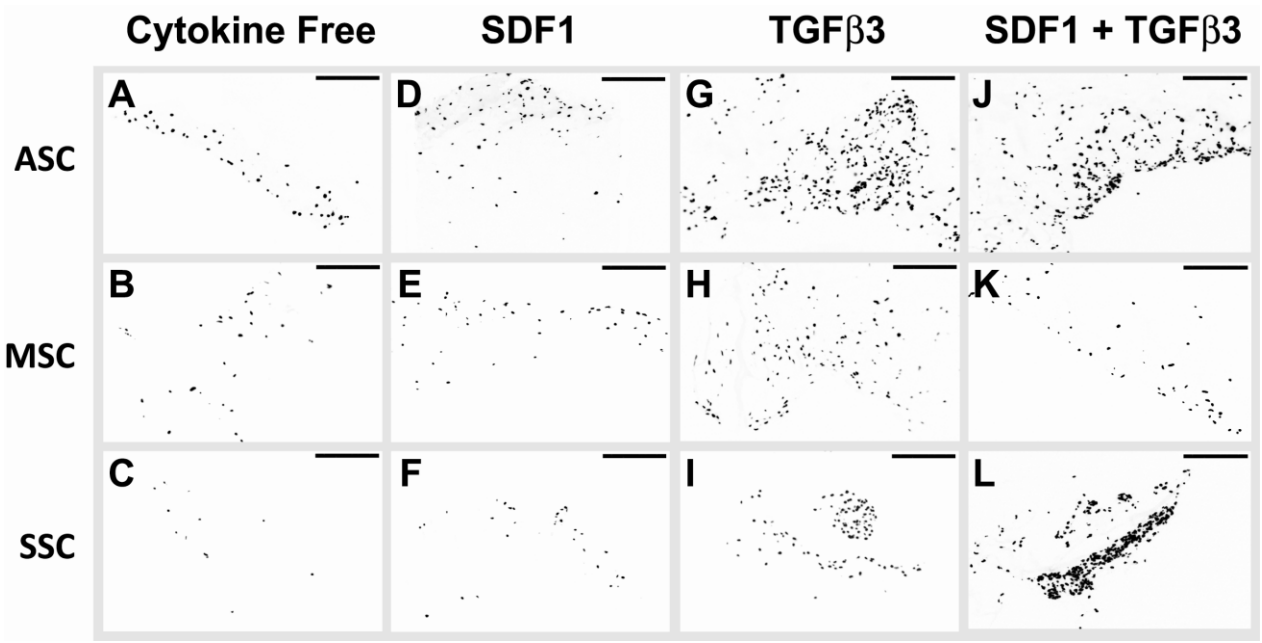

Figure 2.4. Chemokine mediated recruitment of adipose, mesenchymal and synovium stem cells (ASCs, MSCs and SSCs). After 6-wks in the culture of ASCs, MSCs and SSCs, scaffolds were sectioned and stained with DAPI to visualize the cell nuclei. Sections from the top, middle and bottom of the scaffold were stained (n=8-12). Four conditions were tested: cytokine-free (A-C), SDF1β (D-F), TGFβ3 (G-I) and TGFβ3+SDF1β (J-L) for ASCs, MSCs and SSCs. Scale: 200μm.

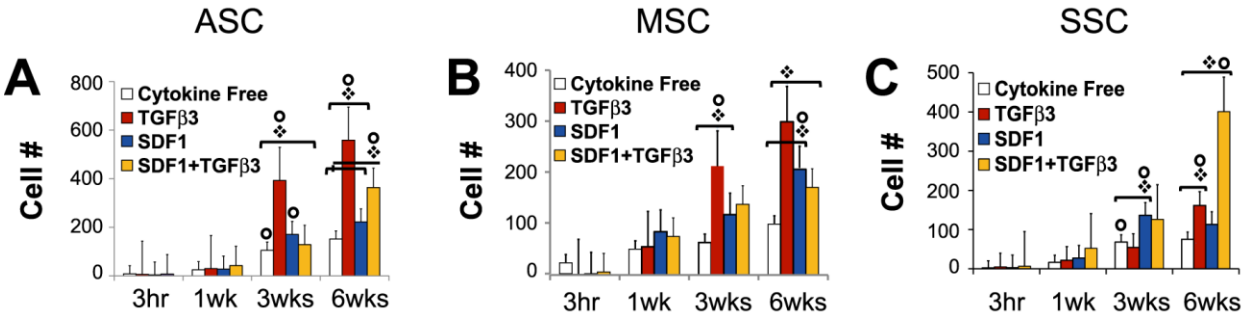

Figure 2.5. Quantification of ASC, MSC and SSC recruitment. DAPI stained sections were quantified to determine the chemotactic effects of SDF1β and/or TGFβ3 on (A) ASCs, (B) MSCs and (C) SSCs. Values shown are mean±standard error. ❖: significant difference over other conditions at same time point ($p<0.05$), °: significant difference over previous time point ($p<0.05$).

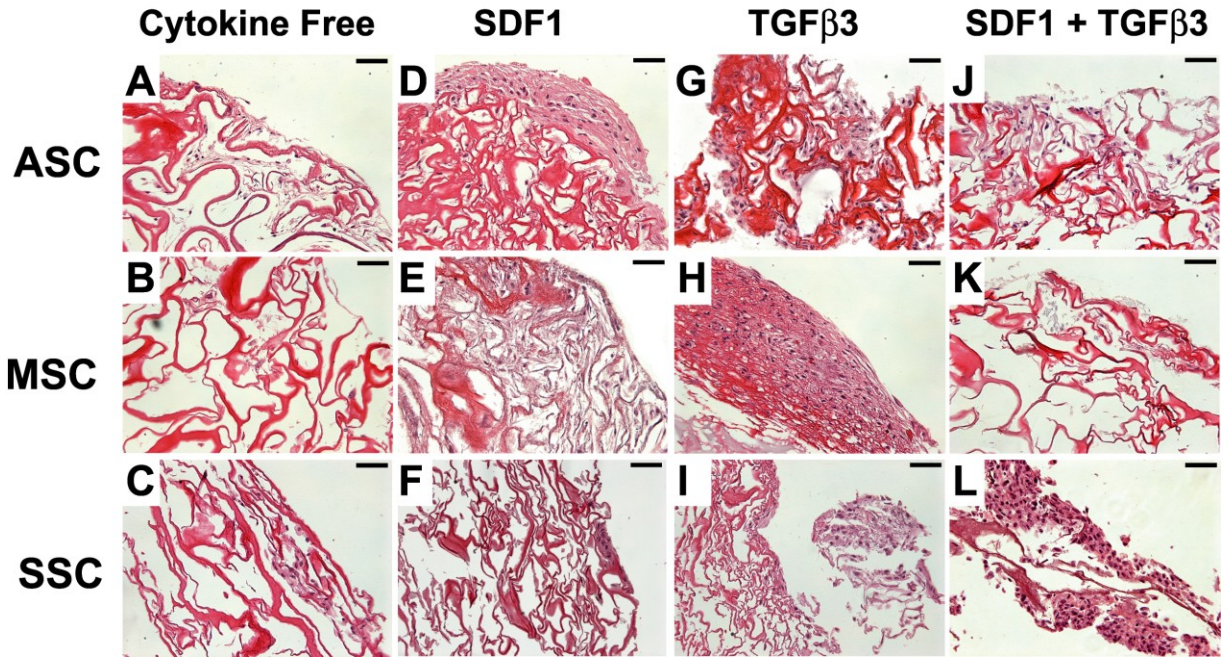

Figure 2.6. Tissue formation upon cytokine-induced cell recruitment. After 6-wks, scaffolds were stained with H&E for each of the four conditions tested: cytokine-free (A-C), SDF1β (D-F), TGFβ3 (G-I) and TGFβ3+SDF1 (J-L) for adipose, mesenchymal and synovium stem cells (ASCs), (MSCs) and (SSCs). Significant matrix deposition can be seen in ASCs due to SDF1β, MSCs due to TGFβ3, and SSCs due to SDF1+ TGFβ3, indicating that the scaffold substrate is conducive to cell attachment (D, H, L). Scale: 50 μm.

significantly more ASCs (558±65) than all other conditions, followed by SDF1β and TGFβ3 co-delivery (363±46.2) (**Figure 2.5A**). TGFβ3 recruited significantly more MSCs (302±52) than SDF1β (208±37) (**Figure 2.5B**). SDF1β and TGFβ3 co-delivery recruited significantly more SSCs (400±120) than all other conditions, followed by TGFβ3 alone (157±18) (**Figure 2.5C**). For all three cell types, significantly fewer cells were present in the cytokine-free group than all other conditions (**Figure 2.5**). Matrix synthesis was evident in some, but not all, groups (**Figure 2.6**). In contrast to little matrix synthesis in cytokine-free samples (**Figure 2.6A-C**), tissue was formed *in vitro* by the recruited ASCs, MSCs or SSCs in SDF1β delivery, TGFβ3 delivery, or SDF1β and TGFβ3 co-delivery samples (**Figure 2.6D-F, G-I, J-L, respectively**).

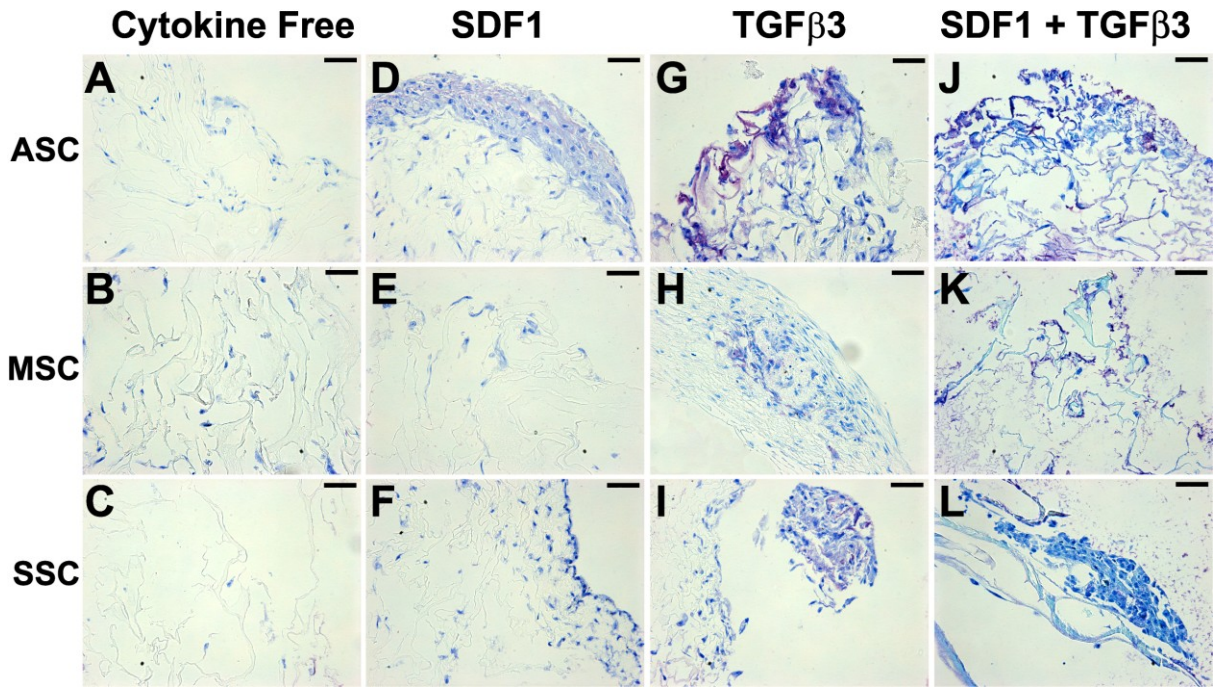

Figure 2.7. Chondrogenic differentiation of chemokine-recruited cells. After 6 wks, sections were stained with toluidine blue for each of the four conditions tested: cytokine-free (A-C), SDF1β (D-F), TGFβ3 (G-I) and TGFβ3+SDF1β (J-L) for adipose, mesenchymal and synovium stem cells (ASCs), (MSCs) and (SSCs). Scale: 50 μm. Positive staining reveals chondrogenesis among the TGFβ3-only group (G-I) and the SDF1β+TGFβ3 (J-L) group for all three cell types.

Chondrogenesis of Recruited Stem/Progenitor Cells.

Cartilage regeneration by cell homing not only requires cell recruitment into an anatomic compartment, but also chondrogenesis of the recruited cells. After 6 wks, toluidine blue staining was most notable in the TGFβ3 group (**Figure 2.7 G-I**) and the TGFβ3 and SDF1β co-delivery

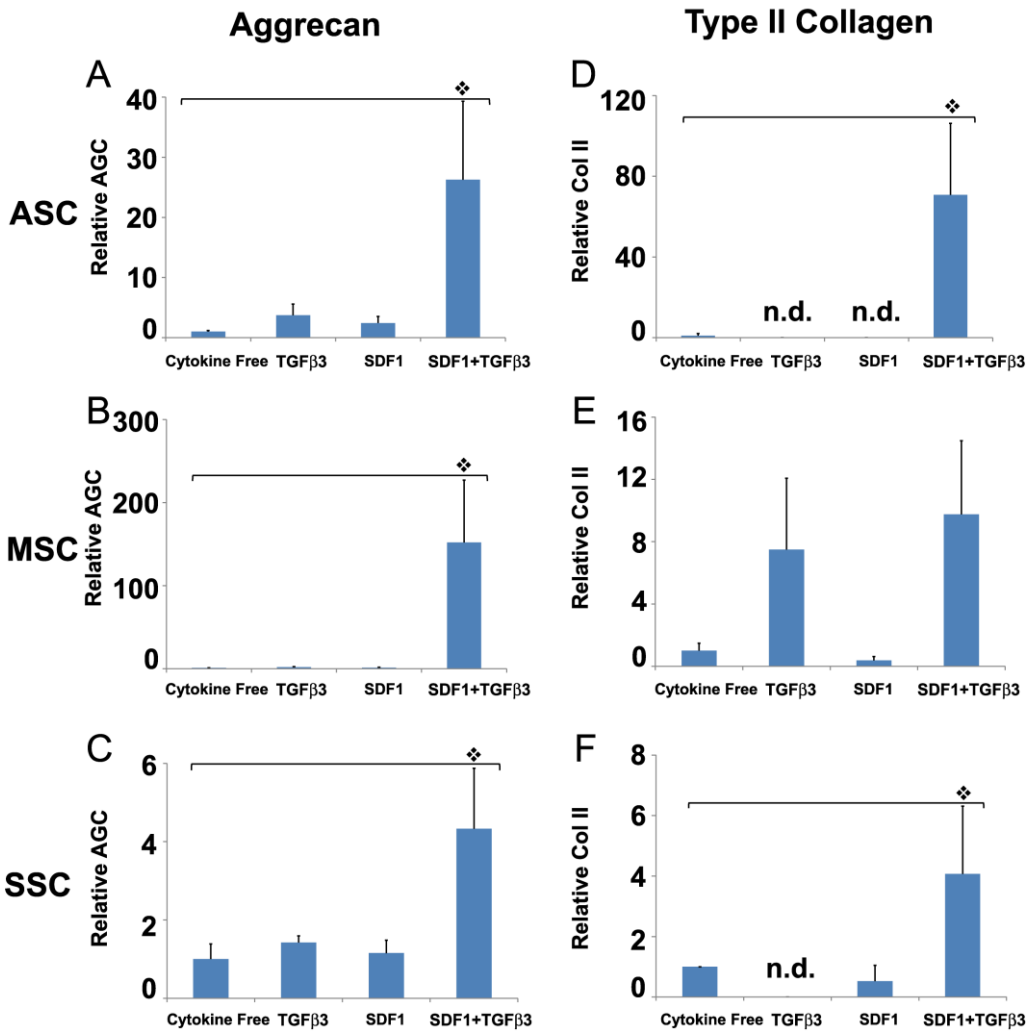

Figure 2.8. Gene expression of aggrecan and type II collagen. After 6 wks, scaffolds were digested, and encapsulated cells were tested for aggrecan expression (A-C) and Col II (type II collagen) (D-F) using RT-PCR (n=3). Relative aggrecan expression was significantly higher upon TGFβ3+SDF1β co-delivery for ASCs, MSCs and SSCs than the cytokine-free groups. TGFβ3+SDF1β co-delivery also induced significantly higher Col II expression for ASCs and SSCs than the cytokine-free group. N.d.: expression below detection limit.

group (**Figure 2.7J-L**) for all 3 cell types. Contrastingly, there was little positive toluidine blue staining in the cytokine-free groups for all 3 cell types (**Figure 2.7A-C**). Aggrecan and type II collagen are two predominant macromolecules in articular cartilage [106]. Quantitative real-time PCR showed significantly higher aggrecan expression upon TGFβ3 and SDF1β co-delivery than the cytokine-free group for ASCs, MSCs and SSCs (**Figure 2.8A-C**). Type II collagen mRNA

was significantly higher for ASCs and SSCs upon TGFβ3 and SDF1β co-delivery than other groups (**Figure 2.8D, F**).

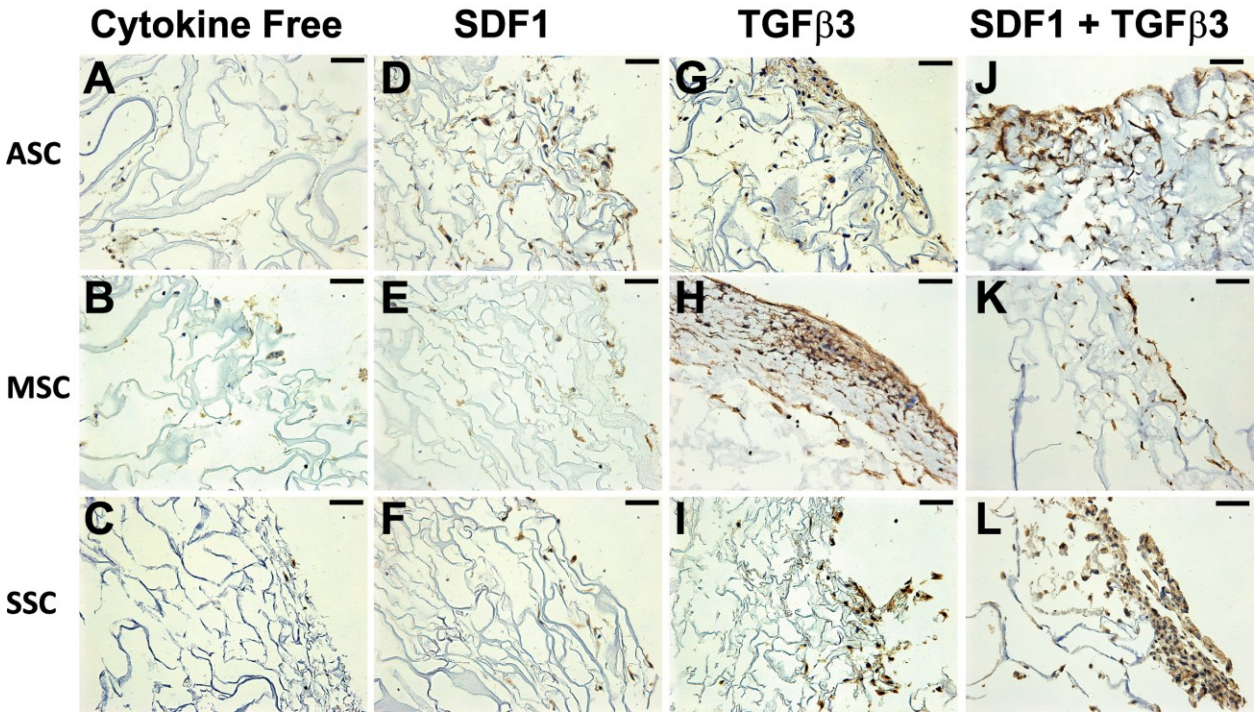

Figure 2.9. Immunohistochemistry staining of aggrecan. After 6 wks, scaffold samples were immunostained with aggrecan antibody for each of the four conditions tested: cytokine-free (A-C), SDF1 (D-F), TGFβ3 (G-I) and TGFβ3+SDF1β (J-L) for adipose, mesenchymal and synovium stem cells (ASCs), (MSCs) and (SSCs). Positive aggrecan staining revealed chondrogenesis among the TGFβ3-only group (G-I) and the SDF1β+TGFβ3 (J-L) group for all three cell types. Scale: 50 μm.

Immunohistochemistry staining revealed aggrecan (**Figure 2.9**) and type II collagen (**Figure 2.10**) expression for ASCs, MSCs, and SSCs, confirming protein synthesis in addition to mRNA expression. Aggrecan antibody staining was present in the extracellular matrix for all three cell types in the TGFβ3 and SDF1β co-delivery group for ASCs, MSCs, and SSCs (**Figure 2.9J-L**) and the TGFβ3 alone group for ASCs and MSCs (**Figure 2.9G, H**). However, aggrecan antibody staining was minimal among the cytokine-free and SDF1β only samples for all three

cell types (**Figure 2.9A-F**). There was marked collagen type II antibody staining for the TGFβ3 and SDF1β co-delivery samples (**Figure 2.10J-L**), as well as the TGFβ3 group for MSCs

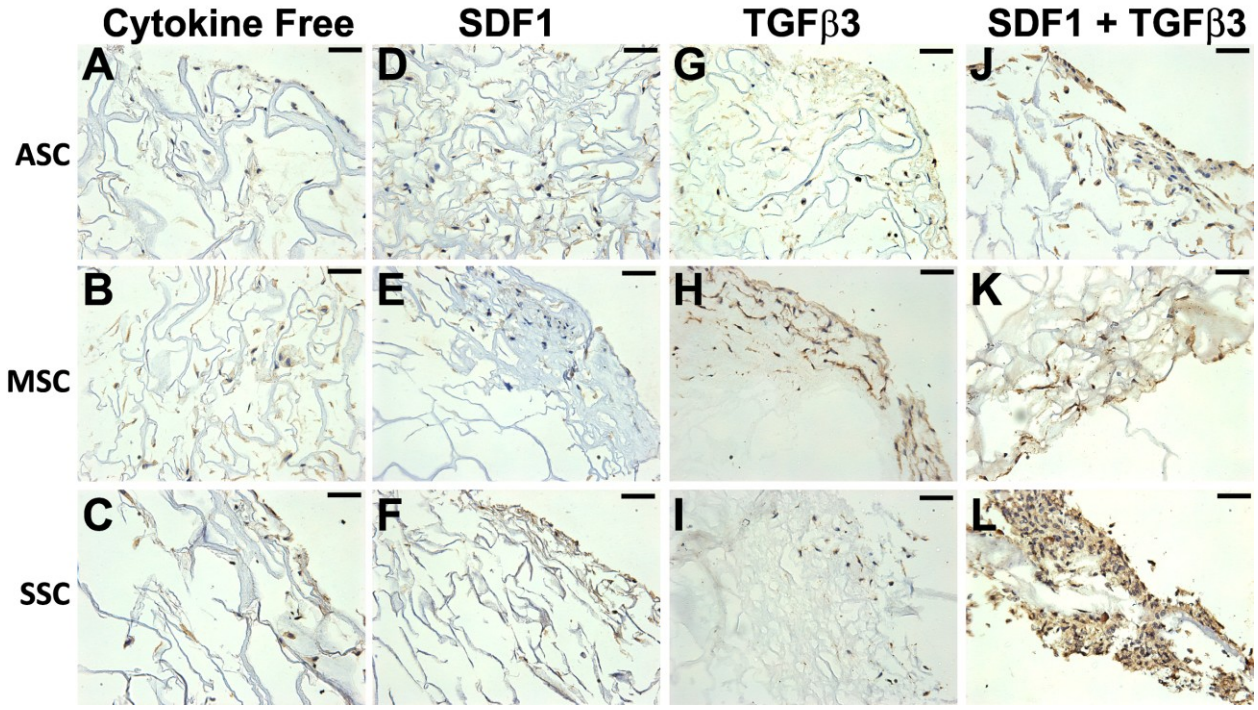

Figure 2.10. Immunohistochemistry staining of type II collagen. After 6 wks, scaffold samples were immunostained with type II collagen (Col II) for each of the four conditions: cytokine-free (A-C), SDF1 (D-F), TGFβ3 (G-I) and TGFβ3+SDF1β (J-L) for adipose, mesenchymal and synovium stem cells (ASCs), (MSCs) and (SSCs). Positive Col II staining revealed chondrogenesis among the TGFβ3-only group for MSCs (H) and the SDF1β+TGFβ3 (J-L) group for all three cell types. Scale: 50 μm.

(**Figure 2.10H**). Positive immunohistochemical staining of aggrecan and collagen type II upon TGFβ3 delivery or combined TGFβ3 and SDF1β co-delivery suggests that TGFβ3 was essential for chondrogenic differentiation of recruited ASCs, MSCs and SSCs.

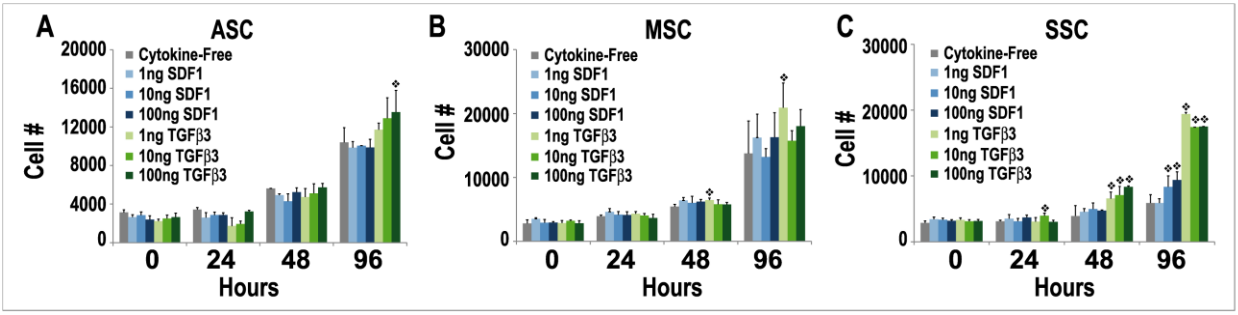

Figure 2.11. Mitogenic effect of SDF1β and TGFβ3. MTS assays were conducted to determine effects of SDF1β and TGFβ3 on cell proliferation. Three concentrations of SDF1β or TGFβ3 were tested: 1 ng, 10 ng and 100 ng (n=3), following 96-hr exposure.

TGFβ3 and SDF1β Have a Modest Effect on Cell Proliferation.

MTS assay revealed that TGFβ3 and/or SDF1β delivery had modest effects on cell proliferation (**Figure 2.11**). A total of 3 doses of TGFβ3 or SDF1β were separately supplemented in ASC, MSC and SSC cultures for up to 96 hrs. Cell proliferation was significantly higher for TGFβ3-treated (1 ng) MSCs than the control (n=3, $P<0.05$). There was also a significant increase in ASC proliferation when treated with 100ng TGFβ3 (n=3, $P<0.05$) over the control. Cell proliferation rates of SSCs increased significantly (n=3, $P<0.05$) over the control in response to 10-ng SDF1β, 100-ng SDF1β and all three doses of TGFβ3.

2.4 Discussion

Previous reports in the literature have highlighted the potent effects of TGFβ3 at inducing chondrogenesis of progenitor cells, but had not demonstrated any chemotactic behavior associated with this biological cue [34, 89]. One of the key findings of the present work is that TGFβ3 not only effectively recruited both adipose and mesenchymal stem cells into the scaffold, but also induced the recruited cells to undergo chondrogenesis. Interestingly, TGFβ3 had somewhat modest effects on the recruitment of synovium stem cells in this *in vitro* system, with the exception of the later time course. TGFβ3's robustness in cell recruitment confirms its

efficacy in the regeneration of an entire articular surface *in vivo* by cell homing in our recent work [85]. Thus, TGFβ3 appears to act as a potent chemotactic molecule and is capable of recruiting at least mesenchymal cells of bone marrow, adipose tissue and perhaps synovium. Given the presently designed slow release rate of TGFβ3, it is conceivable that the initially released TGFβ3 was responsible for cell recruitment, whereas later released TGFβ3 induced chondrogenesis. Contrastingly, SDF1β 's capacity in the recruitment of ASCs and MSCs is below its expected potency as a highly potent chemotactic cytokine for other cell types such as lymphocytes and macrophages [87]. Significant effects of SDF1β in the recruitment of MSCs by 6 wks in our current *in vitro* model is consistent with previous reports of MSC migration by SDF1β [107, 108]. Remarkably, the combined effects of TGFβ3 and SDF1β in the recruitment of ASCs, MSCs and SSCs, suggests their potential synergistic actions. In particular, co-delivery of TGFβ3 and SDF1β seems quite chemotactic for synovium stem cells.

Most cell migration assays are performed in monolayer cell cultures, transwells or Boyden chambers. The present 3D migration system is designed to create an acellular bioscaffold to be populated by cells, including stem/progenitor cells that are purposefully recruited by specific bioactive cues. The motivation for the design of such a system is as follows. First, specific cells that are recruited into an acellular bioscaffold may generate tissues in a cell homing approach for tissue regeneration. It is conceivable that different cell types may be recruited by specific bioactive cues, including peptides, proteins or chemical compounds. This approach may have implications in both tissue regeneration and drug development. Second, identification of bioactive cues in the recruitment of specific cell types may constitute a novel approach for tissue regeneration by cell homing. Cell recruitment into a predesigned bioscaffold *in vivo* may serve as an alternative or adjunctive approach to tissue regeneration by cell transplantation. If certain tissues can be regenerated by chemotaxis of endogenous cells without cell transplantation, development of regenerative therapies may be simplified by

circumventing cell isolation, *ex vivo* manipulation, packing, shipping and sterilization. It is known that most of the tissues and organs thus studied in the body harbor stem/progenitor cells. Targeted chemotaxis of endogenous tissue-forming cells, including stem/progenitor cells, may be capable of regenerating tissues, perhaps without cell transplantation. Initial examples of tissue regeneration by endogenous stem cell homing include regeneration of cartilage, bone, dermal and neuromuscular tissues in severed digits, dental pulp and periodontium [85], [109], [110]. Amphibians such as salamanders are well recognized for their ability to spontaneously regenerate severed limbs, whereas this ability may have been deprived in evolutionally advanced species [111]. However, it remains to be studied whether endogenous regenerative capacity can be reinvigorated by specific, interventional bioactive cues that are delivered at critical times in wound healing. On the other hand, reservations about tissue regeneration by endogenous cell homing, without cell transplantation, include skepticism of the complexity of tissues regenerated, potential toxicity of concentrated bioactive cues, and specificity of a hypothetical match between a given cell type and a bioactive cue. Nevertheless, the presently adopted control-release system, similar to previous work in this area by us and others [112, 113], addresses several potential pitfalls of bioactive cue delivery such as premature cytokine denature and diffusion. Furthermore, the amount of cross-linking of gelatin, which serves as the shell of encapsulated growth factors in the present study, can be adjusted to modulate release kinetics as a function of biological needs.

A number of cytokines are known to induce cell migration including SDF1β, stem cell factor (SCF), insulin-like growth factor-1 (IGF1), and granulocyte colony stimulating factor (G-CSF) [39-41]. The data described here substantiate our recent study [85] that TGFβ3 has potent cell homing capacity, in addition to its reported roles in chondrogenesis and fetal wound healing [114]. Strikingly, we discovered that TGFβ3 is able to recruit both ASCs and MSCs, which natively occupy different anatomic compartments. Remarkably, the TGFβ3 and SDF1β

axis appears particularly potent in the recruitment of SSCs. Positive toluidine blue staining in combination with positive gene expression and protein synthesis of aggrecan and type II collagen suggest *in vitro* chondrogenesis in 3D scaffolds by ASCs, MSCs and SSCs, none of which are known to spontaneously differentiate into chondrocytes in monolayer culture. Importantly, the present findings indicate that SDF1β has little chondrogenic potential. TGFβ3, in addition to its broadly-based cell homing potential, also induces chondrogenesis of recruited stem/progenitor cells. Mitogenic effects of SDF1β and/or TGFβ3 in the present work, most notably for SSCs, are superimposed with cell recruitment and can be further distinguished from cell migration in future studies. However, the net effects of cell proliferation and cell recruitment may be facilitative for tissue regeneration given the frequent shortage of tissue-forming cells in wound healing environments, including cartilage and/or osteochondral defects. Although ASCs, MSCs and SSCs have been investigated as candidate cells for transplantation in the healing of cartilage and osteochondral defects, our present findings provide a strong rationale for additional *in vivo* studies, which will be conducted in Aim 4, to test the efficacy of homing ASCs, MSCs and SSCs, all of which are natively found near a synovial joint, for cartilage regeneration.

Chapter 3. The development of novel microfluidic devices to characterize the process of homing stem/progenitor cells.

3.1 Introduction

In Chapter 2, we successfully devised a method for actively recruiting ASCs, MSCs and SSCs and subsequently inducing their chondrogenic differentiation *in vitro.* This bioactive scaffold represents a potential approach to cell homing for tissue regeneration *in vivo.* In our scaffold design, we incorporated SDF1 and TGFβ3 to induce chemotaxis and/or chondrogenic differentiation. Combinatorial delivery of SDF1 and TGFβ3 was successful at inducing significant migration of SSCs while delivery of TGFβ3 alone was sufficient to induce potent migration of both ASCs and MSCs. Chondrogenic differentiation was induced due to delivery of TGFβ3-alone or due to combinatorial delivery of SDF1 and TGFβ3 for all cell types. Although the bioactive scaffold was able to form tissue that expressed cartilage specific gene and protein markers, the cellularity was low compared to the number of cells seeded on the cell culture plate. Additional cytokines might enhance the cell homing ability of these progenitor cells and lead to improved cartilage tissue formation.

Commonly used migration systems include the Boyden chamber, scratch assay and under-agarose assay. The Boyden chamber uses a membrane to create a cytokine gradient between a bottom media filled chamber and a top cell-seeded layer. However, only end-point migration data can be collected and this system only allows for the testing of one cytokine against one cell type at a time. In the scratch assay, a gap is manually introduced into a confluent cell layer and observed as the cells migrate to repopulate the open area. Because a cytokine gradient cannot be created, studies with this system are limited to those of chemokinesis. Since cells are exposed to gradients of cytokine cues during tissue development, the inability for the scratch assay to form cytokine gradients limits the utility of this method for

studies of tissue regeneration. The under agarose assay functions based on the principle that solidified agarose does not adhere to glass substrates. To conduct this assay, a layer of agarose is solidified onto a glass plate and three holes are punched into the gel for introducing a cell source, a cytokine source and a control source. After cytokine gradients are formed through the agarose, cell migration towards the cytokine or control sources is monitored. However, with this configuration, cells are allowed to migrate in all directions, making it difficult to monitor cell motility over time. Additionally, to study the effects of multiple cytokines, multiple sets of 3 holes would have to be punched from the sample agarose sheet, allowing potential cytokine cross-contamination through the porous gel. Thus, existing migration systems are limited in individual utility, restricting our current understanding of cell-motility.

We developed a novel high-fidelity microfluidic device, based on the principles of the under agarose assay, that was used to conduct multiple cell homing assays concurrently, without any chance of cross-contamination between cytokine gradients. Since cell migration is confined to microfluidic channels, migration can easily be monitored using time-lapse microscopy. Three versions of the device were fabricated. The first device contains 6 identical channels with a fixed length between the cytokine inlet and the cell seeding inlet. With this device, multiple migration assays can be conducted simultaneously to ensure the conditions are identical between experiments. Furthermore, six different cytokines or six different cell types can be tested simultaneously for their chemotactic effects. The second device contains five varying distances between the cell and cytokine inlets to observe how distance affects cell migration. If the same cytokine concentration is tested in channels of varying lengths, depending on the channel length that promotes the most cell migration, one can determine if the cytokine concentration should be higher or lower than the tested concentration. Thus, this device can also be used to narrow down the most effective cytokine concentration for promoting cell migration. The third device contains six channels with a connected inlet and separate outlets.

With this device, a single cell type can be simultaneously exposed to six different cytokines or conversely, the effects of one cytokine can be tested on six different cell types. In this chapter, we will focus on characterizing the optimal conditions for using these devices, and demonstrate the device utility with various cell types.

3.2. Methods

Device Fabrication.

A transparency mask containing the design of the device (**Figure 3.1**) was made using AutoCAD and printed with high resolution (CADArt, Bandon, OR). Using standard photolithography, a silicon master was fabricated with a layer of SU-8 containing a negative imprint of the device pattern and then silanized by evaporation of trichloro (1,1,2,2-perfluoocytl) silane (Sigma, St. Louis, MO). Subsequently, using soft lithography, the master was replicated in polydimethylsiloxane (PDMS) to obtain a positive imprint of the pattern. Briefly, Sylgard 184 silicone elastomer base (Ellsworth Adhesives, Germantown, WI) was mixed at a 1:10 ratio with the curing agent, degassed in a vacuum chamber to remove any air bubbles, and cured in a dry oven at 60°C for 2 hrs. Biopsy punches with a diameter of 1 or 6 mm were used to create the channel inlets (**Figure 3.2**). Devices with uniform length channels and connected channels had a channel length of 5 mm. Devices with varying length channels had channel lengths of 10 mm, 7.5 mm, 5 mm, 2.5 mm and 1.5 mm. All channels had a diameter of 250 μm (**Figure 3.2**). PDMS devices were permanently adhered to pre-cleaned glass slides (25 by 75 mm) using plasma bonding (**Figure 3.2**). Subsequently, the channels were filled with distilled water to maintain a hydrophilic environment.

The microfluidic under agarose assay works as follows. Each channel contains a 1mm diameter inlet in the center through which agarose is injected. Because the inlet is located exactly in the center of the channel, the pressure differential between the agarose inlet and the

two 6mm diameter side wells is equal, which causes agarose to spread to both sides of the channel at the same time. Immediately preceding the inlet to the side wells are two cubes (edge = 50μm). These cubes were designed to increase the surface tension between the agarose and the channel to prevent the agarose from contracting. A very simple setup procedure is required to use the migration assay devices, which includes agarose injection, cell seeding, cytokine loading and cell migration monitoring (**Figure 3.5a**).

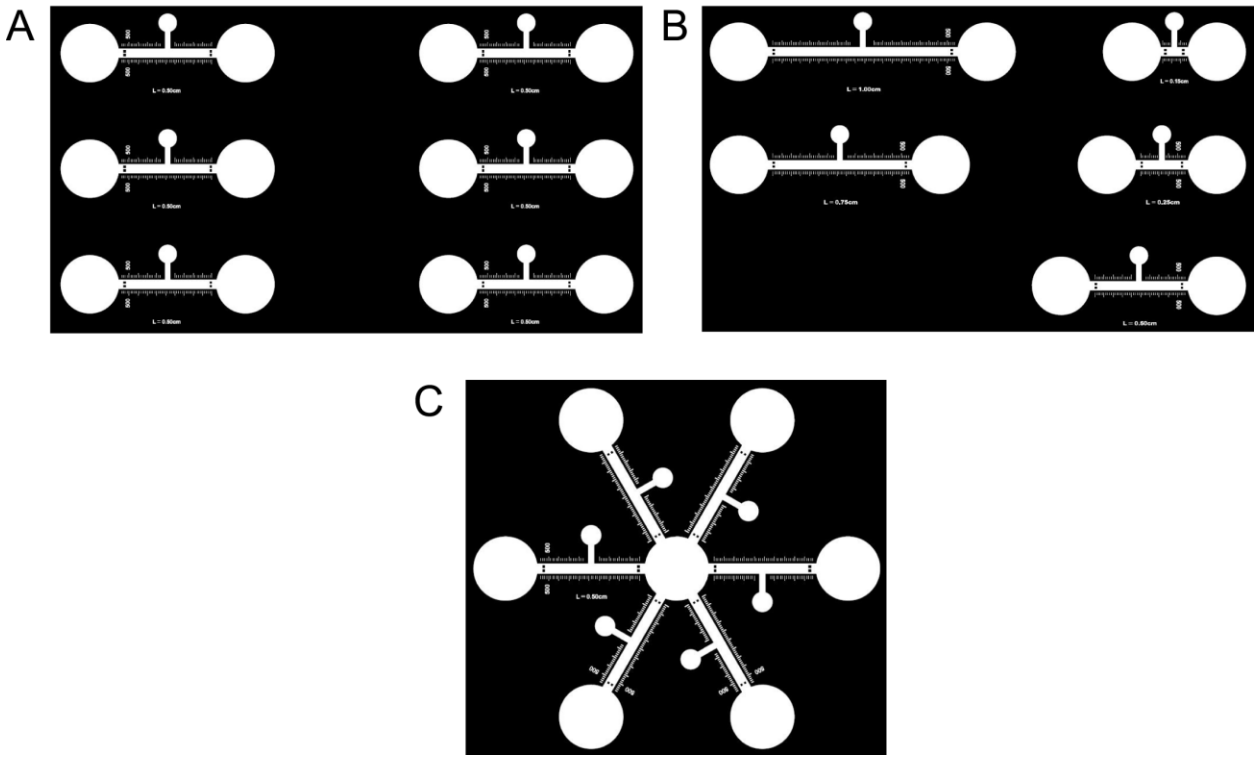

Figure 3.1. Mask designs of microfluidic migration devices. (A) Device 1 contained six identical channels of the same length. (B) Device 2 containing channels with varying lengths. (C) Device 3 containing 6 connected channel of the same length.

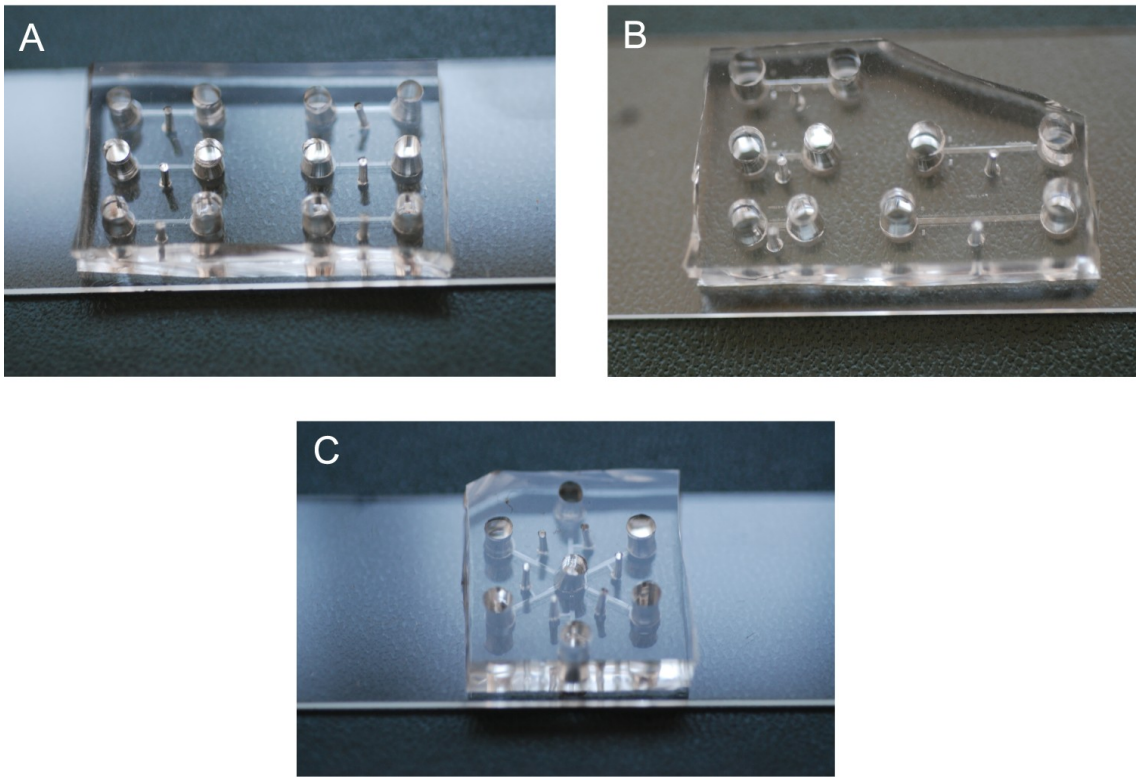

Figure 3.2. Fabricated microfluidic devices after plasma bonding. (A) Device 1 had channels of the same length (1cm), (B) Device 2 had channels with varying lengths (0.15, 0.25, 0.5, 0.75, 1cm), and (C) Device 3 had connected channels of the same length (1cm).

Growth Factor Diffusion Profile and Agarose Contractility Test.

Device characterization was conducted using the device with six identical channels (**Figure 3.1A**). To determine if this microfluidic assay system would be amenable to testing a variety of cytokines, fluorescein conjugated dextrans with molecular weights (3kDa, 10kDa and 70kDa) were infused in the inlets of the channels to generate a concentration gradient and PBS was placed in the channel outlets. The channels were filled with 0.5% agarose (Invitrogen, Carlsbad, CA) mixed with Fluoresbrite® rhodamine carboxylate microspheres with a diameter of 6 μm (Polysciences, Warrington, PA) to determine if the agarose underwent any significant contraction over 12 hours. Time-lapse microscopy captured images every 10 minutes for the

calculation of microsphere position displacement and cytokine diffusion profiles. The fluorescent intensity profiles throughout the channel were determined using ImageJ software.

Isolation of Primary Human MSCs.

Human bone marrow MSCs were isolated from fresh adult donor samples (AllCells, Emeryville, CA) using our prior methods [94, 96, 115]. Briefly, the bone marrow sample was incubated with the RosetteSep® Human Mesenchymal Stem Cell Enrichment Cocktail (Stem Cell Technologies, Vancouver, Canada), placed on top of the Ficoll-Paque™ and centrifuged to separate the layers by density. Mononucleated cells were collected from the Ficoll-Paque™ interface, washed with PBS containing 2% FBS and 1 mM EDTA, and then plated. Mononucleated and adherent cells were cultured in Dulbecco's Modified Eagle Medium (DMEM, Gibco, Carlsbad, CA), 10% FBS (Gibco, Carlsbad, CA) and 5% Antibiotics/Antimicrotics, and only expanded to the second passage for all experiments. These mononucleated and adherent cells are consistent with typical culture of MSCs in the literature [96, 116], although their heterogeneity is recognized by several studies including our recent clonal analysis [112].

Determining Optimal Coating for Cell Attachment to Glass.

To determine the optimal coating to promote MSC attachment to uncoated glass slides, various coatings were tested including fibronectin (Sigma, St Louis, MO), type I collagen (BD Bioscience, Franklin Lakes, NJ), poly-L-lysine (Sigma, St Louis, MO) and 10% FBS (Gibco, Carlsbad, CA). Two types of chamber slides with glass bottoms were also tested for their cell attachment potential including Lab Tek II Chamber Slides (Fisher, Pittsburgh, PA) and Lab Tek II CC2 treated chamber slides (Fisher, Pittsburgh, PA). Uncoated glass slides were used as a negative control and standard cell culture treated plates were used as a positive control. A

PDMS gasket was fabricated and adhered with suction to glass slides to form a small chamber to test all coatings other than the chamber slides and cell culture treated plate (**Figure 3.3**).

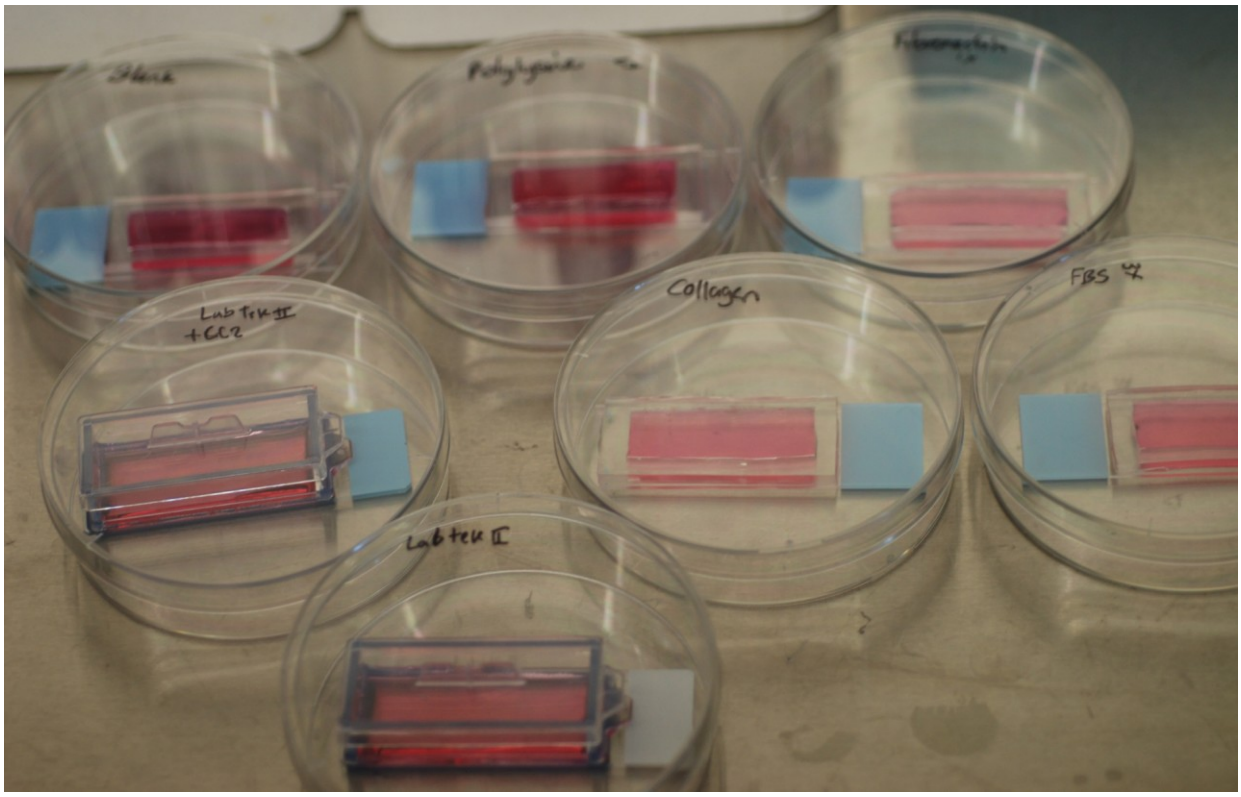

Figure 3.3. Experimental setup to determine optimal glass coating for cell adhesion.

Negative control slides were washed with ethanol for 10 minutes for sterilization, washed with PBS and then seeded with cells. Chamber slides and positive control cell culture plates were seeded directly with cells. All other conditions were washed with ethanol for 10 minutes, washed with PBS, protein coated, rinsed with PBS and then seeded with cells. Type I collagen was made by diluting the stock solution 1:10 with 30% ethanol, spread over the glass, and allowed to air dry. Poly-L-lysine was made into a 0.1% solution, pooled over the glass slide, incubated for 2 hours at room temperature and aspirated. Fibronectin solution was made by diluting 50µg in PBS, pooled over the glass slide, incubated for 45 minutes and aspirated. FBS was coated by

applying a 10% solution to the glass slide followed by one hour incubation. Fourth passage MSCs were seeded at a concentration of 40,000 cells/slide, cultured in DMEM + 1% Ab/AM (serum-free) and imaged after 2, 4.5 and 24 hours.

Cell Seeding for Migration Experiments.

A microfluidic device with channels of uniform length was sterilized for 10 minutes by flowing 70% ethanol through all the channels. The device was washed once with PBS, followed by fibronectin coating (75μg/mL) for 2 hours at 37°C, and then washed with PBS twice. Sterile 1% agarose was diluted 1:2 with cell culture medium and injected into the center inlet. After the gel solidified, any excess agarose in the channel outlets was aspirated. Next, 40,000 third passage human bone marrow derived mesenchymal stem cells (MSCs) were seeded in one of the side wells of each channel and 200ng SDF1β was added to the opposing side wells. The device was kept at 37°C and 5% CO_2 and imaged every 15 minutes for 12 hours using time-lapse microscopy. Individual cell locomotion patterns were observed.

Serum-Free Migration Experiment.

Devices were characterized to promote optimal cell culture conditions for uniform cell attachment and maximal cell migration numbers. Competition migration devices were seeded with 40,000 third passage MSCs and the peripheral wells were loaded with 200ng of SDF1β, TGFβ1, TGFβ3, PDGFBB and IGF1 with PBS as a control. After cell seeding in the device, serum-free cell culture media was used during the migration assay, consisting of DMEM + 5% AB/AM. Devices were fixed with 10% formalin after 24 hours and imaged for quantification of cell migration number and distance. An identical experiment was performed using serum-supplemented medium and the results were compared.

Blood-Derived Biologics for MSC Migration.

To test the range of chemotactic factors and cell types that would be amenable for use in the microfluidic migration devices, a separate experiment was conducted with equine derived cells and biologics, in collaboration with the Cornell University School of Veterinary Medicine. Background material on equine derived biologics can be found in Appendix 1. MSCs were isolated from the sternum of three donor race horses and combined for culture in DMEM media containing 2mM L-glutamine, penicillin (100 units/mL), streptomycin (100 units/mL), basic fibroblastic growth factor (bFGF, 1 ng/mL) and 10% fetal bovine serum. Biologic factors were derived from equine blood and bone marrow sources and consisted of: bone marrow aspirate (BMA), bone marrow aspirate concentrate (BMAC), platelet rich plasma isolated using Arthrex method (Prp-A), platelet rich plasma isolated using Harvest method (Prp-H) and cryoprecipitated fibrinogen (FIB).

To obtain BMA and BMAC, horses were sedated and the sternum was aseptically prepared and infiltrated with local anesthetic. Bone marrow was aspirated from two sternal marrow spaces (35 mL each) into syringes containing heparin to create a final concentration of 15U heparin/mL of BMA. The two syringes were mixed together to obtain one homogenous sample of BMA and an aliquot was removed for use as BMA in the migration assays and for cytological analyses. BMAC (60 mL) was placed into a bone marrow aspirate concentrate disposable container (BMAC® Harvest Technologies, Plymouth, MA) and processed in a SmartPReP2® centrifuge (Harvest Technologies, Plymouth, MA) for removal of the bottom cell layer and buffy coat to yield 6 mL of BMC.

Both Prp solutions were isolated from peripheral blood samples. However, the difference in isolation methods between Prp-A and Prp-H yielded a lower ratio of platelets to leukocytes for Prp-A (800:1) compared to Prp-H (40:1). These two disparate types of PRP were generated by

simple centrifugation of venous blood using commercially available centrifuge containers, Arthrex and Biomet.

FIB was generated by separating the plasma layer from a whole blood sample, freeze-thawing followed by centrifugation and isolating the concentrated plasma pellet. The center chamber of the device was seeded with 40,000 fifth passage equine MSCs and 40µL of each biological factor was placed in the peripheral wells. After 24 hours of migration, devices were fixed with 10% formalin, stained with DAPI (Vectorshield, Burlingame, CA) and imaged for quantification of cell migration number and distance.

Cell Polarization Investigation by Cytoskeleton Staining.

A separate investigation was conducted to confirm that cells are both polarizing and aligning their cytoskeleton in the direction of increasing cytokine concentration. The competition migration device was used to observe the effect of increasing concentrations of 5 different cytokines on MSC cytoskeleton alignment and polarization. The center chamber of the device was seeded with 40,000 third passage MSCs and the peripheral wells were injected with 200ng of MIP1α, PDGF, Lymphotactin, TNFα, TGFβ3 or PBS as a control. Cells were allowed to migrate for 24 hours, followed by fixation with 10% formalin and cytoskeleton was stained using Alexa Fluor® 488 Phalloidin (Invitrogen, Carlsbad, CA). Briefly, formalin fixed cells were washed twice with PBS followed by cell membrane permeabilization with 0.1% Triton X-100 in PBS, two PBS washes, 20 minute phalloidin staining, and nucei counterstaining with DAPI (Vectorshield, Burlingame, CA).

Additionally, the effect of increasing distance between the cell source and the cytokine source on cytoskeleton alignment was examined. The microfluidic assay device containing 5

varying length channels was used to test the chemotactic effects of 200ng PDGFBB on 40,000 third passage MSCs seeded in the device. Cells were allowed to migrate for 24 hours, followed by fixation with 10% formalin and cytoskeleton staining using Alexa Fluor® 488 Phalloidin (Invitrogen, Carlsbad, CA) with DAPI (Vectorshield, Burlingame, CA) nuclear counterstaining, using the methods described above.

3.3 Results

Fibronectin Coating Promotes Optimal Cell Attachment.

To determine the optimal coating for a glass substrate, MSCs were seeded on various protein coatings and phase microscopy images were taken after 2, 4.5 and 24 hours. Cells attached the fastest to the poly-L-lysine coated glass (**Figure 3.4D**). FBS promoted significant cell clumping after 2 hours (**Figure 3.4G**). Remarkably, after 4 hours the cells were able to spread out, but not all cells were attached (**Figure 3.4G**). Cells cultured on the Lab Tek II and Lab Tek II CC2 substrates appeared rounded and small in size, indicating that the cells were not able to fully attach to the substrate and spread out (**Figure 3.4E & F**). After 24 hours, MSCs were able to attach on all substrates. However, there were fewer morphological changes when MSCs were plated on fibronectin and poly-L-lysine coated plates (**Figure 3.4B & D**) compared to standard tissue culture plates (**Figure 3.4H**). Thus, fibronectin was selected as the coating for use in all subsequent microfluidic experiments.

Verification of Diffusion Gradient and Minimum Agarose Contractility.

The device was rigorously characterized by determining diffusion profiles and agarose contractility to ensure reproducibility between experiments. To determine whether a cytokine

gradient was formed, we first studied the diffusion profiles of various fluorescein conjugated dextrans in agarose filled channels (**Figure 3.5B-D**). Dextrans with molecular weights of 3, 10 and 70 kDa were selected to represent the range of molecular weights of the cytokines analyzed in this present work. A gradient of decreasing fluorescence intensity was observed in the agarose over time (**Figure 3.5D**) indicating the suitability of agarose as a means of forming a cytokine gradient. Despite similar diffusion patterns, dextrans with small molecular weights diffused more rapidly than those with larger molecular weights (**Figure 3.5E**). The agarose was mixed with rhodamine carboxylate microspheres to determine agarose contractility, if any, by analysis of position displacement over time. Up to the observed 12 hrs, agarose underwent minimal contraction, as evidenced by the minimal standard deviations both along the X and Y directions (**Figure 3.5F**). In the horizontal direction, the average standard deviation between two carboxylate beads at different time points was 0.175 (**Figure 3.5F**). In the vertical direction, the average standard deviation between two carboxylate beads at different time points was 0.338 (**Figure 3.5F**). Thus, the microfluidic agarose assay can be used without significant contraction and promotes relatively uniform diffusion parameters.

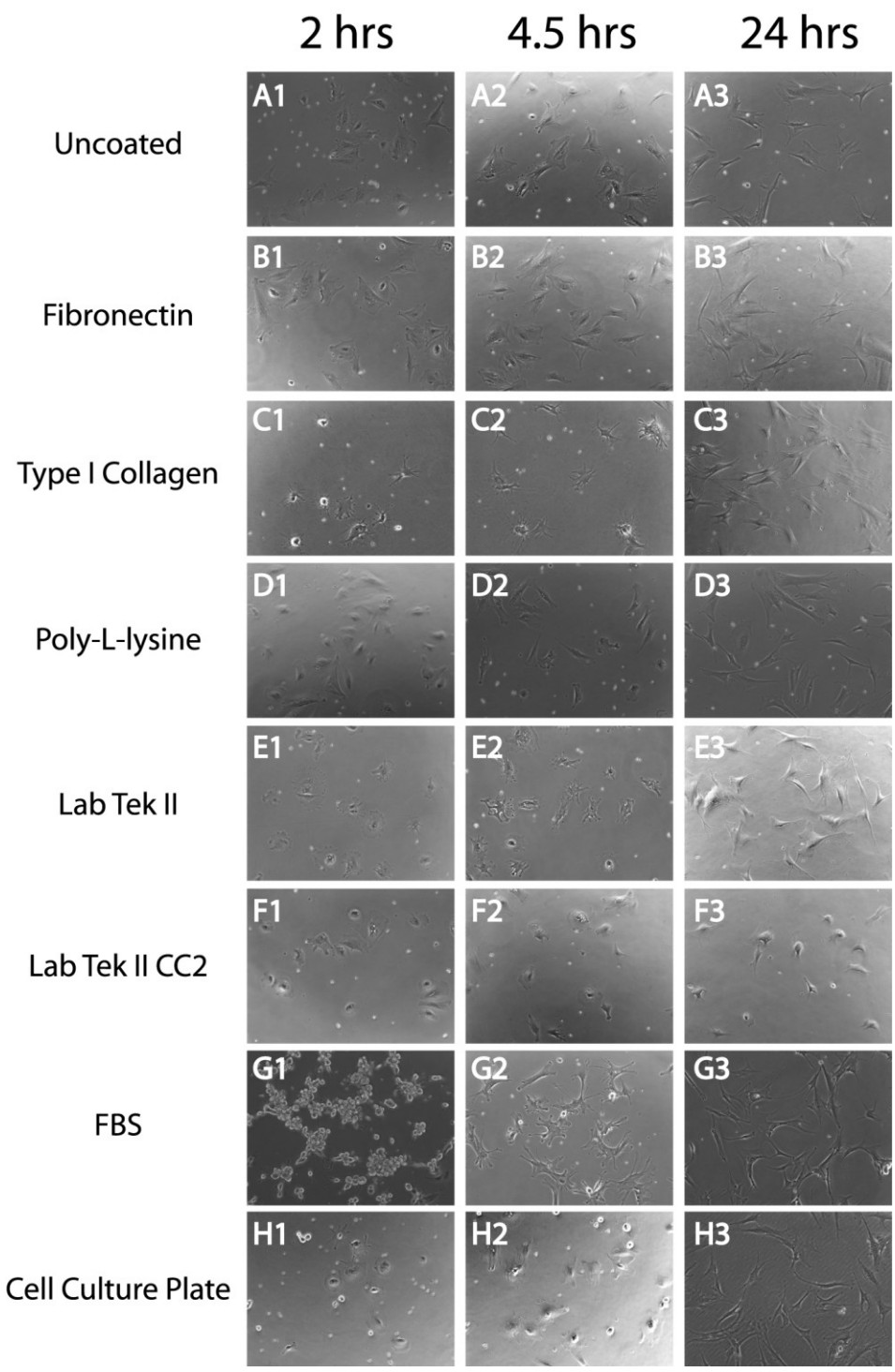

Figure 3.4. MSC morphology on various coatings for glass substrates. (A) No Coating, (B) Fibronectin, (C) Type I collagen, (D) Poly-L-Lysine, (E) Lab Tek II, (F) Lab Tek II CC2, (G) FBS, (H) Polystyrene cell culture plate. Scale = 200μm.

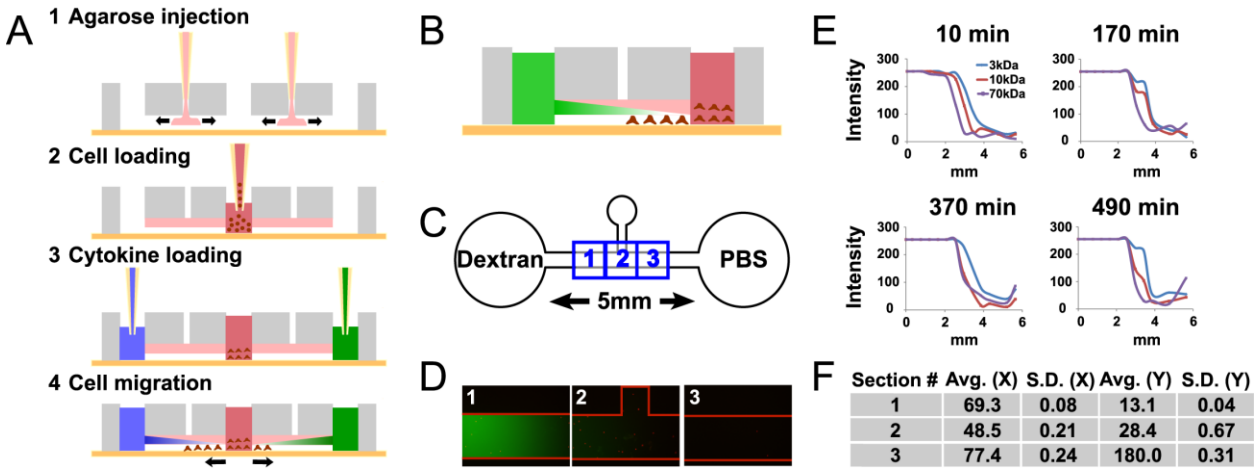

Figure 3.5. Experimental schematics and device characterization. (A) Schematics of agarose loading and cell seeding. 1. Agarose is injected into the chamber and allowed to flow and fill the entire microchannel. 2. Cells are seeded into the center chamber. 3. Cytotactic cues are loaded into the peripheral wells. 4. A gradient of cytotactic cues is established over time to form a descending concentration towards the center chamber. (B) Channels were filled with agarose and fluorescently tagged microspheres. The peripheral wells were infused with fluorescently tagged dextrans of varying molecular weights. (C) Three consecutive regions centered in the channel, each with a length of 600 μm, were selected to measure agarose contractility. (D) A gradient of fluorescence intensity (10 kDa) was formed throughout the three regions within the observed 70 min. (E) Diffusion profiles of fluorescently tagged dextrans (3, 10, and 70 kDa) after 10, 170, 370 and 490 min. (F) The modest standard deviations (S.D.) of the average (avg) microsphere position displacement in each of the three regions indicate minimal agarose contraction over the observed 490 min.

SDF1β Promotes ASC Migration Within 2 hours of Cytokine Exposure.

Using the microfluidic under agarose assay platform with fixed channel lengths, ASCs were exposed to 400ng of SDF1β for 12 hours. Cells were able to evenly attach and spread out, demonstrating that fibronectin is a suitable substrate coating for the migration device. Using time-lapse microscopy, MSCs could be seen migrating under the agarose gel towards the increasing cytokine concentration over 6 hours (**Figure 3.6**). Interestingly, cells could be seen polarizing with their leading edge towards the direction of increasing cytokine concentration (**Figure 3.6B**). The results from this pilot study served as an initial proof-of-principle to demonstrate the functionality of the microfluidic assay platform for studying cell migration.

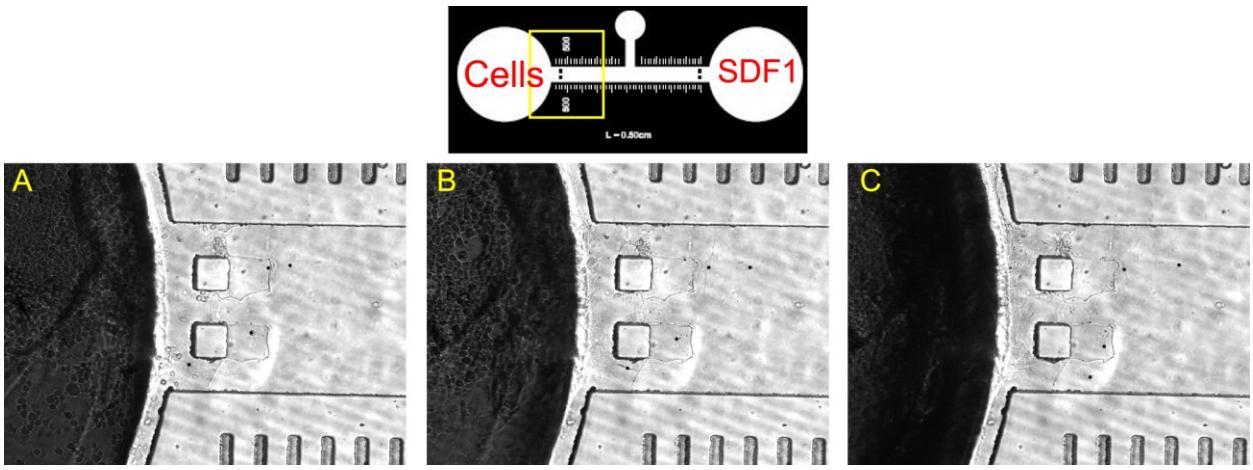

Figure 3.6. ASC migration toward a gradient of 400ng SDF1β. Time lapse images were taken after (A) 2 hours, (B) 4 hours and (C) 6 hours of cytokine exposure. Cells were marked with a black dot to enhance visualization.

MSCs Polarize and Align in the Direction of Increasing Cytokine Concentration.

When cells migrate on a substrate, they undergo classic physiologic changes affecting the organization of their cytoskeleton and cell morphology. After exposure to high cytokine concentrations, cells begin to reorganize their cytoskeleton to align in the direction of increasing cytokine concentration. Adhesive complexes form along the cell body providing points of traction for cell movement and at the leading edge of the cell, causing the plasma membrane to protrude. When adhesive complexes located at the rear end of the cell are released, a net displacement of the cell occurs. To investigate if our devices promote physiological cell migration with classic morphology changes, cell cytoskeleton arrangement was investigated.

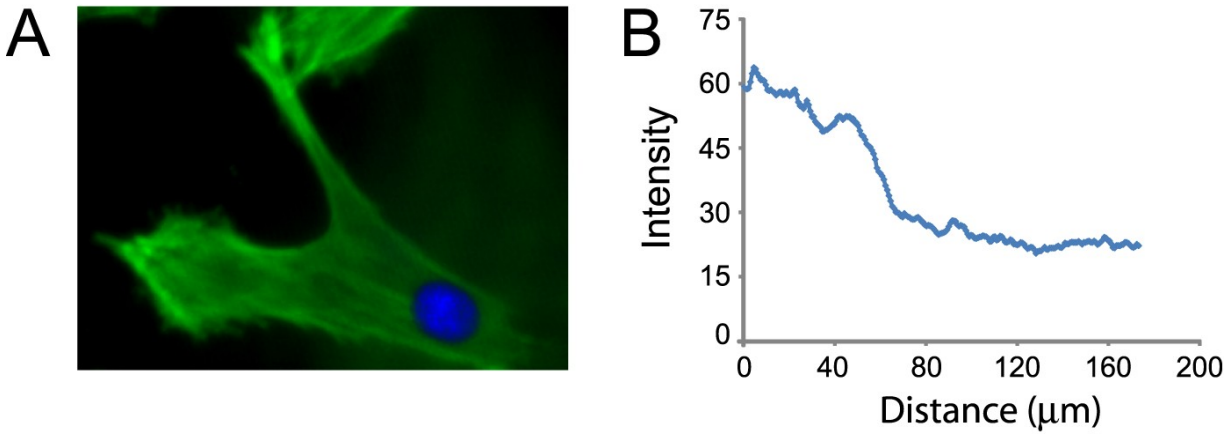

Figure 3.7. MSC polarization and cytoskeleton rearrangement in the direction of increasing PDGFBB concentration. (A) Cytoskeleton staining with Alexa Fluor® 488 Phalloidin indicated cell alignment in the direction of PDGFBB with increased fluorescent intensity at the leading edges of the cell. (B) Fluorescent intensity profile from the leading edge to the nucleus indicating an increasing level of fluorescence towards the leading edge, confirming the presence of focal complexes at the leading edge. Thus, the microfluidic migration devices are able to promote physiologic cell morphology and cytoskeleton arrangement during migration.

Cytoskeleton staining with Alexa Fluor® 488 Phalloidin revealed that the cells were able to polarize and orient their leading edge in the direction of increasing PDGFBB concentration (**Figure 3.7**). Adhesive complexes containing densely arranged integrin receptors, actin filaments, and proteins were present at the leading edge of the cell as indicated by an increase in fluorescent staining intensity (**Figure 3.7A**). To confirm this observation, a fluorescent intensity profile generated from the cell nucleus to the leading edge of the cell indicated a gradient of increasing fluorescence intensity (**Figure 3.7A**). Increasing the distance between the cell source and the PDGFBB source did not promote any noticeable difference in cell alignment or cytoskeleton arrangement (**Figure 3.8**). However, cells could be seen polarizing in the direction of increasing PDGFBB concentration during migration in channels of all lengths (**Figure 3.8**). The ability for cells to polarize in the direction of increasing cytokine concentration was confirmed for additional cytokines including Lymphotactin, MIP1α, TGFβ3 and TNFα (**Figure 3.9**).

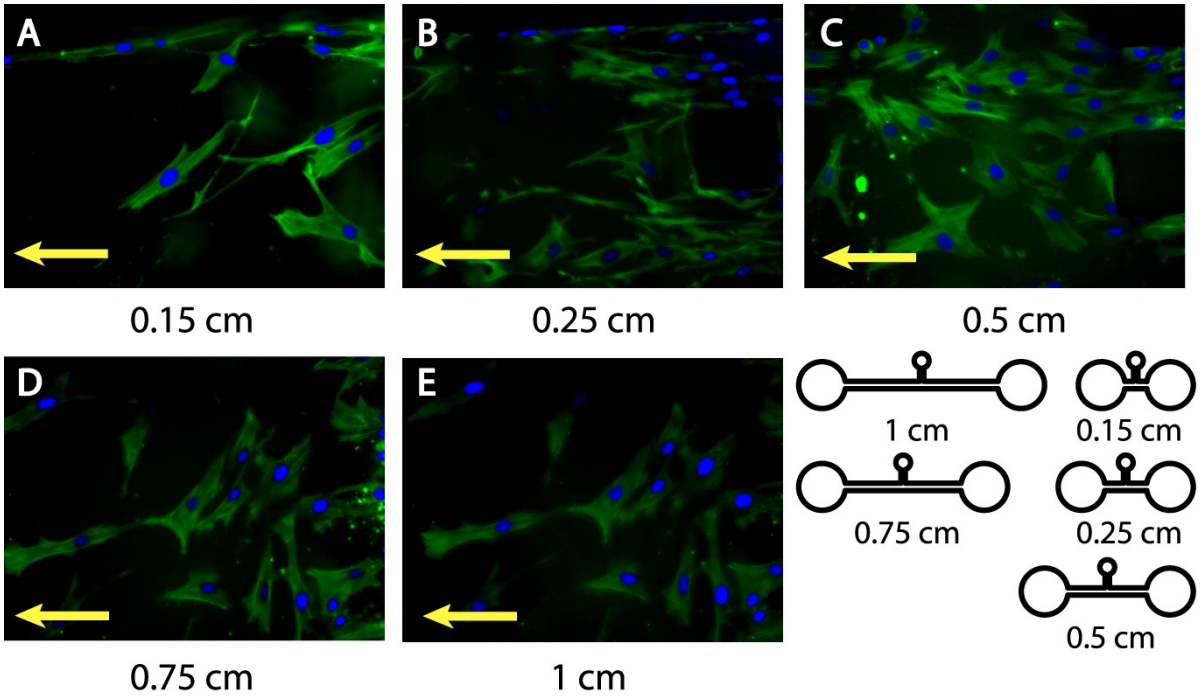

Figure 3.8. Effect of MSC alignment on channels with varying distances between the cell source and the PDGFBB source. MSC cytoskeleton staining was conducted to reveal changes in cell alignment during migration due to channel lengths of (A) 0.15cm, (B) 0.25cm, (C) 0.5cm, (D) 0.75cm and (E) 1cm. No visible difference in cell alignment could be seen due to variation in channel length but cell polarization was present in every channel. Yellow arrows indicate the direction of increasing cytokine concentration.

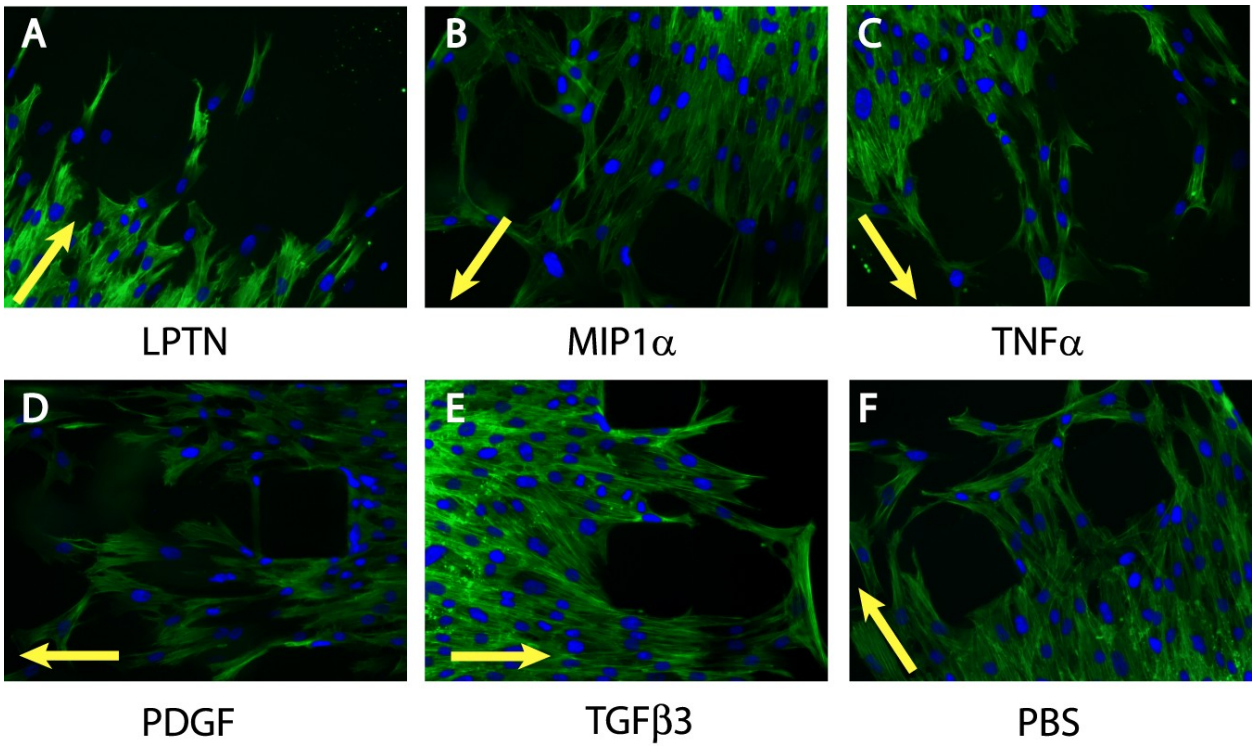

Figure 3.9. Effect of MSC alignment in response to various cytokine signals. Cytoskeleton staining was conducted in MSCs after 24 hours of migration in response to (A) Lymphotactin (LPTN), (B) MIP1α, (C) TNFα, (D) PDGFBB, (E) TGFβ3 and (F) PBS. Yellow arrows indicate the direction of increasing cytokine concentration. Cytoskeleton staining indicates a general alignment and cell polarization towards the direction of increasing cytokine concentration.

Microfluidic Migration Assay is Effective Across Species.

To test if the microfluidic migration devices could be used with cell types or biologic factors from various species, a set of experiments was conducted using competition devices with equine MSCs and biologics. After 24 hours of migration, MSCs could be seen migrating in all device channels to varying degrees (**Figure 3.10**). Quantified cell migration numbers revealed that Prp-H, BMA and FIB induced a general trend of increased migration compared to the PBS control. BMAC showed minimal chemotactic effects on MSCs. However, because there

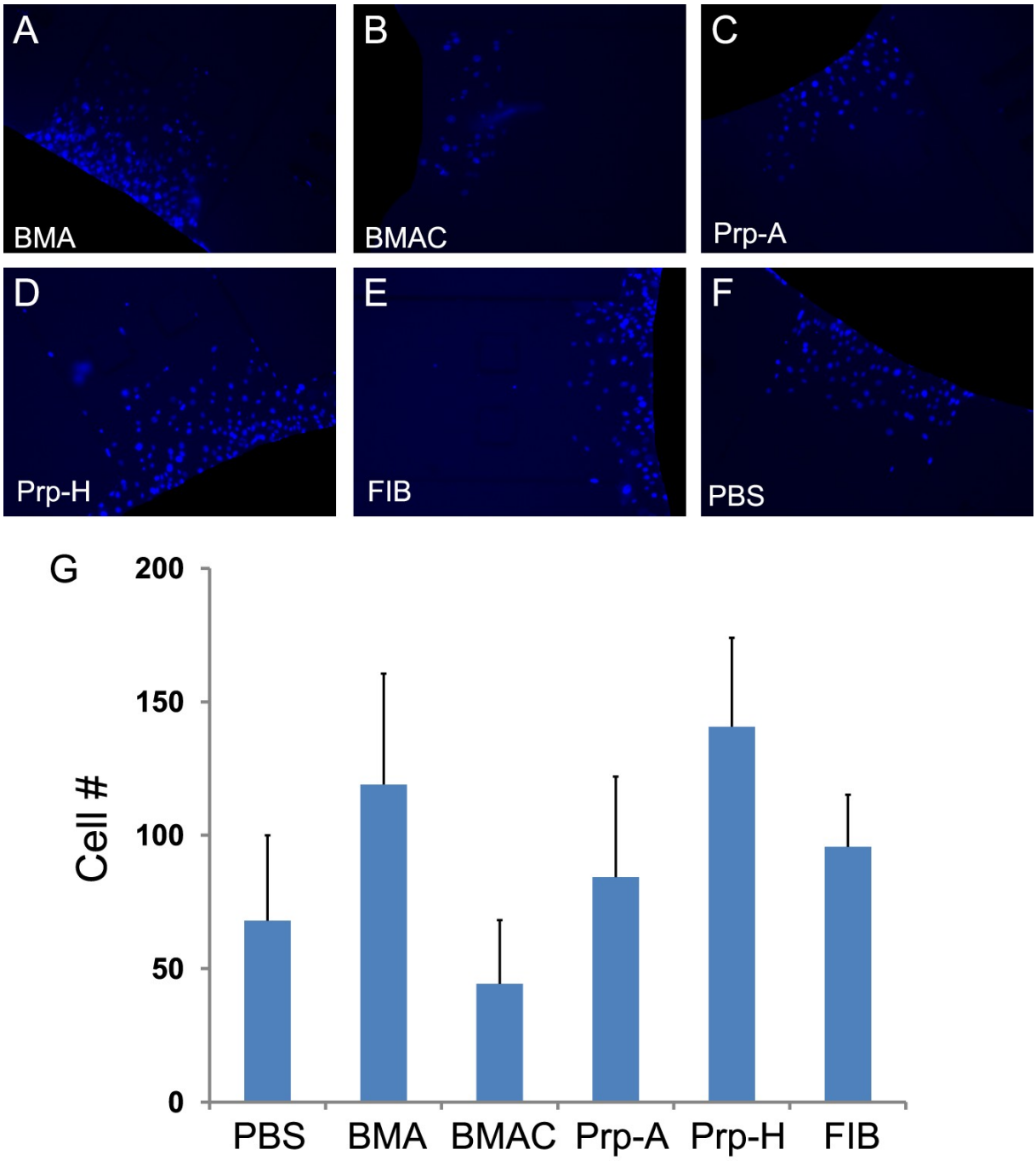

Figure 3.10. Equine MSC migration in response to equine biologics derived from bone marrow and whole blood sources. After 24 hours of migration, DAPI stained MSCs could be seen migrating in the device channels in response to, (A) BMA, (B) BMAC, (C) Prp-A, (D) Prp-H, (E) FIB and (F) PBS (Control). (G) DAPI stained images were quantified to reveal the total number of migrated cells in response to each biologic factor.

was a large variation amongst samples, these values were not statistically significant. A possible reason for large variation between experiments was because bone marrow aspirate and Prp-H were not homogeneous solutions and led to sedimentation over the course of the experiment. Although each outlet in the device received 40μL of solution, because of the solution heterogeneity, it is possible that some devices received more chemotactic constituents than others. Future improvements to obtain a more homogenous solution could include filtration or centrifugation for testing of only the supernatant.

Serum-Free Medium Yields Insufficient Cell Migration Numbers.

To determine the optimal conditions for promoting maximum cell migration numbers and distances, a comparison between serum-supplemented medium and serum-free medium was conducted. MSCs were seeded in microfluidic devices with serum-supplemented or serum-free medium and exposed to gradients of IGF1, SDF1β, TGFβ3, TGFβ1, PDGFBB or PBS as a control. Quantification of cell migration numbers revealed that serum-free medium inhibited cell migration by over 50% compared to serum-supplemented medium (**Figure 3.11A,C**). Cell migration distance values in the presence of serum-free culture were also substantially decreased (**Figure 3.11B,D**). Since serum-supplemented medium was found to be critical for enhancing cell migration behavior, serum-supplemented medium was used in all subsequent experiments.

The use of serum-supplemented medium for culture during migration assays poses some concerns. Serum naturally contains various cytokines that might be chemotactic such as IL1β and IL6. In a sample of DMEM containing 10% FBS, concentrations of IL1β and IL6 were found to be 10ng/mL and 12.5ng/mL respectively [117]. To run one migration assay using our

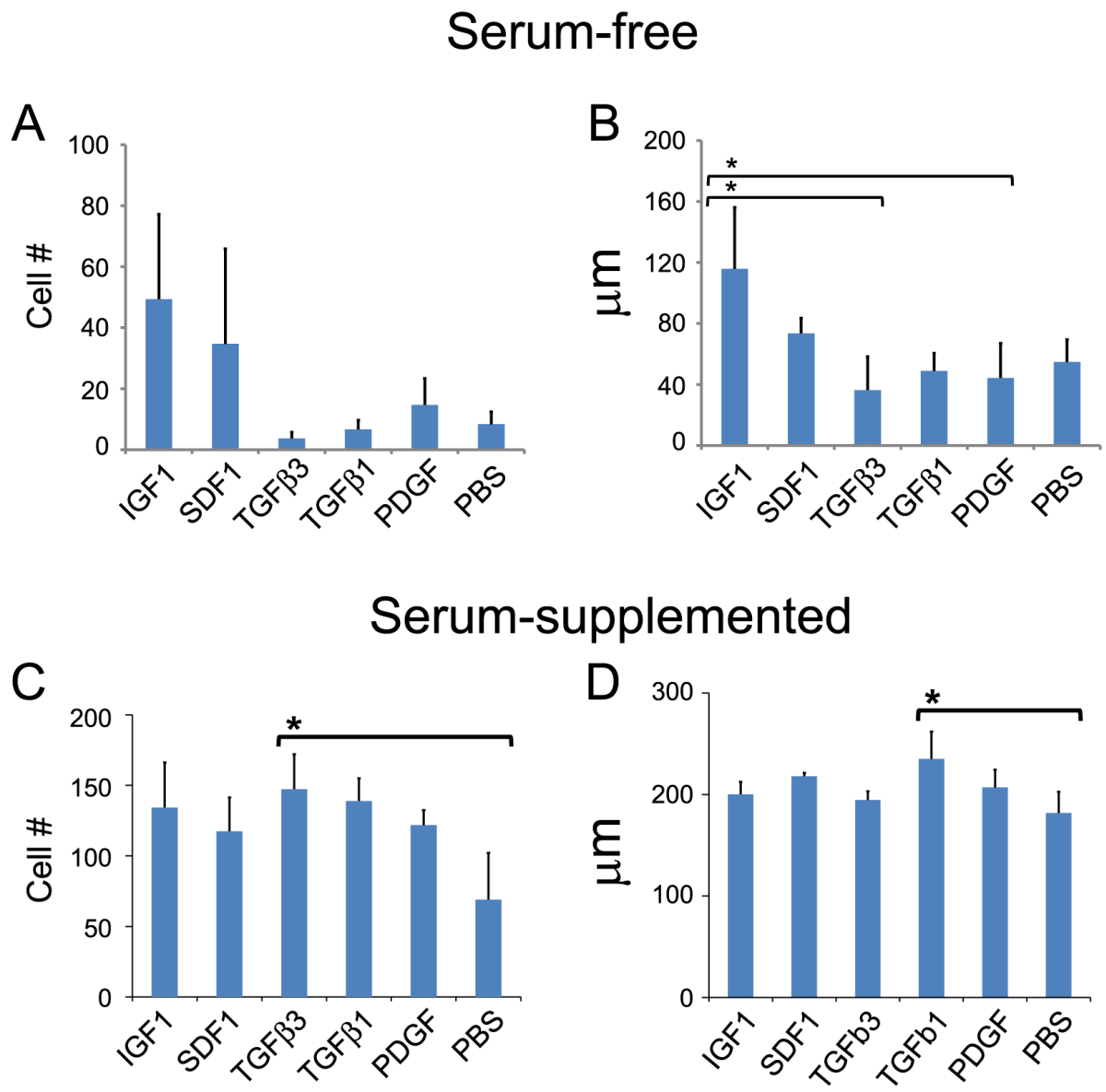

Figure 3.11. Serum Free MSC Migration in response to various chemotactic cues. To characterize the optimal conditions for promoting cell migration, MSCs were allowed to migrate in response to IGF1, SDF1β, TGFβ3, TGFβ1, PDGF and PBS (control) in the presence of serum-free or serum-supplemented medium. Cell migration number (A,C) and migration distance (B,D) were quantified. *: significant difference over other factors ($p<0.05$).

system requires 40μL of media containing 10% FBS, which would correlate to a concentration of 0.4ng IL1β or 0.5ng IL6. For each migration assay, 200ng of cytokine was injected in the device,

which is significantly higher than the medium cytokine concentrations. Although the low levels of serum are not expected to induce any major chemotactic effects, any effect observed due to the serum-supplemented medium would be uniform for each tested cytokine. Therefore, the chemotactic effect observed for each tested cytokine can be distinguished by a net increase in the overall enhanced effect of the serum-supplemented culture. An additional concern lies in the potential inconsistency in serum properties between donors and thus, using serum-supplemented medium for experiments poses a risk for increased variation between experiments. To minimize the variation, an effort was made to use serum from similar lot numbers between experiments.

Shorter Channel Distances Yield More Potent Cell Migration.

An important consideration in developing novel strategies for tissue regeneration by cell homing is effective distances at promoting cell migration between a cell population and a bioactive scaffold. Thus, to investigate how distance from a cytokine source affects cell migration behavior, a microfluidic assay device was designed with varying channel lengths between the cell source and the cytokine source, ranging from 0.15cm to 1cm. MSCs were seeded in this device and 200ng of PDGFBB was placed in each opposing channel end. After 24 hours of migration, quantification of migration numbers and migration distances revealed a general trend of increasing migration with decreasing channel lengths **(Figure 3.12)**. A channel length of 0.15cm promoted a significantly greater cell migration number due to PDGFBB exposure compared to the PBS control. Additionally, the same channel length (0.15cm) promoted a significantly greater cell migration number among cells exposed to PDGF than all other channel

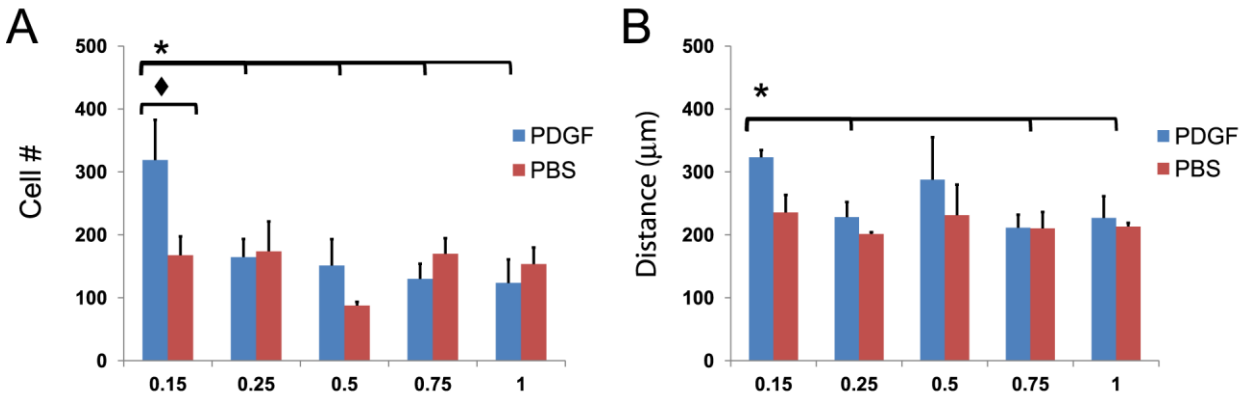

Figure 3.12. Effect of MSC migration in channels with varying distances between the cell source and the PDGFBB source. After 24 hours of migration, DAPI stained devices were quantified to yield (A) cell migration numbers and (B) cell migration distances. A channel length of 0.15cm promoted a significantly greater cell migration number compared to the PBS control for this channel length (♦ $p<0.05$). Additionally, a channel length of 0.15cm promoted a significantly greater cell migration number than MSCs migrating in response to PDGFBB in all other channel lengths and significantly greater migration distance than MSCs migrating in response to PDGFBB in channels 0.25, 0.75 and 1cm long (∗ $p<0.05$).

lengths. Migration distances followed a similar trend, yielding significantly higher distances due to a channel length of 0.15cm among cells exposed to PDGFBB compared to channel lengths of 0.25cm, 0.75cm and 1cm. Because the cytokine concentration was constant between channels, by decreasing the channel length, the cells were able to more quickly experience a higher cytokine concentration. Therefore, testing the effect of channel length on cell migration is synonymous to testing the effects of increasing cytokine concentrations on cell motility. Since shorter lengths between the PDGF source and the MSC source were more effective at promoting greater migration numbers and distances, this implies that higher PDGFBB concentrations are more effective at promoting cell migration.

3.4 Discussion

The microfluidic under agarose assay proved to be an effective method for testing cell migration. An initial device characterization revealed that a cytokine gradient could be generated across the agarose filled channels within minutes after introducing the cytokine into the device. Dextrans of varying sized molecular weights were able to diffuse through the agarose, demonstrating the potential to use this device for testing a wide range of cytokines. The device was able to maintain uniform parameters over the course of the migration experiment as evidenced by the minimum agarose contraction. Serum-supplemented medium during the migration assay was found to be critical for promoting sufficient cell migration numbers and distances. An investigation into optimal glass coatings for cell attachment revealed fibronectin coating to be the most effective at promoting MSC attachment while preserving the native cell morphology.

A unique feature of this microfluidic migration device is the ability to monitor motility over time with time-lapse microscopy. Images captured after 2, 4 and 6 hours displayed individual ASCs as they migrated towards an increasing concentration of SDF1β, which is not possible to observe using migration systems such as the Boyden Chamber. Cytoskeleton staining of migrated cells confirmed that the cells in the device were polarizing and orienting themselves towards an increasing cytokine concentration. The microfluidic under-agarose device was amenable to migration assays with multiple cell types including human MSCs, human ASCs and equine MSCs. In addition to investigating the chemotactic effects of cytokines, biologic factors derived from whole blood and bone marrow sources could also be successfully assayed for their chemotactic effects using this system.

Microfluidic platforms have a number of advantages over existing migration assays including low cost, reproducibility and minimal volumes of reagents required for use.

Additionally, multiple migration assays could be conducted concurrently on the same device, thus ensuring the environmental factors remained consistent between experiments. Despite the vast benefits provided by such a system, a limited number of cells can access the channel entrance at a given time because of the small size of the channels. On the other hand, in a Boyden assay, the entire cell population is seeded on top of the porous membrane so the total number of cells on the bottom of the membrane represents the total number of migrated cells. Thus, in the microfluidic assay, a smaller percentage out of the total population of cells can be monitored at a given time for migration. Furthermore, since only cells migrating within the channel are quantified and not those migrating within the cell chamber, the total number of migrated cells in the channel is not necessarily an indication of the total percentage of migrated cells.

By utilizing the microfluidic device with varying channel lengths in combination with fixed cytokine and agarose concentrations, we were able to investigate the effect of varying the distance between the cell and cytokine source on cell migration. Shorter distances were shown to be more effective at inducing MSC migration in response to PDGFBB. This in turn could also indicate that a higher PDGFBB concentration is more effective at promoting cell migration because shorter channel distances allow the cell source to experience higher cytokine concentrations sooner. The results from this experiment could be useful in identifying the ideal distance to place a bioactive scaffold from a native cell source *in vivo* to induce cell migration.

This novel device offers a rare opportunity for screening of cell homing efficacy, potentially applicable to any stem cell population including embryonic, iPS, skeletal, muscular, neural, cardiac and adipose. A number of basic biological questions regarding cell migration can be addressed by studies using such a device such as cell motility and migratory distances. Determining which combinations of cytokines are the most effective at maximizing cell homing

may offer novel approaches for tissue regeneration without the need for cell delivery, which will be further examined in Chapter 5. Besides tissue regeneration, this device can also be used to identify ways to prevent cancer cell aggregation and spread, wound healing, drug development and studies of native development. Future directions include modifying the design features of the device to incorporate a larger number of channels on an individual device, thus making it feasible to conduct a test of multiple cytokines concurrently.

Chapter 4: An Investigation of the Homing Behavior of Stem/Progenitor Cells Due to Competing Cytokine Signals.

4.1 Introduction

Cells are constantly exposed to multiple cytotactic cues, concurrently or in purposeful sequences, during fundamental biological processes such as development, wound healing or cancer metastasis. Closely regulated signals are necessary for the maintenance of stem cell quiescence and immune balance in postnatal homeostasis [118]. In either trauma or cancer metastasis, locally present or systemically circulating endogenous cells migrate to and from the tissues of interest [28, 119]. Cancer cells secrete a large number of cytokines and chemokines that invite the sprouting of blood and lymphatic vessels in ways that benefit metastasis. A synovial joint in a patient with rheumatoid arthritis is filled with various inflammatory cytokines, which could conceivably be harnessed for tissue regeneration [120]. Interventional therapies for tissue regeneration rely on transplanted cells and/or host endogenous cells that, when aggregated, begin to reorganize and regenerate tissues. However, our understanding of cell motility, one of the most fundamental processes in cell biology, remains fragmented. Proteins, peptides, and chemical compounds that regulate cell motility may act as targets for a broad range of therapeutic purposes [121]. Whereas cell therapy has long been practiced in blood transfusion and bone marrow transplantation, recent interest has focused on the delivery of stem cells in numerous disease models involving virtually all tissues and organs [119]. Mesenchymal stem cells (MSCs) are the most widely delivered adult, non-hematopoietic cells in a broad range of preclinical and patient studies. In several disease and trauma models, MSC delivery shows various efficacy that remains to be further evaluated [116, 122-124]. However, the putative therapeutic potential of MSCs, which is still superficially understood for the majority of tissues and organs, is frequently attributed to the effects of MSCs on immune modulation,

chemotaxis, and regulation of inflammation and angiogenesis, rather than necessarily serving as replacement cells for tissue repair [122-125]. Recently, we showed that host endogenous cells were recruited by TGFβ3 into microchanneled biomaterial scaffolds and led to the regeneration of the entire cartilage layer of a synovial joint *in vivo* [85]. However, the roles played by TGFβ3 could potentially be enhanced by other factors [85]. Cytotactic cues that are most efficacious in the regeneration of a given tissue are largely elusive.

Common cell migration assays including the Boyden chamber, scratch assay and under agarose assay are based on numerous reproducible experiments, but are invariably of low efficiency, typically allowing the study of one factor and one cell type at a time [59, 67, 126]. The Boyden chamber and under agarose assays are not amenable for real time monitoring of cell motility patterns. The scratch assay does not allow for the formation of a cytokine gradient that is typically responsible for cell motility *in vivo* [127]. The conventional under-agarose assay is problematic for studying gradients formed by multiple cytokines that may cross-contaminate through the porous agarose. Several newly designed devices can test the effects of two opposing chemotactic signals, but do not appear to test competitive recruitment of a given cell population in response to multiple cytotactic cues in one single system [67, 68]. In particular, cells exposed to multiple cytokines that yield synergistic and/or antagonistic effects cannot be revealed by currently available cell migration assays.

In Chapter 3, we introduced a novel cell migration assay that was developed to allow simultaneous analysis of competitive cell recruitment by multiple cytotactic cues. These conditions mimic *in vivo* microenvironments where cell populations are continuously exposed to multiple cytokine signals. The device has six microfluidic channels, each with separate outlets for cell seeding and cytokine infusion. Given that cell migration is confined to microfluidic channels, the process of migration can be monitored in real time using time-lapse microscopy as we demonstrate below. By reversing directionality, the effects of a single cytokine could be

concurrently tested on 6 different cell types. In this chapter we will further demonstrate the utility of this multi-channel cell migration assay with a specific case study investigating potent migration cues found in the synovial joint in health and/or arthritis. This migration system has potential broad applications for the study of tissue development, cancer metastasis, infection, wound healing and tissue engineering.

4.2 Methods

Competition Device Characterization.

Separate diffusion experiments were conducted to determine if uniform cytokine diffusion can occur from the center chamber towards the peripheral chambers. Dextran conjugated with rhodamine B (10 kDa; Invitrogen, Carlsbad, CA) was infused into the center chamber, with 0.5% agarose in the channels and ultrapure water in the peripheral wells. Images were taken after 5 and 21 hrs of diffusion and the average pixel intensity in the six channels was calculated to assess the suitability of the device for testing the cytotactic effects of one cytokine in the center chamber on six different cell types that can be readily seeded in the peripheral wells. Additional experiments were conducted to determine if any fluorescent contamination occurs between the six channels, when cytokines are diffused from the peripheral wells towards the center chamber. Dextran (10 kDa) conjugated with rhodamine B or fluorescein was infused into alternating peripheral wells, and imaged after 5 and 21 hrs.

Cytokine Competition to Recruit MSCs.

Devices were fabricated and assembled using standard photolithography and soft-lithography techniques, as described in Chapter 3 (**Figure 4.1**). Microfluidic devices were

sterilized for 10 min by flowing 70% ethanol through all the channels. Devices were washed once with PBS, followed by fibronectin coating (75 µg/mL; Sigma, St Louis, MO) for 2 hrs at 37°C, and then washed with PBS twice. Sterile 1% agarose was diluted 1:2 with cell culture

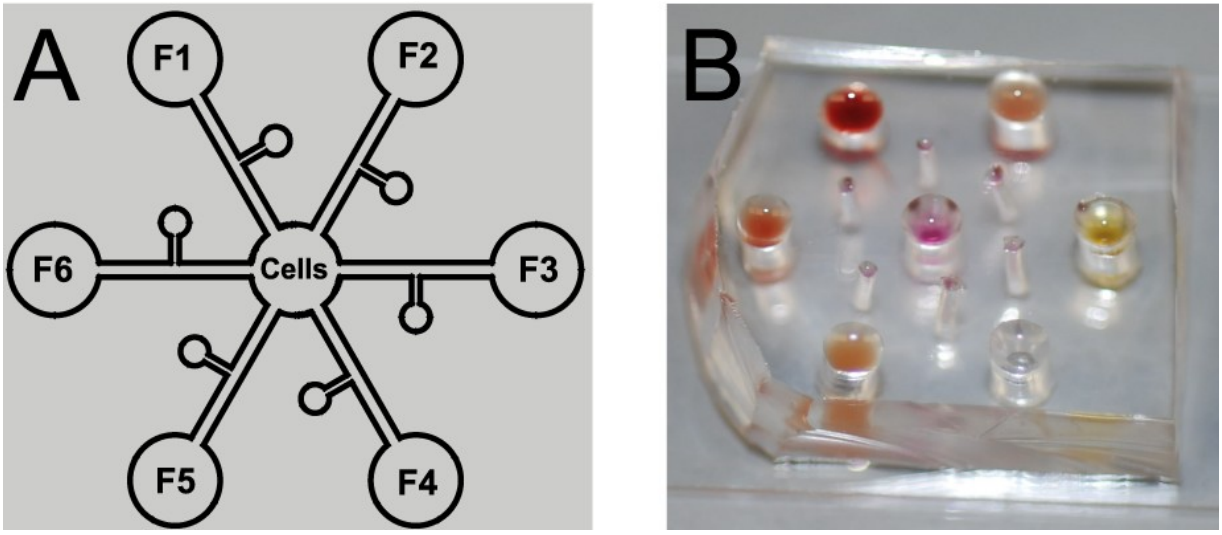

Figure 4.1. Competition device design schematic. (A) Design of a novel microfluidic device for competitive cell migration assays. Cells are seeded in the center chamber, whereas cytotactic factors (F1-F6) are infused in peripheral wells. A channel (dia: 250 µm) connects the center chamber to each of the peripheral wells. (B) Photograph of the fabricated microfluidic device.

medium and injected into the center inlet (**Figure 4.1A**). Following solidification, any excess agarose in the channel outlets was aspirated. The center chamber of the device was seeded with 40,000 MSCs. The following cytokines were selected for their high prevalence in the synovial joint in health and arthritis: TGFβ3 (Cell Sciences, Canton, MA); PDGFBB, Lymphotactin, Fractalkine, SDF1β, IGF1, MIP1α, MIP1β, MCP1, IP10 (R & D Systems, Minneapolis, MN); TGFβ1, TNFα, VEGF (Peprotech, Rocky Hill, NJ); FGF and IL6 (Invitrogen, Carlsbad, CA). Cytokines were randomly assigned to three different competition groups and each group had a cytokine-free control of PBS (**Table 4.1**).

Table 4.1: Cytokine group assignment for cell migration assays. Cytokines that are crucial for arthritis were randomly allocated into 3 groups with PBS as a control for each group. The 'top performers' from the first three groups (in red) were selected for the 'final' round, which yielded the final group capable of robust cell recruitment.

Group 1	Group 2	Group 3	Final
IGF1	bFGF	MCP1	MIP1α
SDF1	Fractalkine	Lymphotactin	PDGF
TGFβ3	TNFα	IP10	Lymphotactin
TGFβ1	VEGF	MIP1α	TGFβ3
PDGF	IL6	MIP1β	TNFα
PBS	PBS	PBS	PBS

Cytokines listed in **Table 4.1**, each at a dose of 200 ng, were placed in the peripheral wells. The cytokines from groups 1-3 that induced the maximal number of cells to migrate were grouped together to form the 'final' round. The winner of this round represented the most chemotactic cytokine among all cytokines tested. A minimum of 3 separate experiments were conducted for each group and the final round in **Table 4.1**, with devices maintained for 24 hrs at 37°C and 5% CO_2 in an environmental chamber. Randomly selected experiments were time-lapse imaged. Subsequently, cells were fixed with 10% formalin and stained with DAPI to visualize the nuclei. The total number of migrated cells, migration distances and migration indices were quantified using ImageJ software.

Cell Migration by PDGFBB Only.

The device shown in **Figure 4.10A**, containing individual channels (that were identical in dimensions to each of the channels in the connected 6-channel devices) was used to test the chemotactic effect of PDGFBB on MSCs in a non-competition setting. All experimental conditions were consistent with the connected channel device experiments, including seeding the MSCs at a density of 40,000 cells from the same donor, infusion of PDGFBB at a dose of 200 ng and all post-migration procedures including cell fixation, data acquisition and analysis.

Statistical Analysis.

Quantitative data for each condition were pooled from at least three independent experiments. Upon confirmation of a normal data distribution, One-way ANOVA with *post hoc* LSD tests were used with α values of $p \leq 0.05$.

4.3 Results

We designed and fabricated a novel microfluidic migration device (**Figure 4.1**) and tested the chemotactic effects of multiple cytokines on human mesenchymal stem cells (MSCs). The device requires minimal setup, including agarose injection, cell seeding and cytokine loading. The device was rigorously characterized by determining diffusion profiles to ensure a fair cytokine competition and reproducibility between experiments.

Verification of Competition Diffusion Gradient

Separate diffusion experiments were conducted to determine whether a given cytokine may uniformly diffuse from the center well to the peripheral wells. This configuration would be

used to test the effects of a single cytokine on competitively recruiting six different cell types (**Figure 4.2**). Dextran conjugated with rhodamine B (10 kDa) was infused into the center chamber, whereas the peripheral wells were filled with ultrapure water. A dextran gradient was formed in each agarose (0.5% w/v) filled channel over 21 hrs (**Figure 4.2A**). The average pixel intensity and associated standard deviations through all six channels were calculated (**Figure 4.2B).** The minimum standard deviations of the pixel intensity after 5 hrs (3.4) and after 21 hrs (1.6) indicate the formation and maintenance of uniform diffusion patterns in each of the six channels.

To determine if any fluorescence contamination occurs between the device channels, dextran conjugated with rhodamine B or fluorescein was infused into alternating peripheral wells (**Figure 4.3**), whereas the center chamber was filled with ultrapure water. The device was imaged after 5 and 21 hrs of diffusion. After 21 hrs, alternating gradients of fluorescence intensity could be readily visualized (**Figure 4.3A**). We observed a continuous distribution of dextran (**Figure 4.3B and D**), with sustained fluorescence intensity above zero throughout the channel's entire length (**Figure 4.3C**). Interestingly, the fluorescence intensity increases in the center chamber, demonstrating the potential of ample cytokine exposure to cells seeded in the center chamber (**Figure 4.3D**).

A

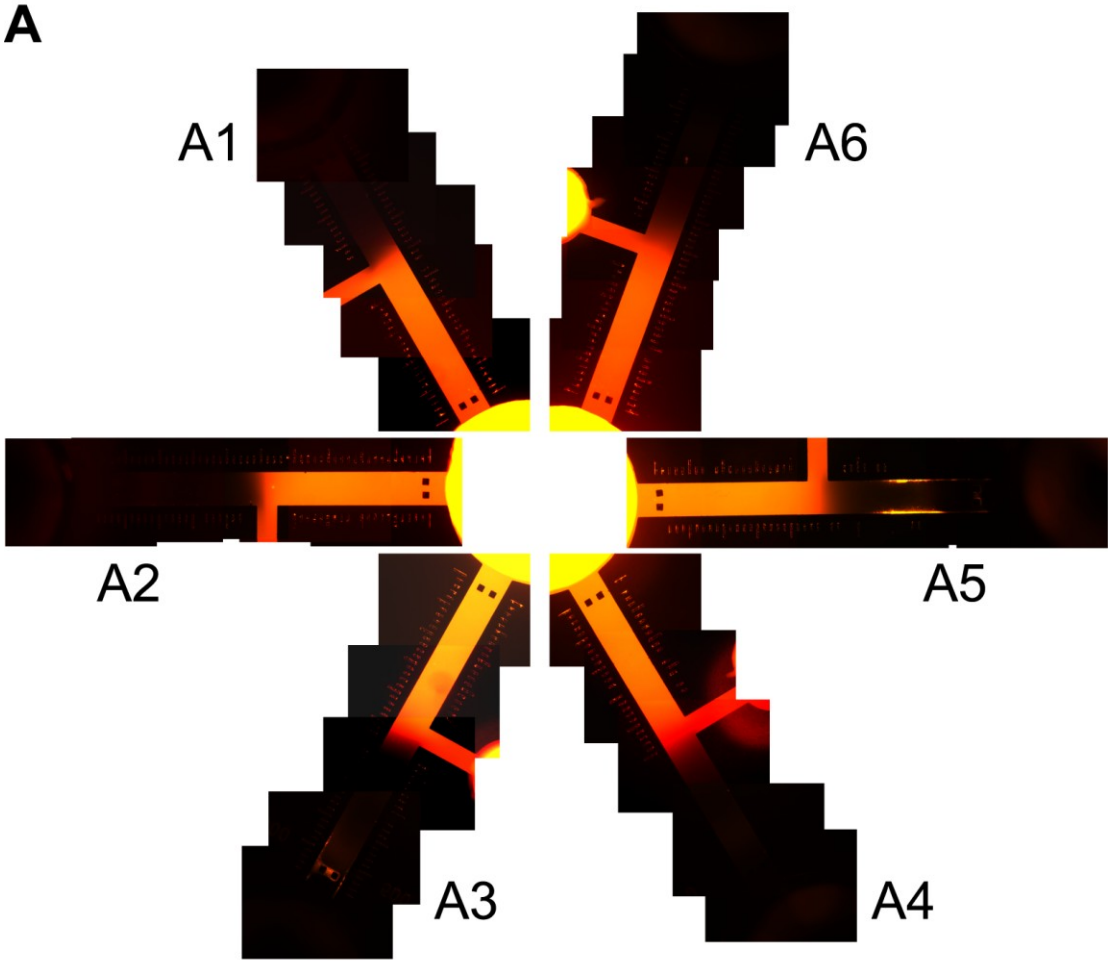

B

Intensity	5 hrs	21 hrs
Avg	99.3	133.8
S.D.	3.4	1.6

Figure 4.2. Diffusion profiles from the center chamber towards the peripheral chambers. A: Dextran conjugated with rhodamine B (10 kDa) was infused into the center chamber. The channels were filled with 0.5% agarose. The peripheral wells were filled with ultrapure water. Gradients formed in all channels over the observed 21 hrs. B: The average pixel intensity in all six channels was 99.3 after 5 hrs and 133.8 after 21 hrs. The modest standard deviations (3.4 and 1.6 respectively) demonstrate the suitability of the device for testing the cytotactic effects of a given factor on six different cell types.

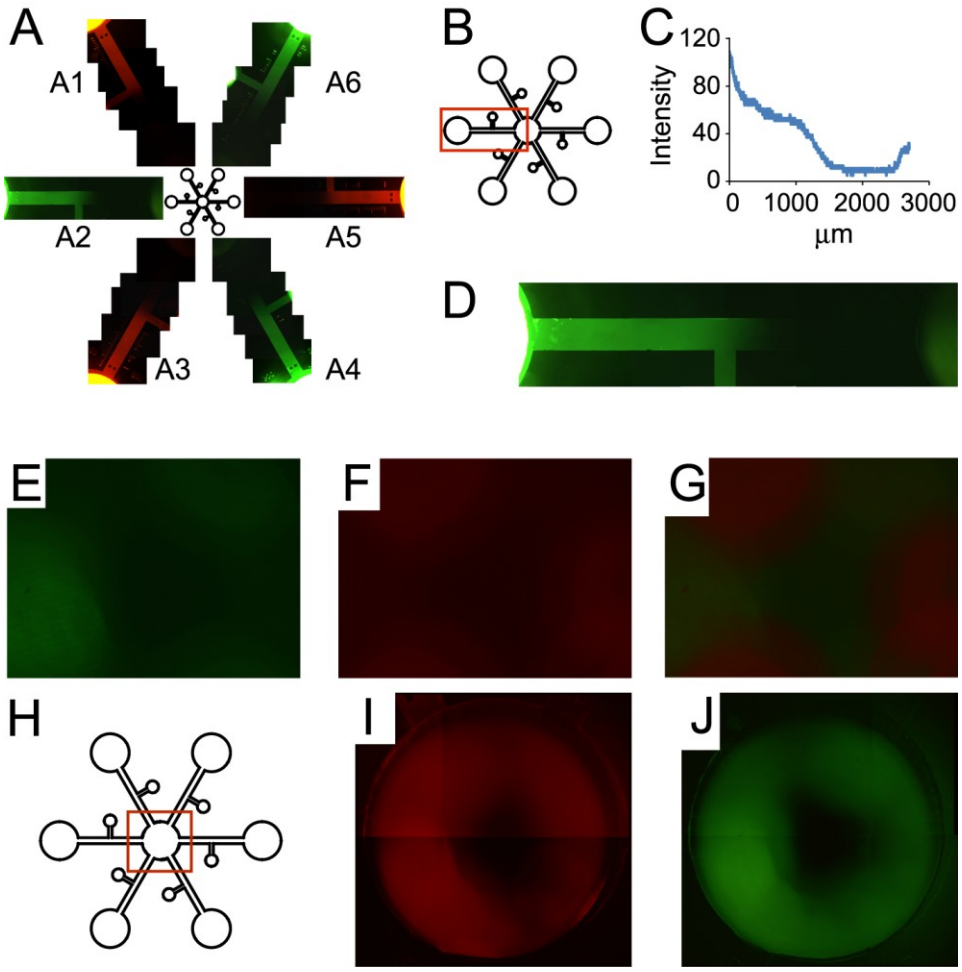

Figure 4.3. Gradients converge from peripheral wells to the center chamber. Dextran (10 kDa) conjugated with rhodamine B or fluorescein was infused into alternating peripheral wells. The channels were filled with 0.5% agarose. The center chamber was filled with ultrapure water. A: After 21 hrs, fluorescent gradients can be seen in each channel (A1-A6) with minimal fluorescent cross-over between channels. B: A single channel (A2) was used to determine the intensity profile of dextran conjugated with fluorescein (10 kDa) over the entire channel length after 21 hrs. C: The intensity profile remains above zero over the entire channel length, indicating a continuous cytokine distribution over the entire channel. Interestingly, the fluorescence intensity increases in the center chamber, demonstrating robust cytokine exposure to cells when they are seeded in the chamber. D: Enlarged image of A2. E: Fluorescein presence at the center chamber after 5 hrs. F. Rhodamine B presence at the center chamber after 5 hrs. G: Merged fluorescence images after 5 hrs. Distinct regions of rhodamine B or fluorescein can be seen surrounding each channel inlet, with minimal cross-over between channel inlets. H: Schematic of the center region imaged for E-G. I: Rhodamine B presence at the center chamber after 21 hrs. J: Fluorescein presence at the center chamber after 21 hrs. Continuous rings of rhodamine B or fluorescein can be seen filling the center channel, indicating a uniformity in cytokine exposure to all potentially seeded cells in the center chamber and demonstrating competition among cytokines placed in the periphery.

The center chamber imaged after 5 hrs displayed distinct regions of rhodamine B or fluorescein surrounding each channel inlet, with minimal crossover between channel inlets (**Figure 4.3E-H**). In the observed 21 hrs, continuous concentric rings of rhodamine B or fluorescein had reached and filled the center chamber, demonstrating that cells seeded in the center chamber are exposed to multiple cytotactic factors infused in the peripheral wells and therefore may be recruited competitively by the most robust cytotactic cue(s) among the six factors infused in the peripheral wells (**Figure 4.3I-J**).

Competitive Cell Migration Assay.

As a case study, we tested the migration of MSCs in response to multiple simultaneous cytotactic cues. The disease model we selected for this case study is arthritis, not only because of its high prevalence and our familiarity with this model, but also because of the excessive cost associated with arthritis treatment, over $80 billion per year in the U.S. [128]. Over 65 cytokines have been shown to play important roles in rheumatoid arthritis [129]. We selected a subset of these cytokines, some of which are not typically considered cell homing cues, based on their known molecular characteristics [120, 129, 130]: TGFβ3, TGFβ1, PDGFBB, lymphotactin, fractalkine, SDF1β, IGF1, MIP1α, MIP1β, MCP1, IP10, TGFβ1, TNFα, VEGF, bFGF and IL6 (**Table 4.1**). Cytokines were randomly allocated into Groups 1, 2 or 3 (**Table 4.1**), and tested for their efficacy in cell recruitment. Top performer(s) of each group were selected to 'compete' in a final round (Final in **Table 4.1**). MSCs migrated under the agarose gel towards a cytokine gradient over the observed 4, 8 and 24 hrs (**Figure 4.4**). Likely due to the presence of serum (10%) in peripheral wells, MSCs even migrated in the PBS control group (**Figure 4.4**) in a process known as chemokinesis. For example, an abundant number of MSCs had migrated after only 4 hrs of lymphotactin (LPTN) exposure in comparison to the control (**Figure 4.4G**), consistent with its

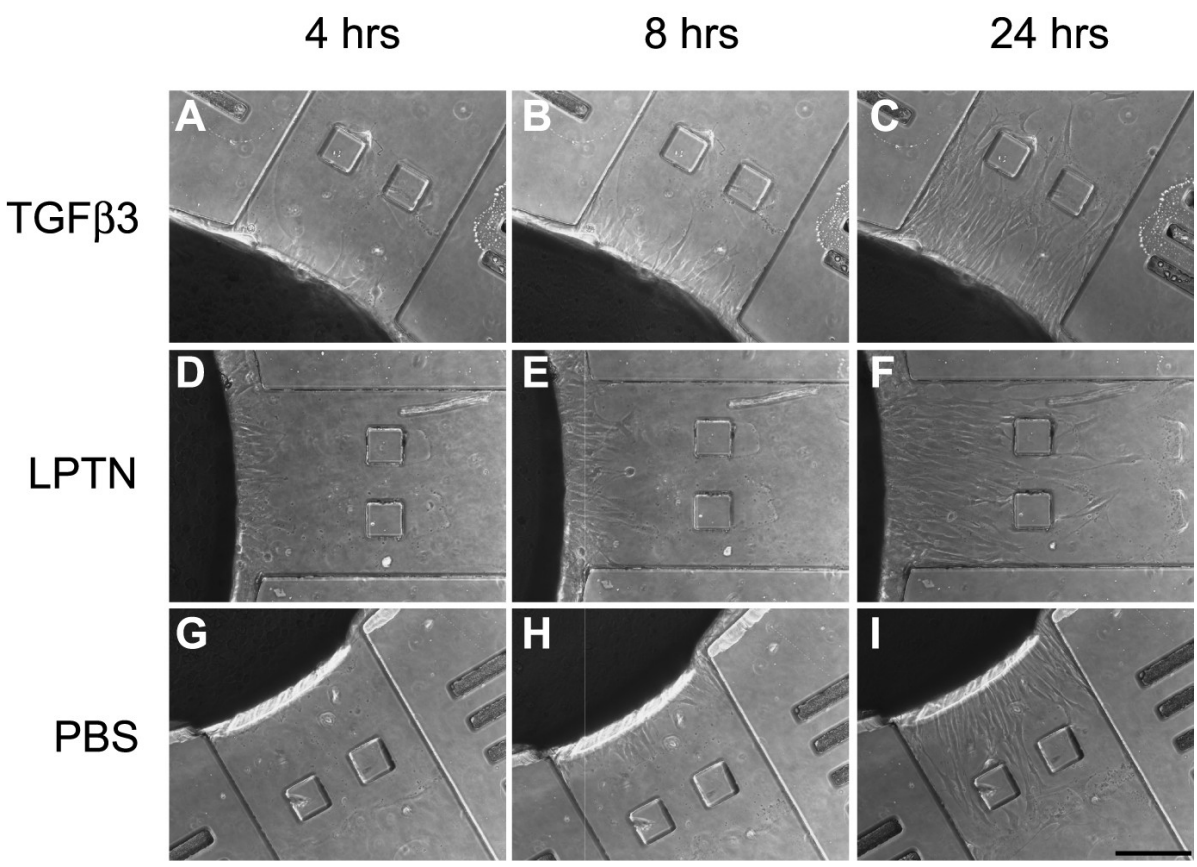

Figure 4.4. Representative time-lapse images of induced cell migration. Cell migration was time-lapse imaged at 4 hrs (A, D, G), 8 hrs (B, E, H) and 24 hrs (C, F, I) after exposure to gradients of cytotatic cues. TGFβ3 (A-C), Lymphotactin (LPTN; D-F) and PBS (G-I; control) induced marked differences in the number and distances of cell migration after 24 hrs following infusion.

previously observed chemotactic effects on MSCs [131]. By 24 hrs, TGFβ3 induced marked cell migration (**Figure 4.4C**) as compared to the control (**Figure 4.4I**), consistent with previous reports [109, 115]. The migratory effects of multiple cytokines were concurrently monitored in real time, representing an advantage over conventional cell migration assays that only allow collection of endpoint data. MSCs seeded in the center chamber can be seen continuously migrating towards an increasing concentration of IGF1, as an example, in the peripheral well on the right side over the observed 12 hrs.

Following each cell migration experiment, cell nuclei were stained with DAPI and imaged with phase contrast and fluorescence microscopy (**Figure 4.5**). Clearly, the six factors in the final round recruited different numbers of MSCs (**Figure 4.5**). DAPI stained nuclei were quantified to determine the total number of cells that had migrated into each channel (**Figure 4.6**), the migratory distance (**Figures 4.7 and 4.8**) and the migration index (**Figure 4.9**). Significantly more MSCs were recruited by TGFβ3 in Group 1 (147 cells), TNFα in Group 2 (128 cells) and MIP1α in Group 3 (132 cells) than the control by 24 hrs (**Figure 4.6A, B and C,** respectively). In the 'final' round with top performers of cell recruitment selected from Groups 1,

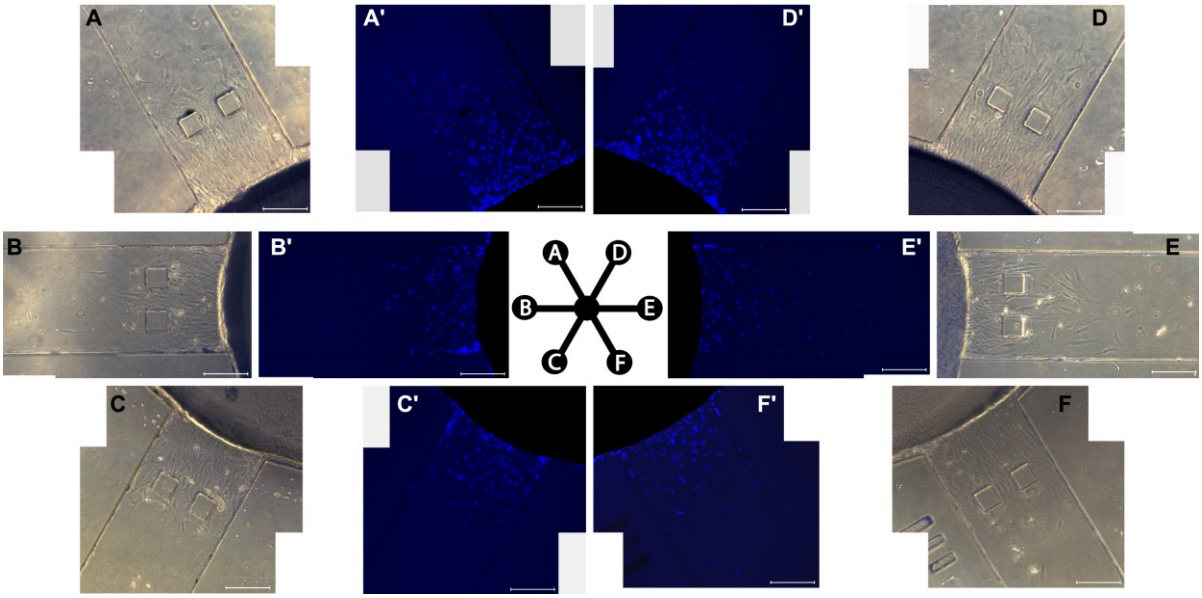

Figure 4.5. Competitive cell migration from the final round of cytotactic cues that were selected as the most robust from the first three groups (c.f. Table 1). A-F show phase contrast images at 24 hrs following exposure to MIP1α, TGFβ3, TNFα, Lymphotactin, PDGFBB and PBS (control). Following phase contrast imaging, the cells were stained with DAPI (A'-F') to visualize the abundant number of cells that had migrated in response to gradients formed by MIP1α (A'), TGFβ3 (C'), TNFα (D'), Lymphotactin (LPTN: E') and PDGFBB (F') in comparison to PBS (control; B'). DAPI images were subsequently used to quantify the number of migrated cells, migratory distance and migration index.

2 and 3, significantly more MSCs were recruited by PDGFBB (115 cells), TGFβ3 (120 cells), and TNFα (125 cells) (**Figure 4.6D**) compared to the control.

The distance over which cells migrate is of interest in stem cell biology, neutrophil motility, tissue regeneration and cancer metastasis. The most robust cytokines that induced significantly longer migratory distances were TGFβ1 (235 μm) in Group 1; bFGF (255 μm) and IL6 (241 μm) in Group 2, lymphotactin (214 μm) in Group 3, and TGFβ3 (264 μm) in the 'final' round (**Figure 4.7A-D**). Remarkably, TGFβ3 promoted both significant cell recruitment and induced the longest migration distance of MSCs, which appears to account for our recent *in vivo* finding that TGFβ3 not only recruited an abundant number of cells, but also promoted the regeneration of the entire articular cartilage surface of a synovial joint [102, 103, 115]. To further demonstrate the robustness of this system, the cell migration distance in the final round was stratified into categories of <100 μm, 100-200 μm and >200 μm (**Figure 4.8**). MIP1α and PDGFBB induced significantly more cells that migrated >200μm compared to the number of cells that migrated 100-200μm (**Figure 4.8**). TGFβ3 and TNFα induced significantly more cells that migrated >200μm compared to the number of cells that migrated in all other distance categories as well as the number of cells that migrated >200μm for PBS control (**Figure 4.8**).

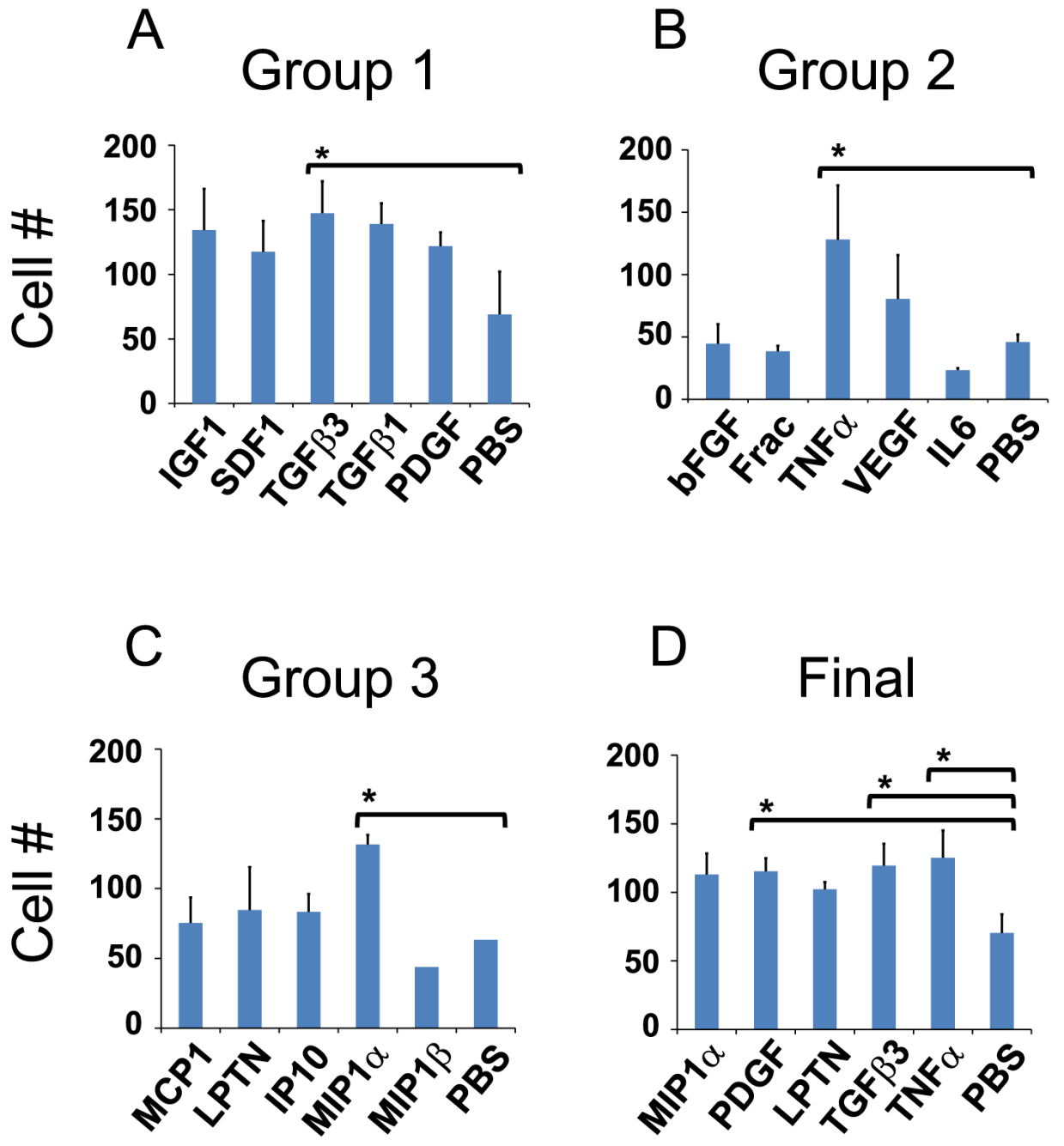

Figure 4.6. Quantification of migrated cells in competition assay. A-D:The total number of migrated cells was quantified for the first three groups of cytotactic cues, and also for the final round of the most robust cues. Significantly more cells migrated than the control in response to TGFβ3 in Group 1, TNFα in Group 2, MIP1α in Group 3 and TNFα, TGFβ3, and PDGFBB in the final. *: $p<0.05$.

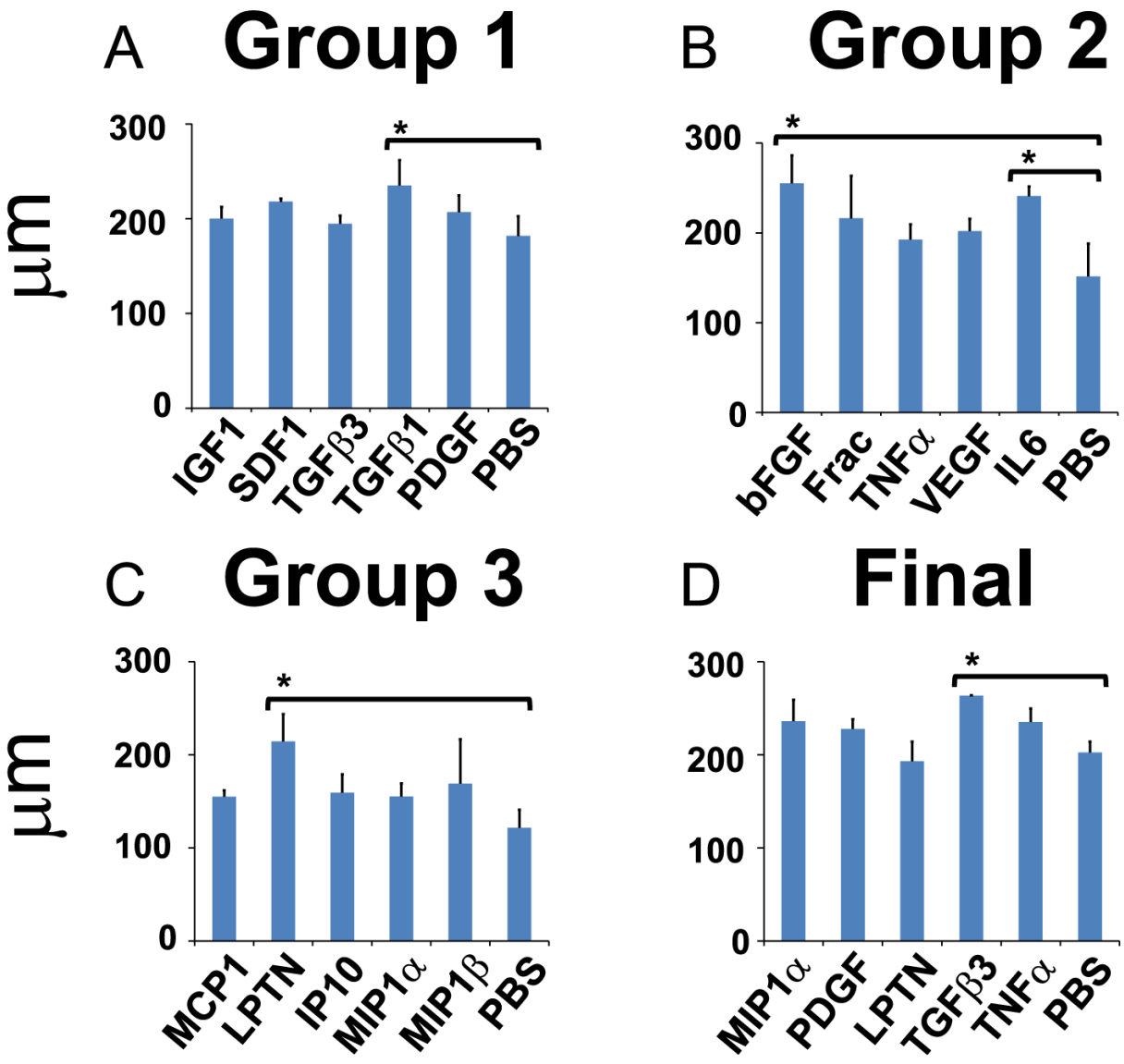

Figure 4.7. Quantification of cell migration distance in competition assay. A-D: Cells migrated significantly longer distances than controls in response to TGFβ1 in Group 1 , bFGF and IL6 in Group 2 , LPTN in Group 3, and TGFβ3 in the final. *: $p<0.05$.

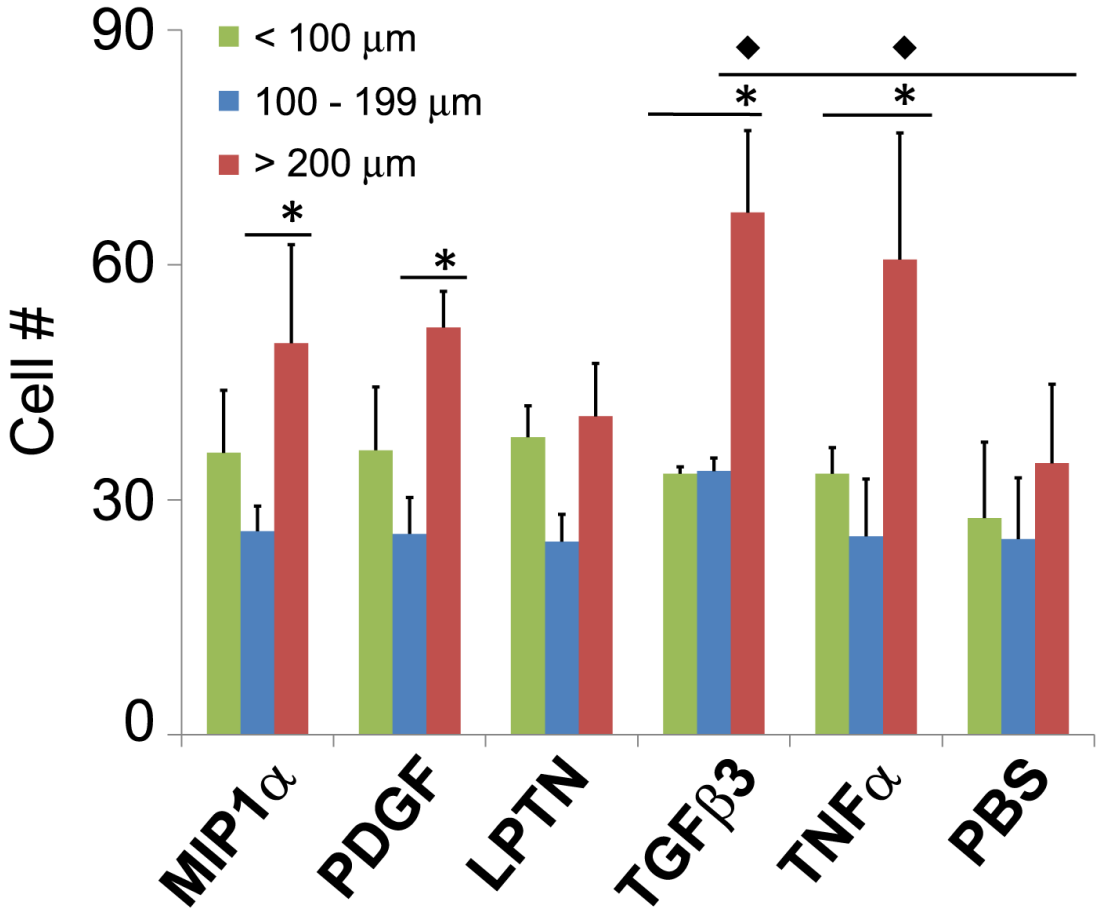

Figure 4.8. Distribution of migration distances for final round. Cell migratory distances were stratified into categories of <100 µm, 100-200 µm and >200 µm. ∗ indicates significance ($p<0.05$) over other distances for a given one factor. ♦ indicates significance ($p<0.05$) of one factor over the control group for the same distance value. *: $p<0.05$.

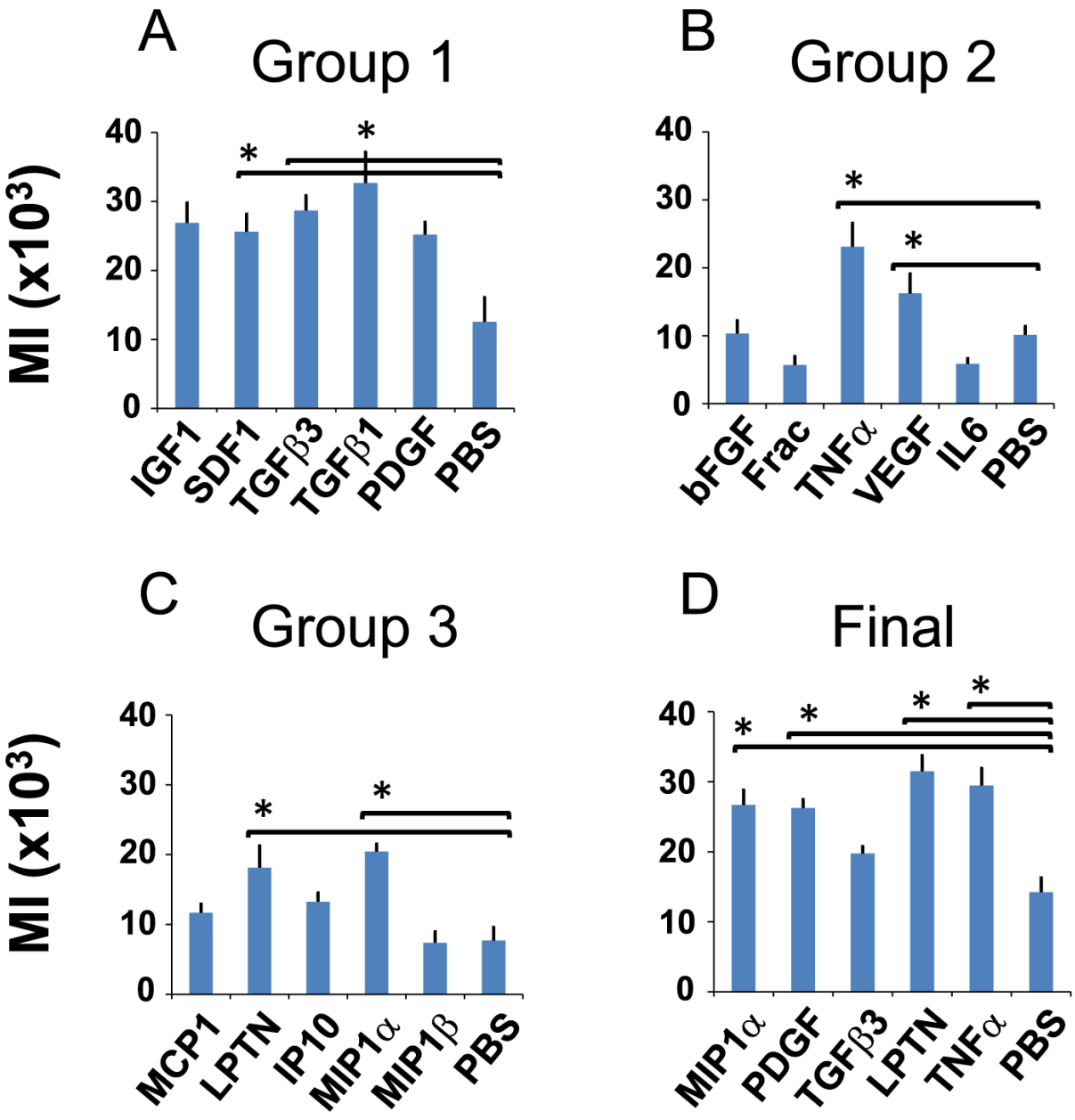

Figure 4.9. Quantification of Migration Index (MI) in competition assay. A-D: The cell migration index was derived by multiplying the total number of cells migrated into the channel by the migratory distance. Significantly greater MI was induced than controls by SDF1β and TGFβ3 in Group 1, TNFα and VEGF in Group 2 , LPTN and MIP1α Group 3 and MIP1α, PDGFBB, LPTN, and TNFα in the final. *: $p<0.05$.

Additionally, cell migration index (MI) was quantified by multiplying cell numbers by migration distances (**Figure 4.9**). SDF1β and TGFβ3 induced significantly greater MI (26 and 33 respectively) than the PBS control (13) in Group 1 (**Figure 4.9A**). TNFα and VEGF induced significantly greater MI (23 and 16 respectively) than the control in Group 2 (**Figure 4.9B**). LPTN and MIP1α induced significantly greater MI (18 and 20 respectively) than the control in Group 3 (**Figure 4.9C**). MIP1α, PDGFBB, LPTN, and TNFα induced significantly greater MI (27, 26, 20 and 29 respectively) than the control in the final (**Figure 4.9D**).

Given that fluorescent dextran diffusion in each channel reached the center chamber (**Figure 4.3**), cell migration data substantiate the possibility of competitive recruitment of cells by multiple cytokines in each group. For example, MIP1α in Group 3 induced significantly more MSCs to migrate than the control (**Figure 4.6C**), but failed to induce significantly more MSCs to migrate in the final round (**Figure 4.6D**), suggesting that other cytokines in the final round, PDGFBB, LPTN, TGFβ3 and/or TNFα, may have exerted even stronger cytotactic effects than MIP1α. A similar pattern was observed for MSC migratory distances in response to TNFα, which showed modest effects on migratory distance in Group 2 (**Figure 4.7B**), but enhanced cytotactic effects in the final round (**Figure 4.7D**), similar to previous observations that TNFα enhances the effects of other chemokines [132]. Remarkably, TGFβ3 only had modest effects on MSC migratory distance in Group 1 (**Figure 4.7A**), but induced a robust increase in migratory distance on MSCs in the final round (**Figure 4.7D**), likely owing to a putative synergistic effect with other cytokines including MIP1α, PDGFBB, LPTN, and/or TNFα. When cells are exposed to multiple cytokines *in vivo*, chemotactic effects may be enhanced or reduced depending on the presence of synergistic or antagonistic factors. To this end, a separate migration experiment was conducted to determine the migratory effects of PDGFBB on MSCs in a non-competition setting (**Figure 4.10**). After 24 hrs, PDGFBB alone in a non-competition setting induced significantly more MSCs to migrate (226 cells) than not only the

control (88 cells) ($p<0.05$) (**Figure 4.10**), but also compared to PDGFBB in a competition setting in Group 1 (122 cells) (**Figure 4.6A**) or the final (**Figure 4.6D**) (115 cells). The chemotactic effects of PDGFBB on MSCs are also consistent with previous findings [132, 133].

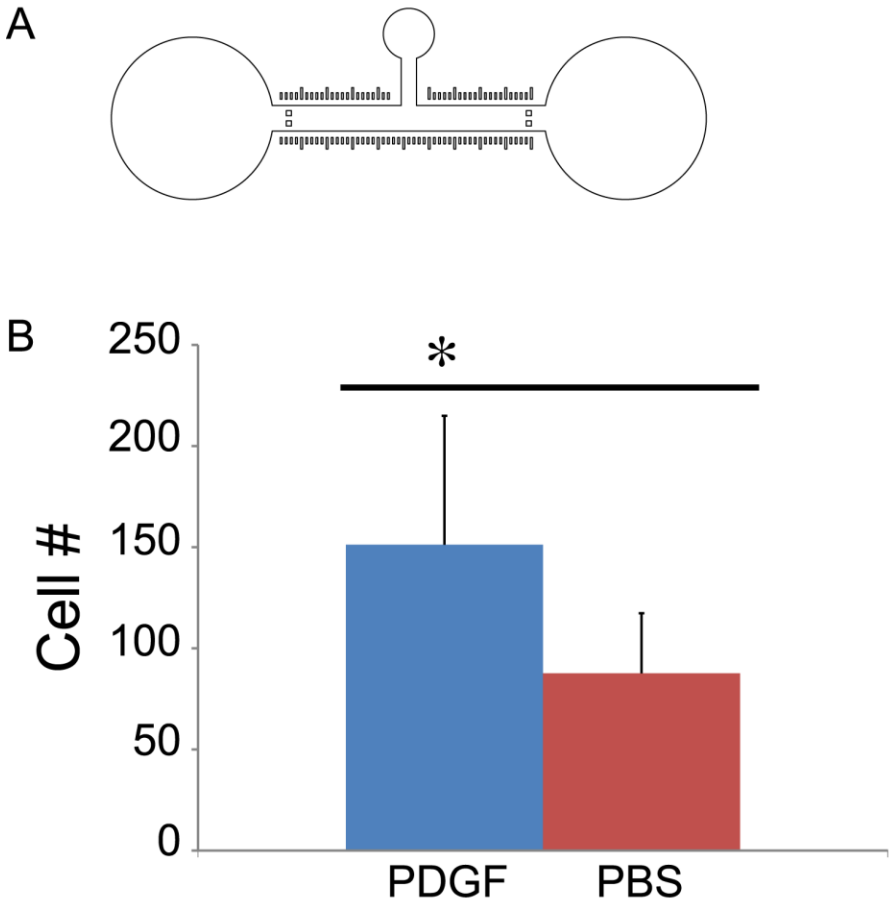

Figure 4.10. PDGFBB effects on cell migration in a non-competition setting. A: A separate under-agarose migration device was fabricated with a single channel consisting of two chambers, one for cell seeding and the other for cytokine loading with the same configuration as a single unit of the 6-channel device. B: Significantly more MSCs migrated in response to PDGFBB (226 cells) compared to the control (88 cells) ($p<0.05$). Differences in cell migration in response to PDGFBB in a competition setting (122 cells in Group 1) compared to a non-competition setting (226 cells) indicate that the other factors in the 6-channel setting play interactive roles for cell migration.

4.4 Discussion

This novel microfluidic device enables the competitive recruitment of cells that are simultaneously exposed to multiple cytotactic cues under real-time imaging. Multiple chemotactic factors with gradients that converge on cells of interest generate complex synergistic and/or antagonistic effects on cell migration, thus simulating the *in vivo* milieu of chemotactic cues that act on cells in development, cancer metastasis, wound healing or tissue repair. A cytokine gradient is generated along the length of agarose-filled channels within minutes and maintained for the tested 24 hrs. Diffusion of dextrans of varying molecular weights and cell migration data demonstrate the effectiveness of this microfluidic device for testing the simultaneous actions of multiple chemotactic cues. Another conceptual innovation, to be investigated in future experiments, is to assay the effects of a given chemotactic cue on the migration of multiple cell populations, mimicking *in vivo* conditions whereby multiple cell types may be attracted or repelled by a given factor. These two features are not present in typical cell migration assays including the Boyden chamber, Transwell and scratch assays.

Putative synergistic and antagonistic effects of multiple cytokines demonstrate the likelihood that not only do multiple cytokine gradients reach the center chamber where cells are seeded, but also the competitive effects of multiple cytokines in the recruitment of MSCs that are free to migrate into any of the six channels. Additional experiments that can be conducted with this migration system include chemokinesis, migration directionality and importantly clonal fractions of a heterogeneous cell population. Tests to determine the speed of individual migrating cells could be done to delineate if a cytokine is chemokinetic. A chemokinetic factor would promote an increase in cell speed as the cell approaches an increasing cytokine concentration. The effect of increasing cell passage number on migration ability could be tested as well. Since stem cells lose their stemness with increasing passage numbers [3], it is predicted that as the passage number increases, fewer cells will migrate. Determining which

cytokine combinations are the most effective at maximizing cell homing may offer novel approaches for tissue regeneration with or without the need for cell delivery [109, 115]. Specifically, the device may help to determine the spatial location for placement of a cytotactic cue in a bioactive scaffold from a native cell source to induce effective cell migration. Besides tissue regeneration, this device may be used to better understand fundamental biological processes such as development, cancer cell aggregation and spread, motility of inflammatory cells and drug development.

High throughput is desirable for screening the migration of multiple cell populations or the effects of multiple chemotactic cues on the migration of a given cell type. A number of devices allow high throughput screening of cell migration such as the ChemoTx® system (Neuro Probe, Gaithersburg, MD). Microfluidic platforms have a number of advantages over existing cell migration assays, including low cost, high reproducibility and minimal volume of required reagents. The present microfluidic cell migration assay can be readily scaled up by not only using multiple devices, but also by adding more channels to each device to allow for the screening of numerous cytotactic cues or testing the cytotactic effects of a given factor against multiple cell populations. While this system offers a unique platform for monitoring the migration of multiple cell types seeded together in real-time, due to the small size of the device, a limited number of cells can be tested at once. Approximately 40,000 cells can be seeded in one of the wells of the device to ensure sufficient space for cell attachment. If multiple cell types are seeded in the same well, the total number of cells that can be seeded in the well must be divided by the number of cell types. The limited number of cells required for each migration assay is advantageous however, in minimizing the cost of running an individual migration experiment. The present device only allows a limited number of cells to access the channel entrance at a given time because of the small channel diameter (250 μm). Since only the cells migrating within the channel are quantified and not those showing motility within the central

chamber, the total number of migrating cells in the channel is not an indication of total cell motility. To maintain consistency, a uniform concentration of 200 ng was selected to test all cytokines in the present work. It is conceivable that cell migration can be enhanced at higher or lower concentration for a given cytokine. In summary, this microfluidic migration device has the unique advantage of allowing assays of cell migration competitively in response to multiple cytotactic cues with broad applications ranging from drug development to wound healing and tissue regeneration.

4.5 Future Studies

Stem Cell Niche Migration Behavior.

Stem cell niches *in vivo* are in close proximity to multiple cell types and simultaneously exposed to multiple cytokine signals that act to maintain tissue homeostasis or initiate a chemotactic response to injury. Migration assays that emulate the environmental conditions found in a stem cell niche could provide new insight into native stem cell migration behavior. Future experiments have been designed to test the chemotactic effects of multiple cytokines on multiple cell types simultaneously. The ability to conduct multiplexed testing of numerous cells and cytokines represents a unique feature of these migration devices. Preliminary experiments were conducted to create a stem cell niche consisting of MSCs, ASCs and SSCs and investigate the chemotactic effects of the final round of cytokines on these cell types in combined culture. Passage 3-4 ASCs, SSCs and MSCs were separately labeled with CellTracker Green CMFDA (**Figure 4.11A**), Red CMPTX (**Figure 4.11B**) and Blue CMAC (**Figure 4.11C**) dyes respectively (Invitrogen, Carlsbad, CA). To determine which stem/progenitor cell is most chemotactic, the center well of the competition microfluidic device

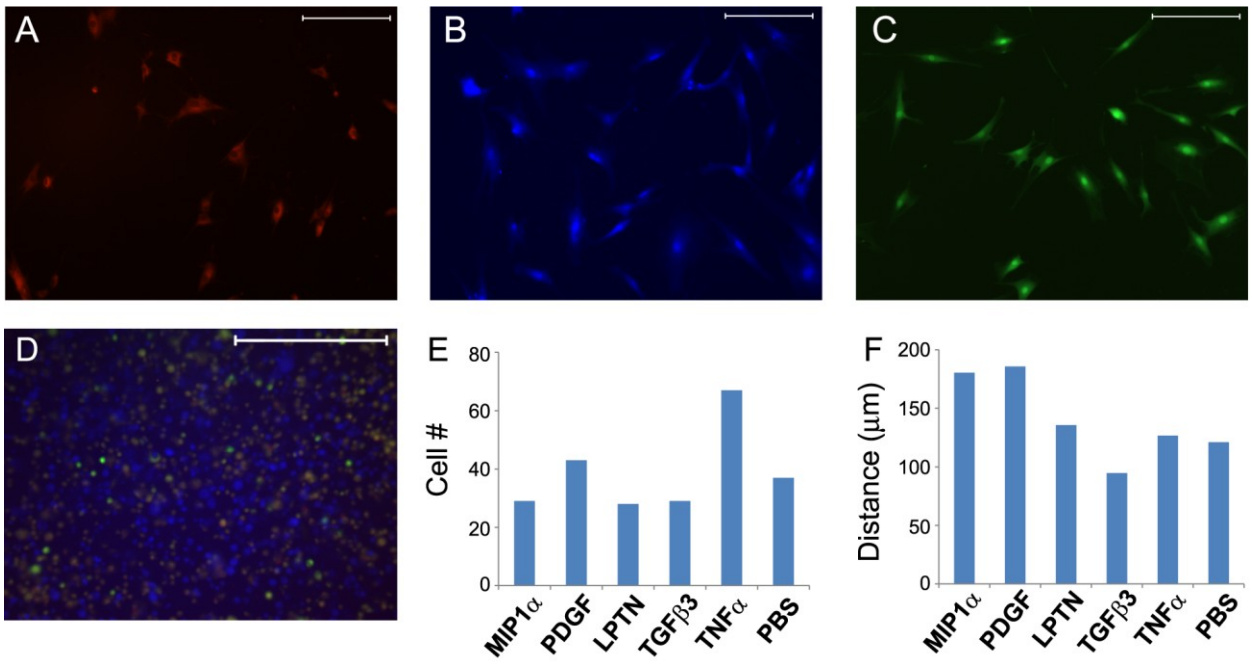

Figure 4.11. Stem cell niche migration behavior. Celltracker labeling of (A) MSCs with Blue CMAC (B) ASCs with Green CMFDA and (C) SSCs with Red CMPTX dye. Images were taken immediately after labeling. (D) Center well initially seeded with labeled ASCs, MSCs and SSCs (E) Total number of migrated cells and (F) cell migration distance in response to cytokines from round 6. Scale for A-C: 50μm. Scale for D: 200μm.

was seeded with a mixture of 12,000 of each labeled cell type (Figure 4.11D) and simultaneously exposed to the cytokines from the final round. All devices were kept for 24 hours at 37°C and 5% CO_2. Subsequently, cells were fixed with formalin and stained with DAPI to visualize the cell nuclei. The total number of migrated cells and the migration distances were quantified using ImageJ software. Preliminary results from quantification of DAPI stained devices revealed that TNFα was most potent at inducing highest cell migration numbers (**Figure 4.11E**) and MIP1α and PDGF were most effective at inducing the farthest cell migration distances **(Figure 4.11F)** among the stem cell niche. Future experiments are planned to

increase the sample size to verify these trends. Additionally, the cell migration numbers and distances will be quantified individually for ASCs, MSCs and SSCs to determine which cell type is the most chemotactic. Comparison studies will be conducted to test MSCs, SSCs and ASCs alone in the presence of the final round factors to evaluate the effect of co-culture on the chemotactic ability of these cell types.

Chapter 5: In Vivo Chondrogenesis by Cell Homing for Rhinoplasty Augmentation

5.1 Introduction

In Chapter 2 we demonstrated that slow-release delivery of TGFβ3 from a bioactive scaffold can direct the migration of MSCs, ASCs and SSCs to the scaffold and subsequently induce chondrogenic differentiation of the recruited cells. To confirm that TGFβ3 is an effective chemotactic agent, MSCs were subjected to rigorous chemotactic testing with 15 cytokines found in a synovial joint in health and/or arthritis. TGFβ3 was found to be the most effective factor among all tested factors at inducing MSC migration, as evident by the promotion of significant cell migration numbers and distances. However, it remained to be seen whether these results could be translated *in vivo* for clinical applications.

We selected to use rhinoplasty augmentation as an exemplary application for testing the effectiveness of cell homing for cartilage regeneration in a small animal model. Although the system designed in Chapter 2 was initially intended for orthopedic cartilage applications, we decided against using our scaffold as an *in situ* cartilage plug for regenerating cartilage defects in the synovial joint for the following reasons. As an initial proof-of-principle, rats were selected for use in our *in vivo* experiments, because of ease of handling and the ability to test a large number of different experimental conditions, with the end goal of switching to a larger animal model after optimal scaffold conditions have been determined. However, a physiological limitation for using rats to regenerate orthopedic defects is the inability for the tibial growth plate to fuse after the animal reaches maturity. Thus, the rat is able to self-heal and form new cartilage as the animal ages, causing a concern for tissue regeneration studies as to whether the regenerated tissue was a result of the applied treatment or a result of the natural self-healing process [71]. Therefore, a less biased model for cartilage formation in a small animal would be an ectopic model, which led to the selection of the rhinoplasty augmentation model.

Rhinoplasty augmentation is a surgical procedure aimed at increasing the natural nasal tip projection. Current procedures utilize a biological or synthetic ectopic structure to maintain an aesthetic shape, but have limitations. While autologous grafts are often preferred, obtaining a large enough tissue graft is challenging and results in donor-site morbidity. Biomaterial-based grafts are readily available, but may be unnatural in appearance and prone to infection or extrusion. Thus, a significant clinical need exists for improved rhinoplasty augmentation implants. An implant that combines the advantages of both autologous and biomaterial grafts would be ideal. We developed a bioactive biomaterial-based scaffold that can home stem/progenitor cells in the nasal dorsum and induce chondrogenesis of the homed cells. Cartilage formation by cell homing, to our knowledge, has never been tested before for rhinoplasty augmentation applications, but could potentially serve as an alternative treatment method and will be explored in this chapter.

5.2 Methods

PLGA Scaffold Characterization.

Because the collagen sponge used in Chapter 2 to fabricate the bottom layer of the scaffolds had weak mechanical properties, poly(lactide-co-glycolide) (PLGA) was tested as an alternative material for *in vivo* studies. Varying concentrations (10%, 20%, 30% and 40% wt/vol) of porous poly(lactide-co-glycolide) (PLGA) scaffolds were fabricated using a salt-leaching method similar to previously published approaches [6, 134]. Briefly, PLGA 50:50 crystals (Sigma, St. Louis, MO) weighing 1-4g were dissolved in 30mL dimethylchloride. Dissolved PLGA solutions were mixed with 27g of sodium chloride (Sigma, St. Louis, MO) that was sieved

to ensure a particulate diameter ranging between 150-500μm, poured into a teflon coated 10cm plate and allowed to air dry overnight. Scaffolds were punched out of the PLGA sheet using a 6mm diameter biopsy punch, salt leached with distilled water and dried using a lyophilizer.

The degradation profiles of the PLGA scaffolds were characterized to determine the optimal bulk concentration for subsequent *in vivo* studies. Scaffolds were sterilized for 10 minutes in 70% ethanol and their wet weights were measured. One scaffold of each PLGA concentration was placed in a separate well of a 12-well tissue culture plate and submerged in 2mL of PBS containing 1% AB/AM. Scaffolds were harvested after 0, 7, 17, 22, 27, 34 and 38 days and their wet and dry weights were determined. Additionally, the scaffold morphology was examined at varying time points to observe internal pore structure using Scanning Electron Microscopy.

Calcium Release From Alginate.

According to a recent article published by *Wu et al*, MSCs exposed to 0.5-4mM $CaCl_2$ experienced an upregulation of the CXCR4 surface receptor and an increase in cell migration ability [53]. Since alginate hydrogel is polymerized with $CaCl_2$, we hypothesized that as the hydrogel degrades over time, calcium would be slowly released into the surrounding environment and increase local cell migration. To test this conjecture, bilayered scaffolds described in Chapter 2 were fabricated with a top alginate (FMC BioPolymer, Philadelphia, PA) layer without gelatin microspheres and a bottom collagen sponge layer (Helistat, Integra LifeSciences, Plainsboro, NJ). The top layer was made using 100μL of 2% alginate and cross-linked using 1mL of 50mM, 100mM or 200mM $CaCl_2$ (Sigma, St. Louis, MO). One scaffold of each $CaCl_2$ concentration was placed in a separate well of a 12-well tissue culture plate (n=3)

and submerged in 1.5mL of PBS containing 1% AB/AM. PBS samples were collected after 0, 1, 2, 4, 7, 11, 17, 24 and 32 days and the calcium content was measured using the Calcium Colorimetric Assay Kit (Biovision, Mountain View, CA).

Pilot In Vivo Studies.

For our initial studies, bilayered scaffolds were fabricated, similar to those described in Chapter 2, with a top 2% w/v alginate layer containing gelatin microspheres encapsulating cytokines and a bottom layer made of either 20% PLGA or collagen sponge. Although collagen sponge is mechanically weak, one group was included in the pilot studies with collagen sponge as the scaffold base material to confirm the positive *in vitro* results observed in Chapter 2 using this material for cell homing and chondrogenesis. Cytokine selection for pilot studies was also based on positive *in vitro* results observed in Chapter 2, using SDF1β and TGFβ3 co-delivery. PDGFBB was selected because of its potent chemotactic effects on MSCs as shown in Chapter 4 and in previously published literature [132, 133]. IGF1 was selected because of its ability to enhance chondrogenesis *in vitro* [135, 136]. Therefore, three scaffold types were tested: 200ng SDF1β and 200ng TGFβ3 co-delivery with a bottom collagen sponge layer (Group 1), 200ng SDF1β and 200ng TGFβ3 co-delivery with a bottom 20% PLGA layer (Group 2) and multi-factor delivery of 200ng SDF1β, 200ng TGFβ3, 200ng IGF1 and 200ng PDGFBB with a bottom 20% PLGA layer (Group 3) (**Table 5.1**).

Table 5.1: Experimental design conditions for pilot *in vivo* study.

Group #	# of Rats	Harvest Time Point	Scaffold Condition
1	3	6 wks	Collagen Sponge Scaffold + 200ng SDF1 + 200ng TGFβ3
2	3	6 wks	PLGA Scaffold + 200ng SDF1 + 200ng TGFβ3
3	3	10 wks	PLGA Scaffold + 200ng SDF1 + 200ng TGFβ3 + 200ng PDGFBB + 200ng IGF1

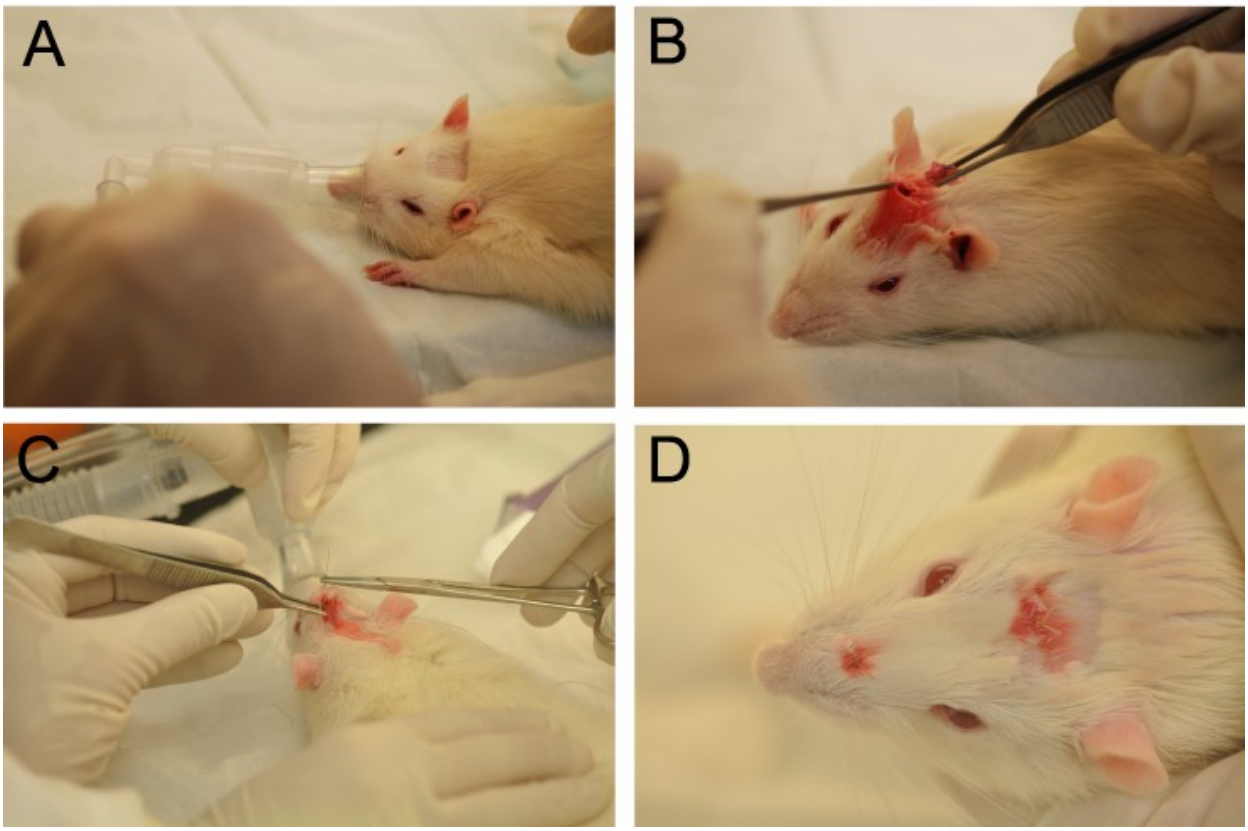

Figure 5.1. Surgical methods used for scaffold implantation. (A) Rats were anesthetized and the surgical incision site was shaved. (B) An incision was created on the top of the head, followed by formation of a subcutaneous pocket leading to the nasal tip. Scaffolds were inserted into the pocket and onto the nasal tip. (C) Incision was sutured closed and an additional suture was placed above the implant to fix it in place. (D) Top-down view of finished surgery.

We received Institutional Animal Care and Use Committee approval to use adult Sprague Dawley rats (aged 10 months; Harlan, Indianapolis, IN, USA). The rats were initially anesthetized and maintained with 3-4% isoflurane (**Figure 5.1A**). An incision was made on the head and the soft tissue was dissected down to the bone forming a subcutaneous pocket (**Figure 5.1B**). To test the most effective scaffold location for promoting cell homing, two different implant locations were tested (**Figure 5.2**). Scaffolds in Groups 1 and 2 were placed on

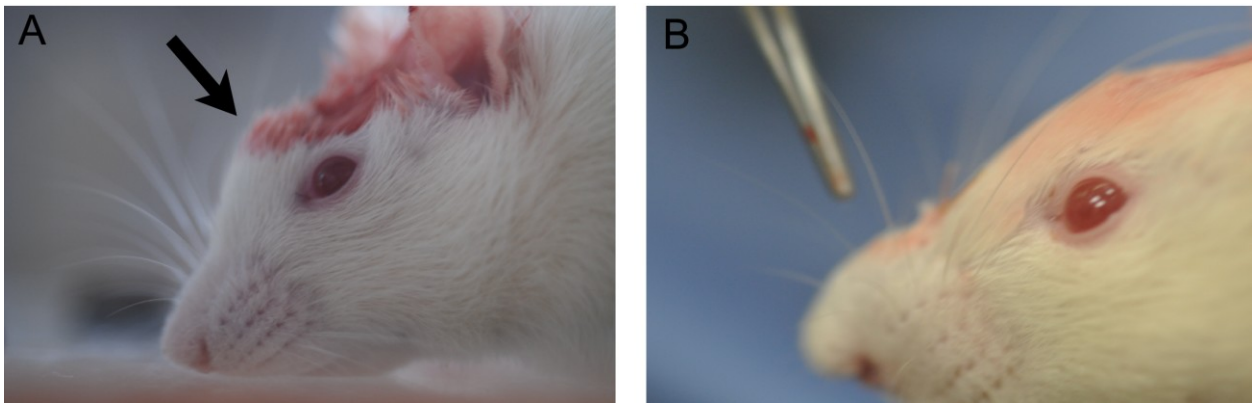

Figure 5.2. Profile pictures of rats immediately after implantation. (A) Groups 1 and 2 were implanted above the bone (B) Group 3 was implanted with half of the scaffold situated above the tip cartilage and half the scaffold above the bone.

top of the nasal bone (**Figure 5.2A**), on the same horizontal plane as the eyes. Scaffolds in Group 3 were placed over the native nasal cartilage, but due to the small size of the native cartilage, half of the implant covered the native cartilage and the other half covered the native bone (**Figure 5.2B**). The incision was sutured closed and one extra suture was placed over the top of the implant to secure it in place (**Figure 5.1C&D**). Two different harvest time points were selected, 6 and 10 weeks, as an initial gage for the time course of tissue formation and whether or not engineered tissue volume could be sustained over time. Therefore, animals from Groups

1 & 2 were sacrificed at 6 weeks and animals from Group 3 were sacrificed 10 weeks postoperatively. Scaffolds were analyzed with histology and immunohistochemistry to evaluate cell recruitment and chondrogenesis.

5.3 Results

PLGA Scaffold Degradation Profile.

PLGA scaffolds made from 10% PLGA appeared to follow a different degradation mechanism compared to 20%-40% PLGA scaffolds. Scaffolds made from 20%-40% PLGA underwent surface degradation, causing their total size to decrease over time (**Figure 5.3A**). On the other hand, 10% PLGA scaffolds underwent bulk degradation. Over time, the scaffold height

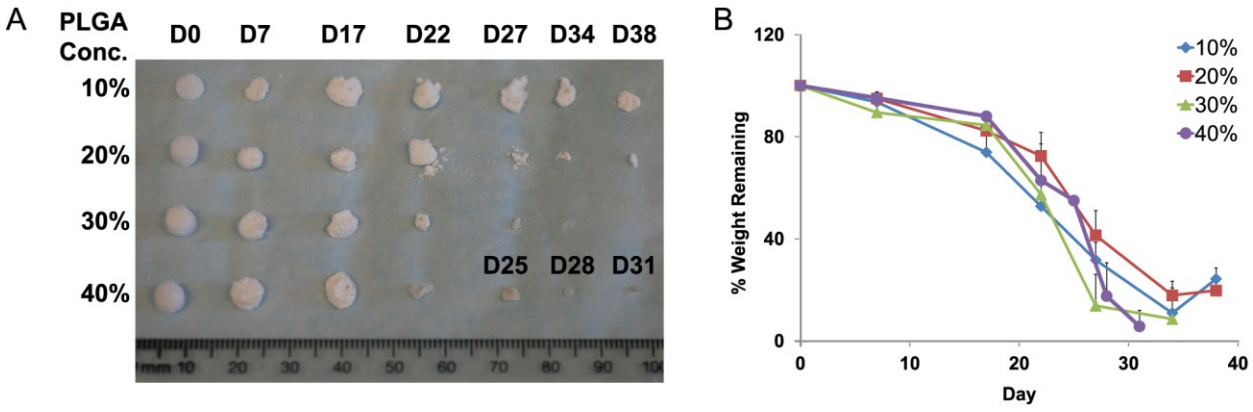

Figure 5.3. PLGA scaffold degradation profile. PLGA scaffolds with concentrations of 10%, 20%, 30% and 40% w/v were subjected to PBS culture for up to 38 days. After each time point, collected scaffolds were lyophilized and (A) imaged to observe scaffold structure. (B) Percent weight change over time was also calculated.

decreased and the width increased, followed by a final structural collapse (**Figure 5.3A**). Scaffolds made from 40% PLGA degraded the fastest of all scaffold types, completely disappearing at 31 days, followed by 30% PLGA scaffolds, which degraded at 34 days (**Figure 5.3B**). Scaffolds made from 10% and 20% PLGA followed a similar degradation time course and were mostly degraded after 38 days. At each time point, the percent weight remaining was higher for 20% compared to 10% PLGA, indicating that 20% PLGA might provide a more stable bulk structure for tissue formation over time (**Figure 5.3B**). Scaffolds imaged using Scanning

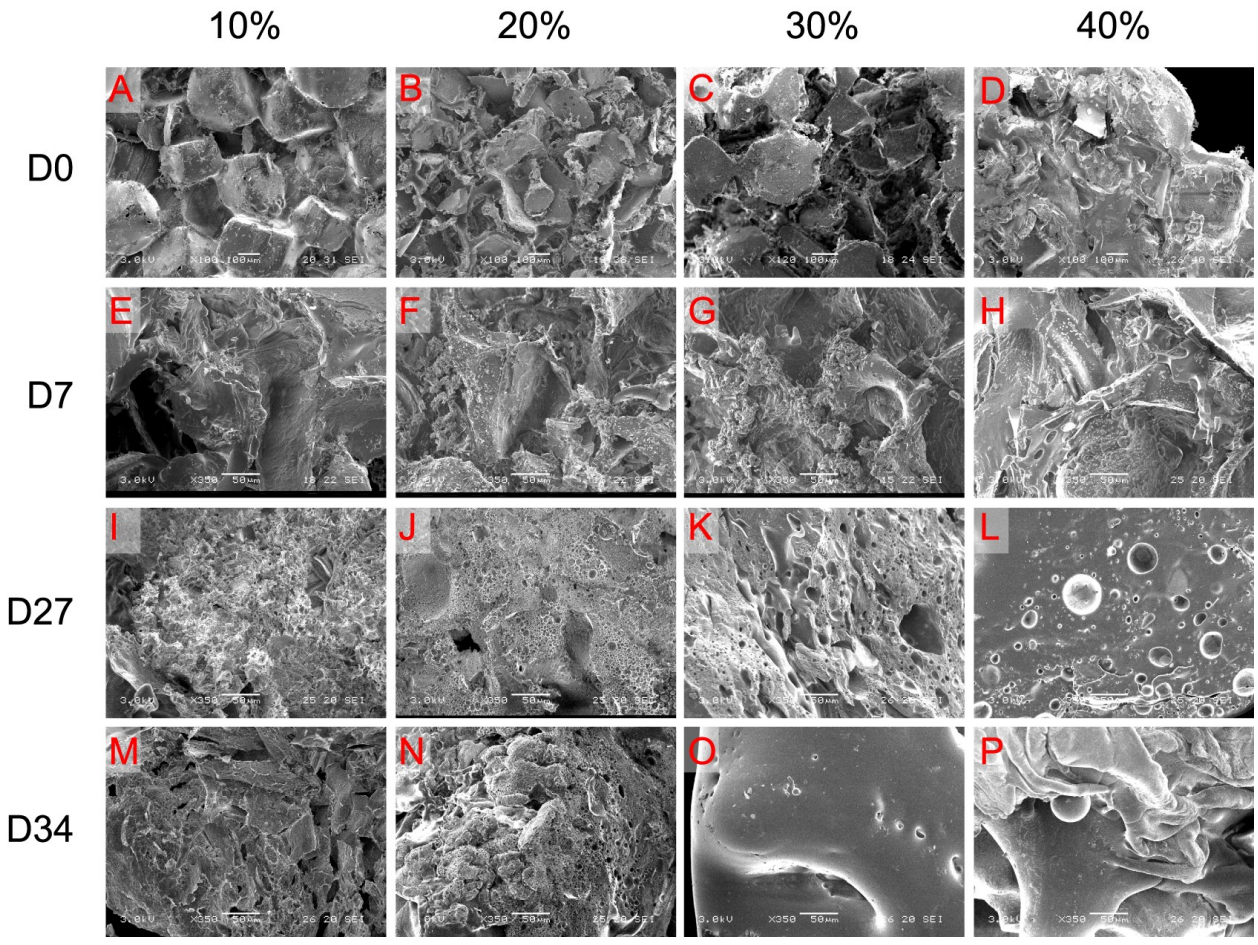

Figure 5.4. SEM images of PLGA scaffold degradation over time. (A-D) Day 0, 100X: 10% (w/v) PLGA, 20% PLGA, 30% PLGA and 40% PLGA, (E-H) Day 7, 350X, (I-L) Day 27, 350X, (M-P) Day 34, 350X. All images were taken at 3.0 kV.

Electron Microscopy revealed a distinct pore structure at the time of fabrication formed by the leaching of salt crystals (**Figure 5.4 A-D**). After 7 days, the smooth internal structural walls began to collapse, and the pore edge roughness increased (**Figure 5.4 E-H**). By day 27, the internal walls of the scaffold were engulfed with small craters (**Figure 5.4 I-L**). A cross-section image taken of 30% PLGA after 17 days of degradation revealed craters forming from the inside of the material, but the material surface remained predominantly smooth (**Figure 5.5**). While the

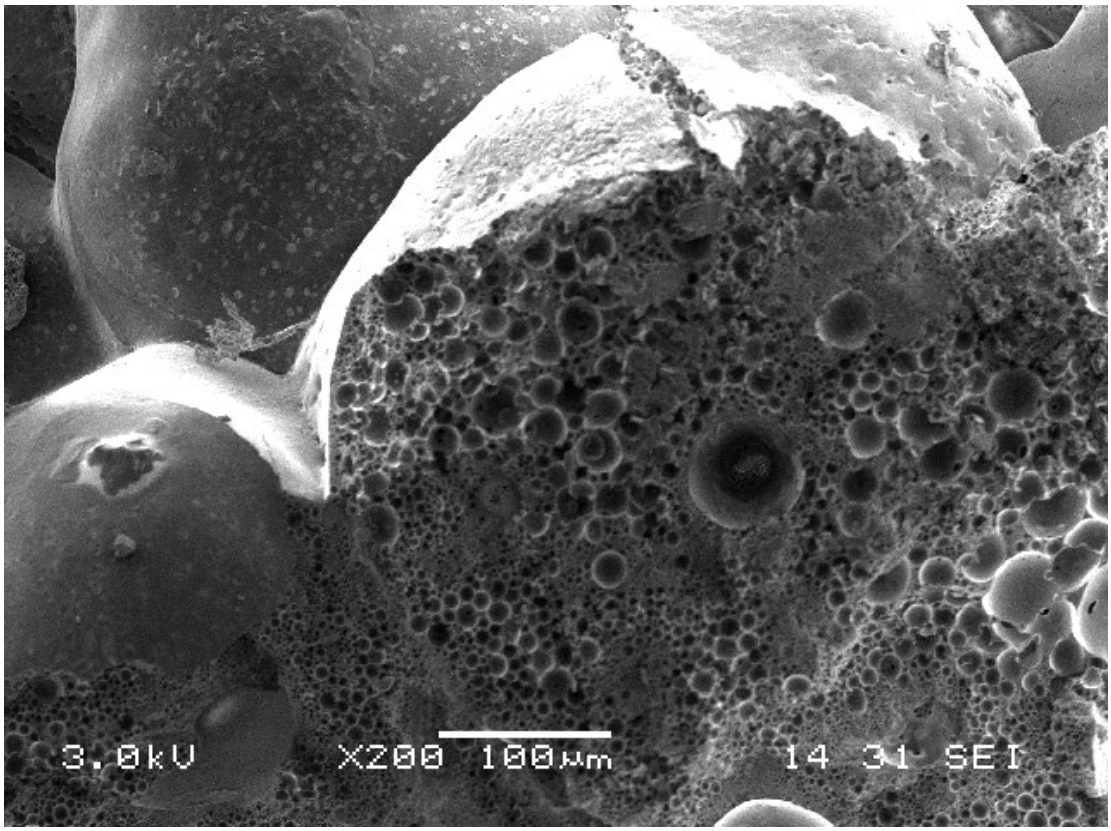

Figure 5.5. Cross-section of 30% PLGA after 17 days of degradation.

internal craters signified bulk erosion, a steady decrease in scaffold size over time indicated surface degradation, thus suggesting that 30% PLGA underwent a possible combinatorial bulk

and surface degradation. The material became physically sticky and difficult to handle by day 34 for 30% PLGA and 40% PLGA scaffolds, likely attributing to the complete pore collapse observed by SEM for 30% and 40% PLGA scaffolds (**Figure 5.4 M-P**).

Calcium Degradation Profile.

To determine if calcium was continuously released from alginate as it degraded, a colorimetric calcium assay was conducted. All three concentrations of $CaCl_2$ used to cross-link alginate promoted a continuous calcium release over time (**Figure 5.6**). At day 32, calcium release from the 100mM samples was a factor of 1.3 greater than the calcium release from the 50mM samples and the calcium release from the 200mM samples was a factor of 2.1 greater than the calcium release from the 50mM samples. Furthermore, at day 32, cumulative release of 200mM $CaCl_2$ was 4.4mM, very close to the value suggested by *Wu et al* for successfully enhancing MSC migration *in vivo*. Therefore, continuous release of $CaCl_2$ by implanted scaffolds fabricated with 200mM $CaCl_2$ should promote an upregulation of the CXCR4 receptor on local stem progenitor cells, which may lead to possible enhanced migration into the scaffold. Thus, all scaffolds fabricated for *in vivo* experiments were made using 200mM $CaCl_2$.

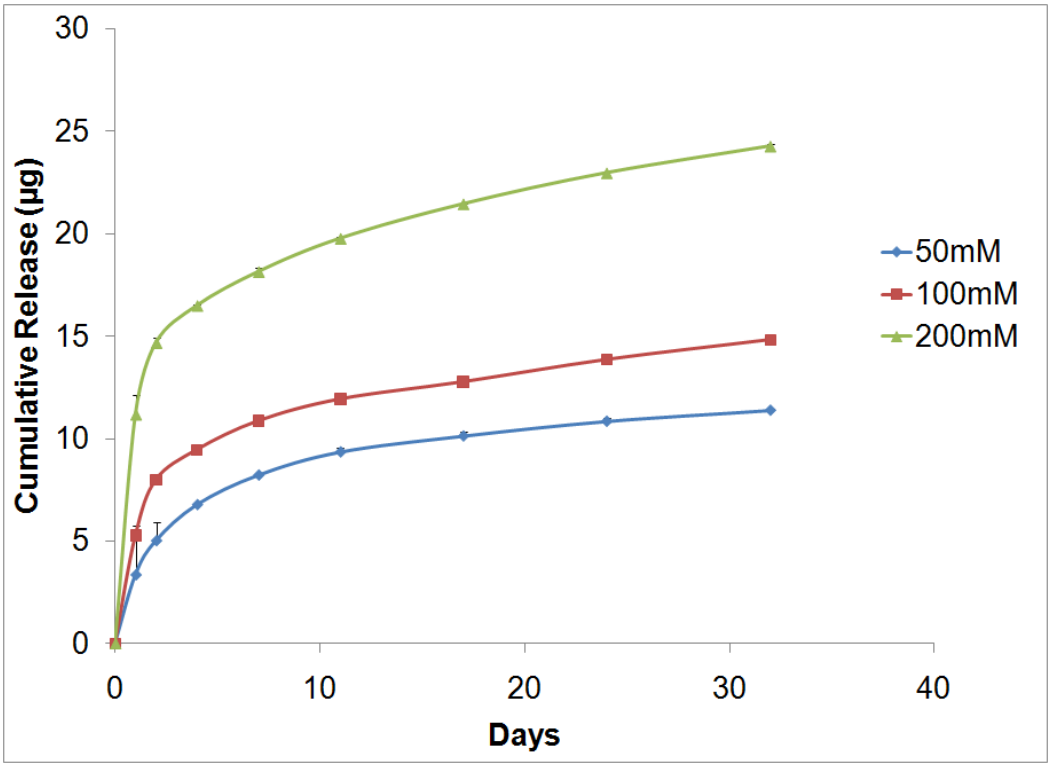

Figure 5.6. Calcium release profile from alginate cross-linked with solutions of 50mM, 100mM and 200mM $CaCl_2$.

Pilot In Vivo Experiments.

Bilayered scaffolds were successfully fabricated with a bottom 20% PLGA layer or collagen sponge layer and a top alginate layer containing gelatin microspheres encapsulating cytokines (**Figure 5.7A**). Gross images of the scaffolds before implantation revealed a very similar morphology among collagen and PLGA scaffolds (**Figure 5.7B & C**). Immediately after implantation, profile images of the rats revealed a distinct augmentation at both implant locations (**Figure 5.2**). After 6 weeks of implantation, harvested scaffolds from all three groups

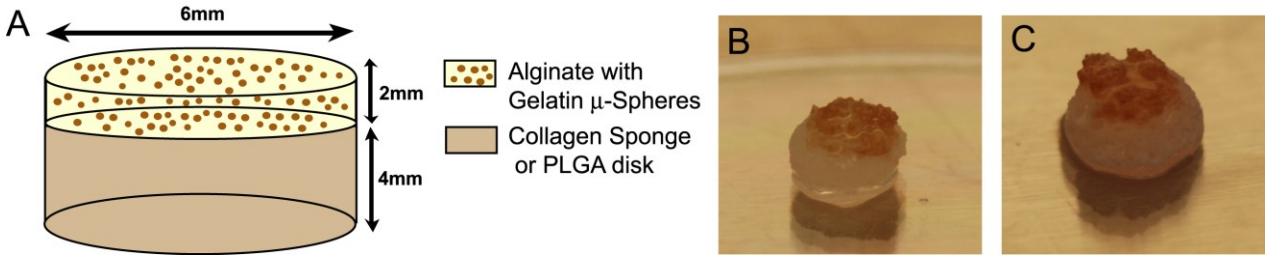

Figure 5.7. Schematics and gross images of rhinoplasty augmentation scaffolds before implantation. **(**A) Schematic of implanted scaffolds. (B) Gross image of collagen based scaffold before implantation and (C) Gross image of PLGA based scaffold before implantation.

displayed cell recruitment into the scaffold and tissue formation (**Figure 5.8**). Interestingly, both the 2-factor PLGA scaffold (Group 2) and the 4-factor PLGA scaffold (Group 3) resulted in tissue formation of the same size (**Figure 5.8B &C)**. Because the 4-factor scaffolds were placed above the native cartilage, scaffold integration with the native tissue could be observed. Remarkably, the 4-factor PLGA scaffold was successful in forming tissue that was integrated with the native cartilage structure (**Figure 5.8C**). Harvested scaffolds were fixed, sectioned, and

Figure 5.8. Gross images of harvested scaffolds from pilot study. (A) Collagen scaffold with SDF1β + TGFβ3 harvested at 6 wks, (B) PLGA scaffold with SDF1β + TGFβ3 harvested at 6 wks and (C) PLGA scaffold with SDF1β + TGFβ3 + IGF1 + PDGFBB harvested at 10 wks. Scaffold was harvested with adjacent native cartilage to demonstrate scaffold integration with native tissue.

subjected to histological analysis to reveal overall cellularity, quality of tissue formation and presence of chondrogenesis. H & E stained scaffolds reveal a large number of migrated cells in scaffolds from each group, indicating the ability for both PLGA and collagen sponge scaffolds to promote cell attachment and tissue formation **(Figure 5.9 A-C)**. Holes present throughout the

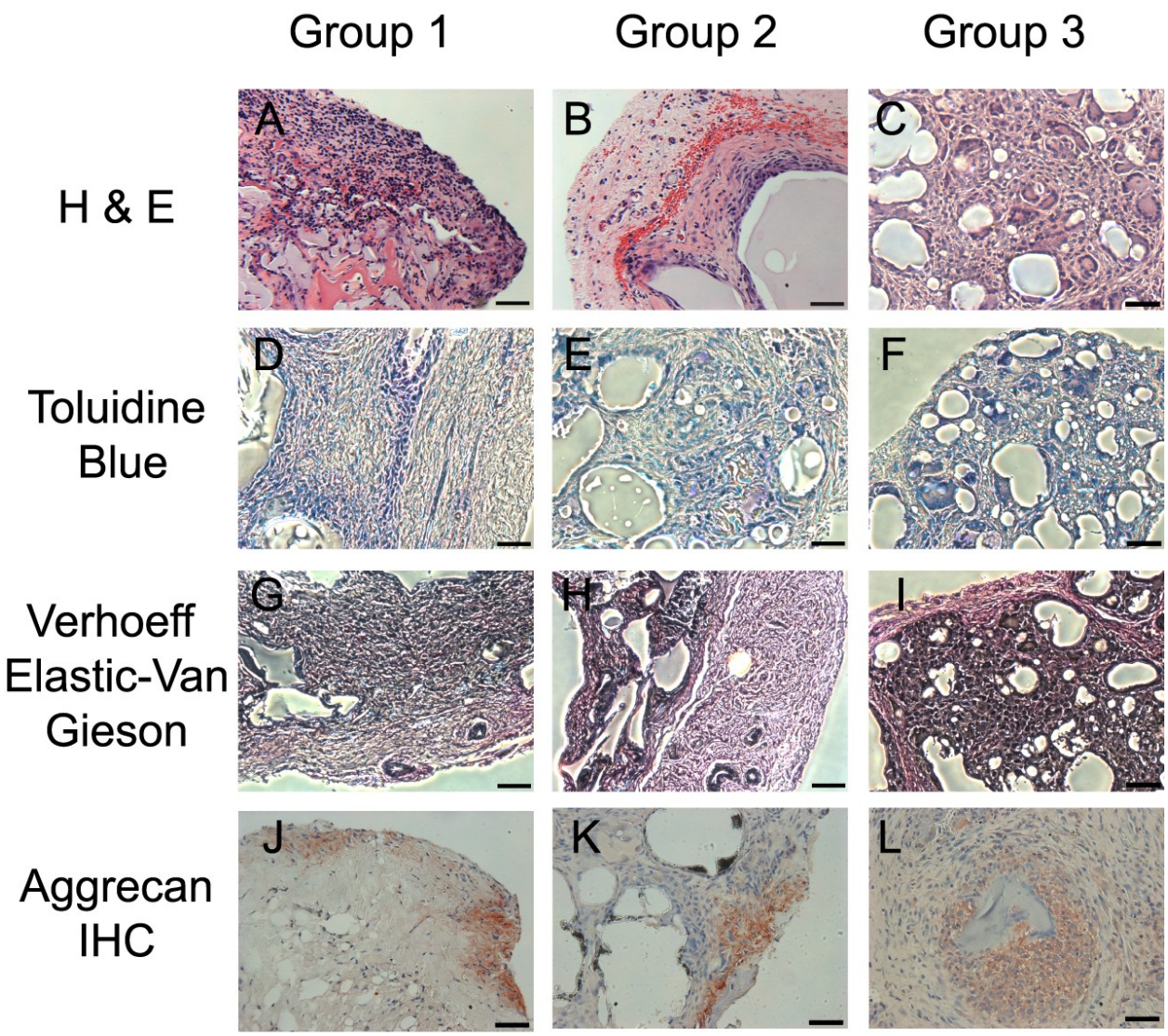

Figure 5.9. Pilot study histological results. Harvested scaffolds were stained for (A-C) Hematoxylin & Eosin (H & E) staining of (D-F) Toluidine Blue, (G-I) Modified Verhoeff Elastic-Van Gieson, (J-K) Aggrecan immunohistochemistry. Scale = 50μm

tissue are thought to be the result of fully degraded gelatin microspheres or alginate that previously occupied the scaffold space, but had not yet filled in with new tissue. Groups 1 & 2 contained a heterogeneous tissue composition, containing an abundant number of red blood cells and inflammatory cells. Group 3 on the other hand, displayed more uniform tissue morphology, with fewer blood cells and immune cells. Toluidine blue staining revealed disperse regions of chondrogenic differentiation for Group 1 and Group 2 with slightly more prominent staining present for Group 3 (**Figure 5.9 D-F**). Modified Verhoeff Elastic-Van Gieson staining for elastic cartilage tissue formation revealed weaker staining for Group 1, increased staining for Group 2, and very prominent staining for Group 3 **(Figure 5.9G-I)**. Immunohistochemistry staining revealed the presence of aggrecan in selected regions of the tissue **(Figure 5.9J-L)**. Aggrecan staining in Groups 1 and 2 was located at the scaffold periphery (**Figure 5.9J-K**), whereas aggrecan staining for Group 3 was located in the region surrounding the gelatin microspheres (**Figure 5.9L**).

Second Round of In Vivo Experiments.

While the number of homed cells present in Groups 1-3 was remarkable, only selected regions of the scaffold became chondrogenic. The cell number present in the scaffold appeared to be higher than the cell number found in native cartilage. The heterogeneous tissue formed in the scaffold was thought to be a combination of chondrogenic cells in addition to immune cells and fibroblasts. The immune cells were believed to be recruited by SDF1β, because in addition to its ability to recruit stem/progenitor cells, SDF1β has also been shown to recruit peripheral blood lymphocytes, monocytes, B-cells and T-cells [137]. Immediately after scaffolds from Group 3 were implanted, significant swelling localized to the rat face was noted but disappeared after 24 hours. This was thought to be the result of PDGFBB that was released locally in the

face. The local inflammation recruited many immune cells to the scaffold location. While PDGFBB was shown to have a strong chemotactic ability in Chapter 4, it also induced inflammation, which was a hindrance to tissue formation. Thus, PDGFBB was not used for subsequent experiments.

Table 5.2: Experimental design for second round of *in vivo* experiments.

Group #	# of Rats	Harvest Time Point	Scaffold Condition
4	3	10 wks	Control – Cartilage Scoring
5	3	10 wks	Control – 20% PLGA Scaffold without GFs + Cartilage Scoring
6	3	10 wks	20% PLGA Scaffold + 200ng TGFβ3 + Cartilage Scoring
7	3	10 wks	20% PLGA Scaffold + 500ng TGFβ3 + Cartilage Scoring
8	3	10 wks	10% PLGA Scaffold + 500ng TGFβ3 + Cartilage Scoring
9	3	10 wks	20% PLGA Scaffold + 1000ng TGFβ3 + Cartilage Scoring
10	3	6 wks	20% PLGA Scaffold + 1000ng TGFβ3 + Cartilage Scoring
11	3	10 wks	40% PLGA Scaffold + 1000ng TGFβ3 + Cartilage Scoring

Pilot study results indicated a need for improved scaffold design to recruit mostly progenitor cells that can become chondrogenic, and limit the number of immune and fibroblast

cells recruited. A second round of *in vivo* experiments was designed (**Table 5.2**) with two control groups (Groups 4-5) and five experimental groups (Groups 6-11). To determine if SDF1β recruited inflammatory cells into the scaffold, Groups 6-11 only released TGFβ3 from the scaffolds. Recently, it was discovered that large numbers of multipotent mesenchymal progenitor cells are present in the superficial and middle zones of adult cartilage [138]. We hypothesized that a method of increasing the number of progenitor cells available locally around the scaffold would be to score the native cartilage tissue to activate and release some of the native progenitor cells. Control conditions were tested to isolate the effects of cartilage scoring alone (Group 4) as well as to delineate the role of the cytokines in tissue formation from that of the biomaterials alone (Group 5). Groups 6-11 tested three different doses of TGFβ3 delivery (200ng, 500ng and 1000ng) to determine the optimal dose for promoting cell migration and chondrogenesis. Because 10% PLGA appeared to undergo a surface degradation compared to 20% PLGA which appeared to undergo bulk degradation, it was hypothesized that the number of holes present in the harvested tissue would be reduced with 10% PLGA. Thus, two groups were included in follow-up studies with the same concentration of TGFβ3 delivery, but one group contained a 10% PLGA scaffold (Group 8) whereas the other group contained a 20% PLGA scaffold (Group 7). At the time of scaffold implantation, the native tip cartilage tissue was scored for all groups. In an effort to further reduce inflammation, all groups also included the administration of Carprofen, a non-steroidal anti-inflammatory drug (NSAID), at the beginning of surgery. To better understand the timeline of cell recruitment and chondrogenesis, two groups were included with identical scaffold conditions, but one group was harvested at an early time point of 6 weeks (Group 10), whereas the other group was harvested after 10 weeks (Group 9). To create a more pronounced augmentation with a stiffer feel, a group was added using 40% PLGA (Group 11). Identical cytokine conditions were used in Group 9 and Group 11 to delineate the effect of scaffold material alone on cell recruitment and chondrogenesis. Three rats were

tested in each group and harvested after 6 or 10 weeks for analysis of cell recruitment and chondrogenesis.

Round 2 In Vivo Experiment Results.

Profile images taken immediately before and after scaffold implantation indicated that both 10% and 20% PLGA scaffolds successfully created an augmentation (**Figure 5.10**).

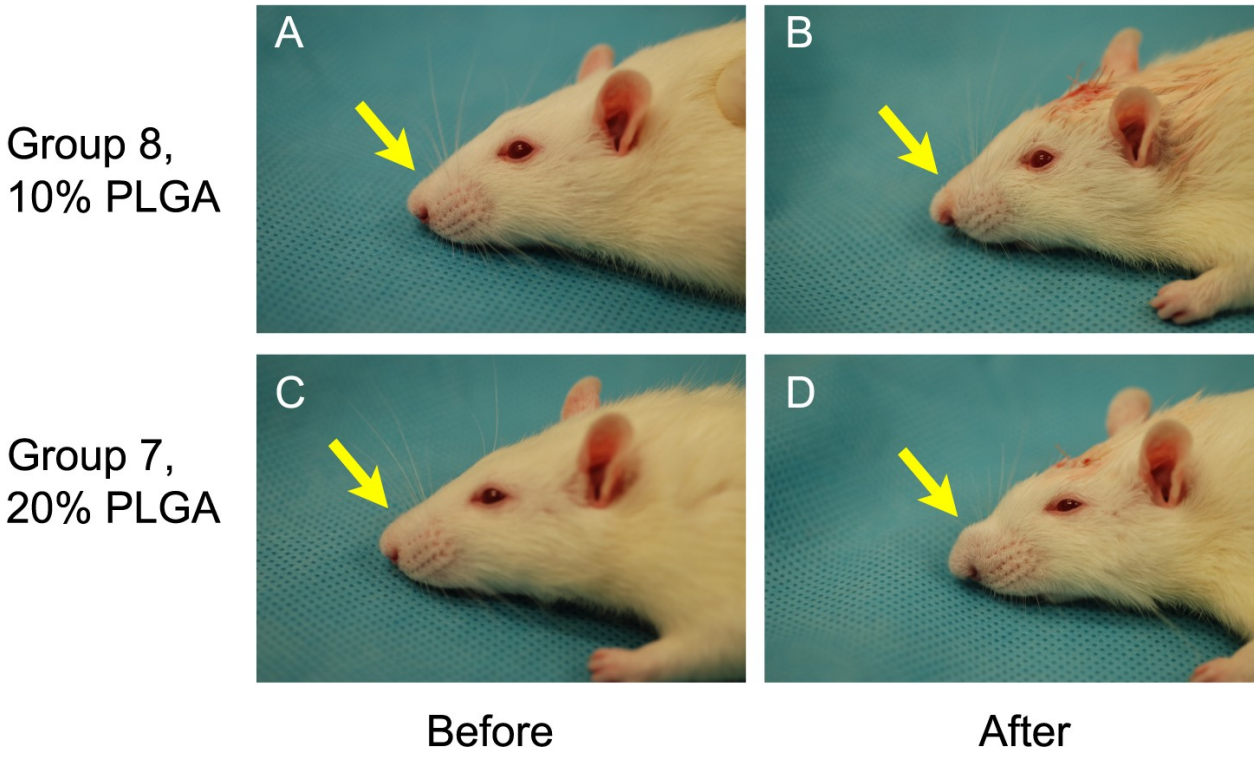

Figure 5.10. Profile pictures of rhinoplasty augmentation before and immediately after surgery. Rat receiving Group 7 scaffold made from 10% PLGA is shown (A) before surgery and (B) after surgical implantation. Rat receiving Group 8 scaffold made from 20% PLGA is shown (C) before surgery and (D) after surgical implantation. The 20% PLGA scaffolds resulted in a larger augmentation immediately after implantation compared to the 10% PLGA scaffolds.

However, 20% PLGA (**Figure 5.10D**) created a distinctly larger augmentation compared to 10% PLGA scaffolds (**Figure 5.10B**). After 10 weeks of implantation, profile images were taken immediately after animal eutheasia to reveal the level of augmentation visibly remaining (**Figure 5.11 A-H**), during the dissection (**Figure 5.11 A'-H'**), and after scaffold dissection to compare scaffold sizes within groups (**Figure 5.11 A"-H"**). No visible ectopic tissue could be seen in Group 4, which only received cartilage scoring. For this group, perichondrium was isolated for use as a control to distinguish engineered tissue in other groups from native perichondrium tissue (**Figure 5.11 A"**). Group 5 control scaffolds displayed minimal ectopic tissue formation in two rats and no visible ectopic tissue formation in the third rat (**Figure 5.11 B"**). An increase in tissue formation could be seen due to increasing doses of TGFβ3 delivery (**Figure 5.11 C", D"** and **F"** respectively). Interestingly, 10% PLGA (**Figure 5.11 E"**) promoted larger ectopic tissue formation compared to 20% PLGA (**Figure 5.11 D"**). Since 10% PLGA underwent surface degradation *in vitro*, a larger scaffold surface area remained over time, potentially providing recruited cells *in vivo* with more space for tissue formation compared to scaffolds made from 20% PLGA. Remarkable glistening white tissue formation could be seen due to the highest dose of TGFβ3 delivery (**Figure 5.11 F'**). The combination of large ectopic tissue size and white tissue color set this group apart from all other groups. After tissue removal in Group 9 (**Figure 5.12A and B**), images of a smooth underlying bone confirmed that the tissue formation was not causing negative pathology to the underlying bone (**Figure 5.12C**). Tissue harvested after 6 weeks (**Figure 5.11 G"**) was much larger than tissue harvested after 10 weeks (**Figure 5.11 F"**). This indicates a potential issue in maintaining tissue volume over time. However, MSCs have been shown to condense in size as they undergo chondrogenesis, which might contribute

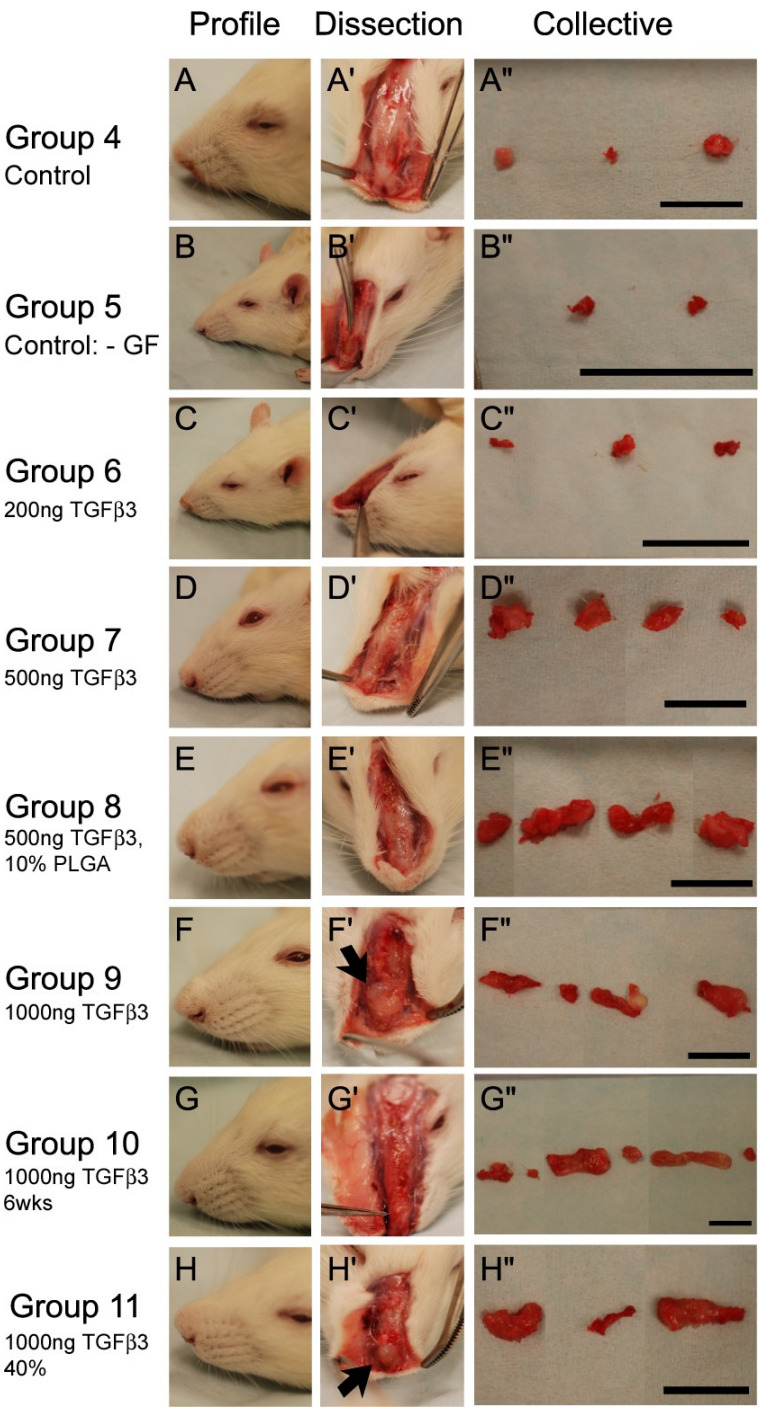

Figure 5.11. Gross images of rhinoplasty harvests for groups 4-11. Profile images were taken immediately after harvest for visualization of remaining augmentation (A-H) and any ectopic tissue formation was dissected out (A'-H'). Harvested tissue from each rat in the experimental group was imaged together (A"-H"). Note: harvested tissue in D", E", F" and G" consisted of two parts for some rats. Scale = 1 inch.

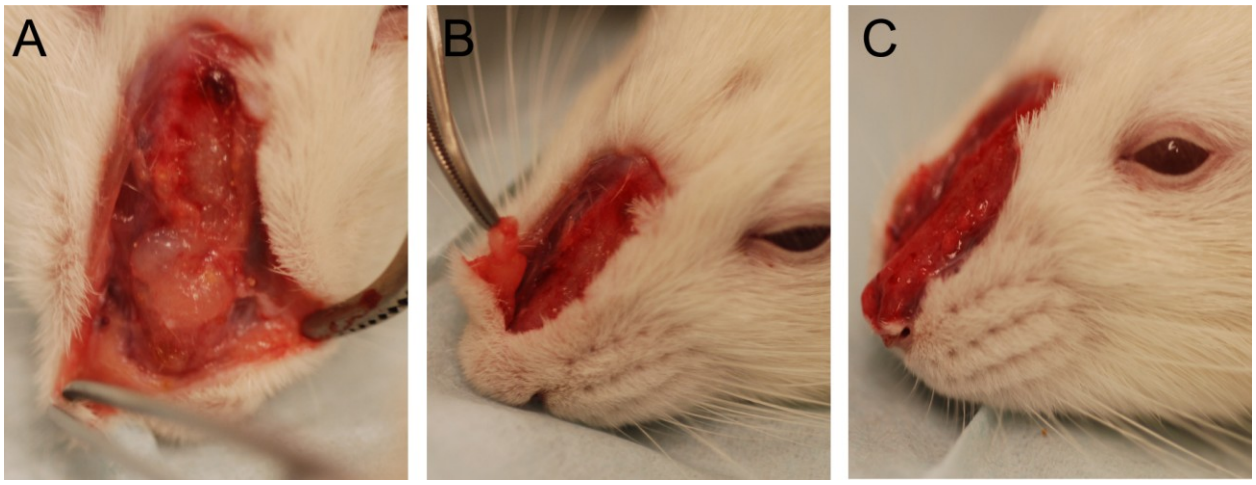

Figure 5.12. Ectopically engineered tissue does not disturb underlying bone. Gross images were taken of the engineered tissue from group 11 (A) before dissection, (B) during dissection and (C) after dissection showing a healthy underlying bone surface.

to the decrease in tissue volume over time [139, 140]. Scaffolds made from 40% PLGA (**Figure 5.14 H"**) did not display a clear difference in tissue size compared to 20% PLGA (**Figure 5.14 F"**). H & E staining of harvested scaffolds revealed no significant differences in tissue morphology between the perichondrium isolated in Group 4 (**Figure 5.13B**) and the fibrous tissue isolated from the growth factor-free scaffolds used in Group 5 (**Figure 5.13C**). Scaffolds in Groups 6-11 (**Figure 5.13D-L**) had distinctly different tissue morphology compared to the Group 4 control (**Figure 5.13B**). None of the scaffolds in Groups 4-11 indicated the presence of blood cells or immune cells (**Figure 5.13**). Thus, blood cells and immune cells previously evident in Groups 1-3 were attributed to SDF1 delivery and/or lack of Carprofen NSAID administration prior to surgery. Fewer holes in tissue formation were evident in Group 8 (**Figure 5.13H**) compared to Group 7 (**Figure 5.13I**), confirming our hypothesis that the holes were a result of material degradation at a speed faster than new tissue formation. Scaffolds made from

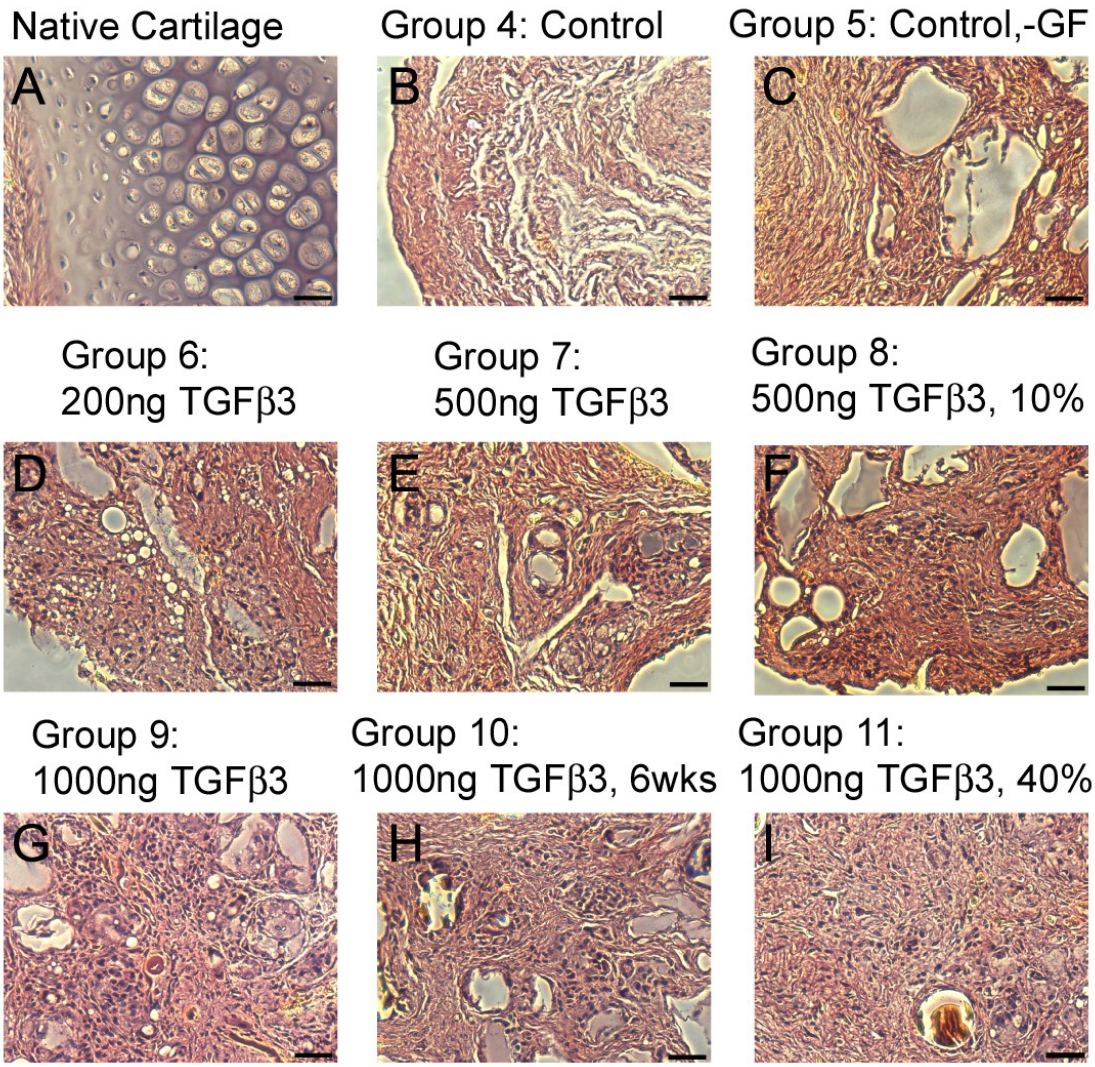

Figure 5.13. Hematoxylin & Eosin (H & E) staining of harvested tissue from second round of *in vivo* experiments. (A) Native Cartilage, (B) Group 4, (C) Group 5, (D) Group 2, (E) Group 1, (F) Group 3, (G) Group 6, (H) Group 7, (I) Group 8, (J) Group 9, (K) Group 10, (L) Group 11. Scale = 50μm

40% PLGA (**Figure 5.13L)** promoted more uniform tissue formation with less residual scaffold material compared to scaffolds made from 20% PLGA (**Figure 5.13J)**, indicating that tissue formed in Group 11 at a rate equivalent to the material degradation time.

Chondrogenic differentiation was observed based on the presence of positive Toluidine Blue staining (**Figure 5.14**) and immunohistochemical staining for aggrecan (**Figure 5.15**). Control groups did not display any positive staining for chondrogenesis among Group 4 (**Figure 5.14B**)

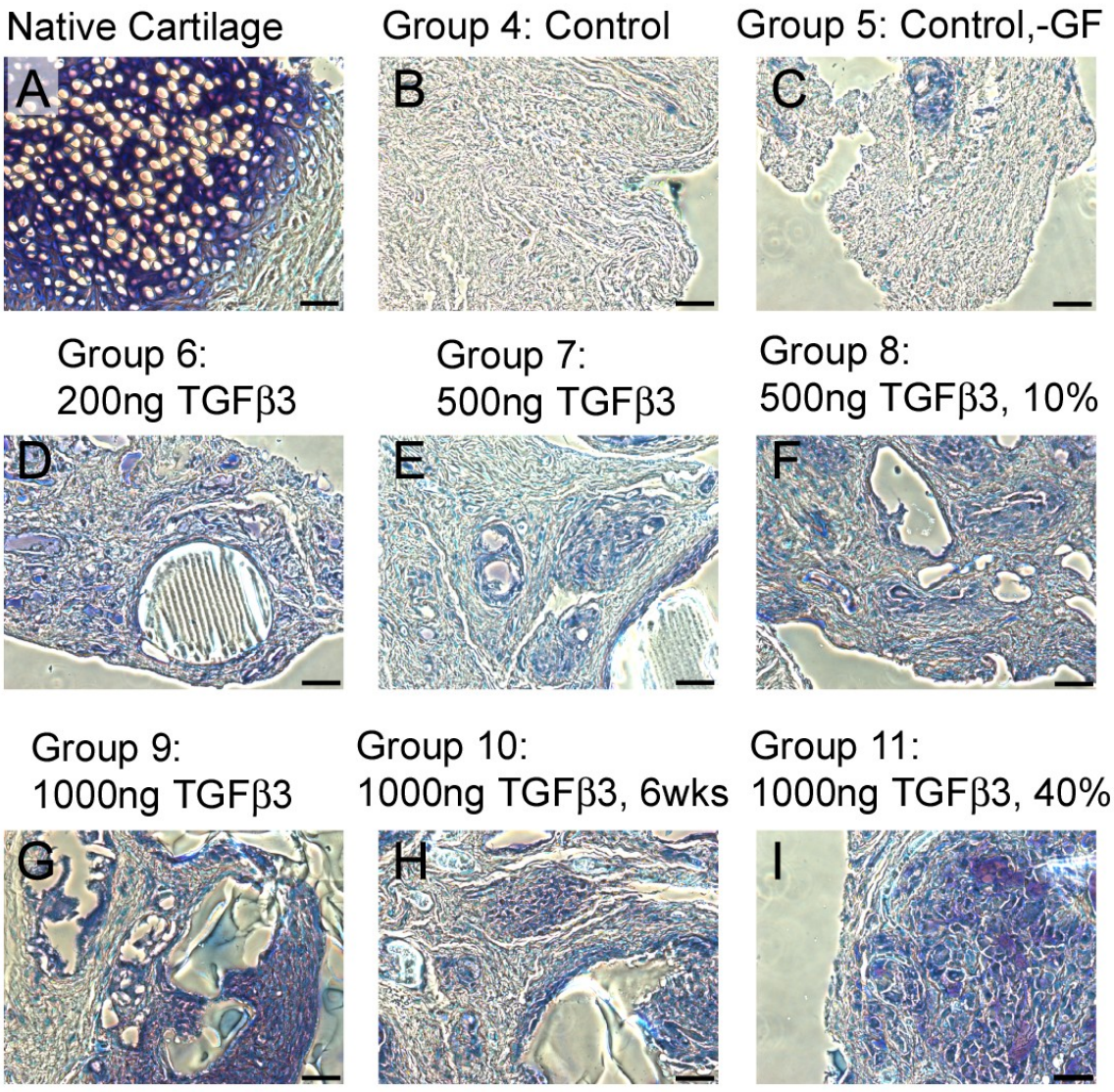

Figure 5.14. Toluidine Blue staining of harvested tissue from second round of *in vivo* experiments. (A) Native Cartilage, (B) Group 4, (C) Group 5, (D) Group 2, (E) Group 1, (F) Group 3, (G) Group 6, (H) Group 7, (I) Group 8, (J) Group 9, (K) Group 10, (L) Group 11. Scale = 50μm

and minimal staining for Group 5 (**Figure 5.14C**). Increasing levels of chondrogenesis was evident due to increasing doses of TGFβ3 delivery (**Figure 5.14 G", I"** and **K"** respectively). Chondrogenic differentiation was more prominent among Group 10 (**Figure 5.14J**) tissue compared to Group 9 (**Figure 5.14K**). Thus, the loss in tissue volume over time might be due to tissue degradation and not condensation due to increasing chondrogenesis. Marked chondrogenesis was observed among Group 11 (**Figure 5.14L**) scaffolds compared to Group 9 (**Figure 5.14K**) scaffolds, suggesting that in addition to cytokine delivery, the higher material concentration used in Group 11 might play a role in chondrogenesis since both Group 9 and Group 11 received identical cytokine delivery. One possible explanation for this effect results from the difference in material stiffness. The stiffer material used in Group 11 might have been able to promote enhanced chondrogenic differentiation compared to the less stiff material used in Group 9, as suggested by previous reports [141]. Cartilage scoring seemed to have an overall effect of increased chondrogenesis (**Figure 5.14G-L**). However, follow-up studies are necessary to confirm these observations, since the groups that did not receive cartilage scoring had varied cytokine delivery.

The results of the toluidine blue staining were confirmed with the presence of positive aggrecan immunohistochemical staining (**Figure 5.15**). Minimal aggrecan staining was present among the control groups (**Figure 5.15 B and C**). Higher doses of TGFβ3 delivery (**Figure 5.15 G-I**) promoted enhanced aggrecan staining compared to lower delivery doses (**Figure 5.15 D-F**). Aggrecan staining was primarily located in the region surrounding the cytokine releasing microspheres (**Figure 5.15 D-I**). This could be an indication that the cytokines were only able to diffuse a limited distance from the microspheres and promote chondrogenic differentiation in this region. Future scaffolds designs should have an increased material permeability to promote more uniform cytokine diffusion and chondrogenic differentiation. Alternatively, including a

higher concentration of microspheres in future scaffold designs could eliminate cytokine diffusion limitations and promote more uniform cartilage formation.

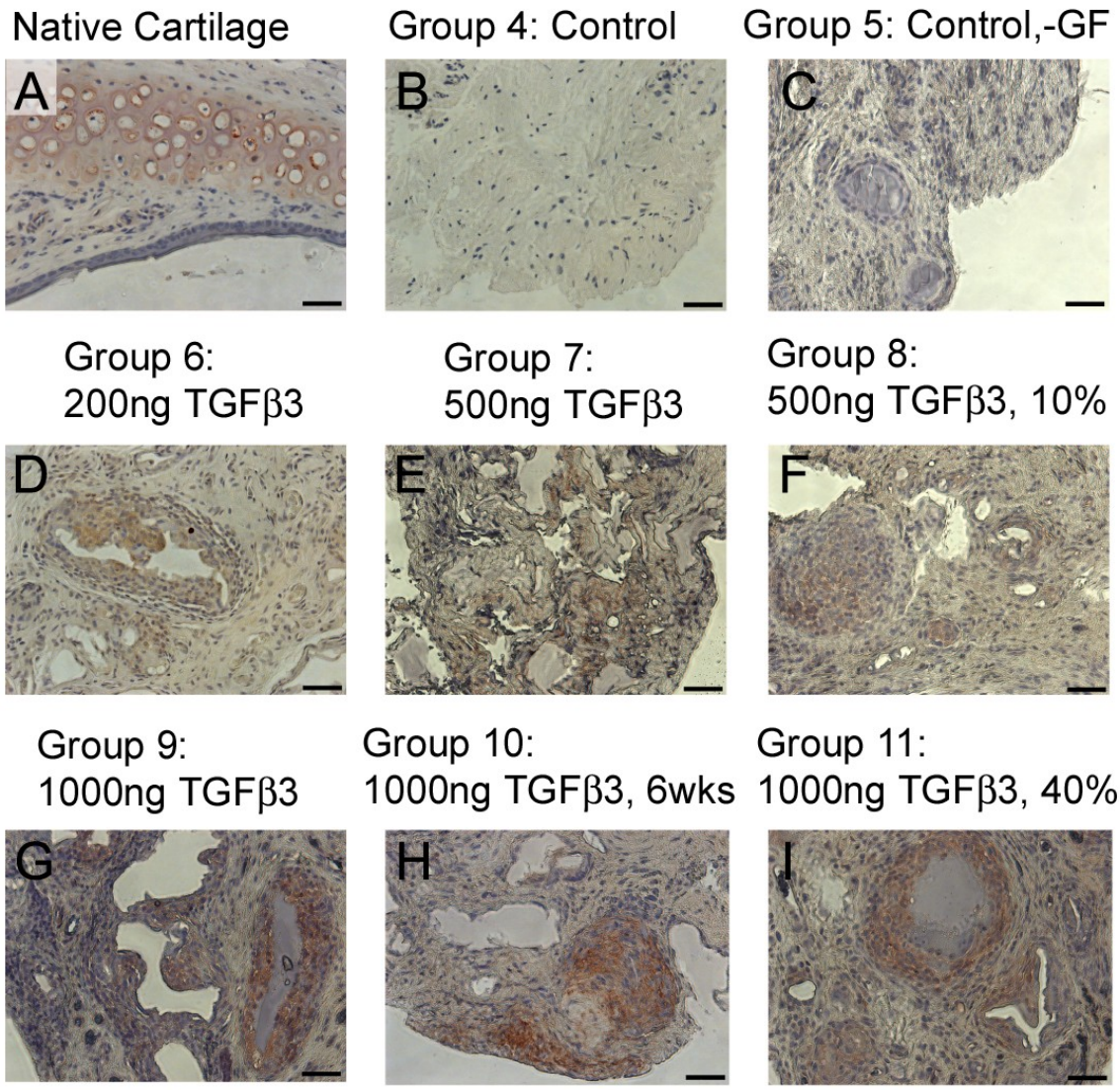

Figure 5.15. Aggrecan immunohistochemical staining of harvested tissue from second round of *in vivo* experiments. (A) Native Cartilage, (B) Group 4, (C) Group 5, (D) Group 2, (E) Group 1, (F) Group 3, (G) Group 6, (H) Group 7, (I) Group 8, (J) Group 9, (K) Group 10, (L) Group 11. Scale = 50μm

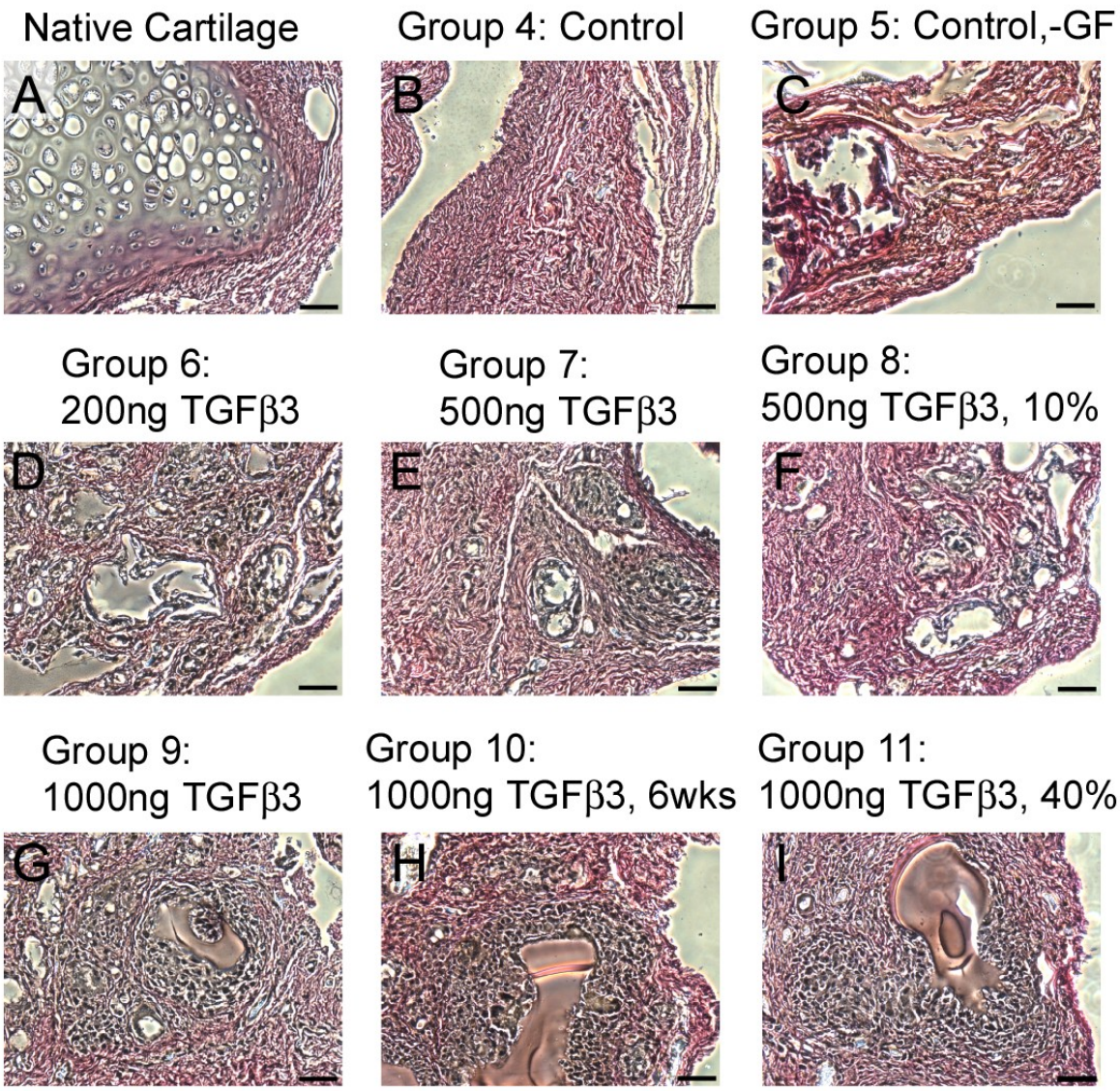

Figure 5.16. Modified Verhoeff Elastic-Van Gieson staining for elastic cartilage of harvested tissue from second round of *in vivo* experiments. (A) Native Cartilage, (B) Group 4, (C) Group 5, (D) Group 2, (E) Group 1, (F) Group 3, (G) Group 6, (H) Group 7, (I) Group 8, (J) Group 9, (K) Group 10, (L) Group 11. Scale = 50μm

Elastic cartilage formation was determined based on the presence of positive modified Verhoeff Elastic-Van Gieson staining (**Figure 5.16**). Positive elastic cartilage formation was not evident in the control groups (**Figure 5.16B** and **C**). Increased elastic cartilage staining was observed among Groups 9-11, which delivered a high-dose of TGFβ3 (**Figure 5.16J-L**),

compared to Groups 6-8, which delivered lower doses of TGFβ3 (**Figure 5.16G-I**). In particular, positive elastic cartilage staining was concentrated around cytokine-releasing microspheres as observed by the aggrecan staining.

5.4 Discussion

Ectopic cartilage-like tissue was engineered using novel bioactive scaffolds with slow-releasing cytokines and without the use of cell-transplantation. To our knowledge, this is the first attempt at applying cell homing approaches to engineer cartilage tissue for rhinoplasty augmentation. This innovative approach combines the advantage of autologous donor tissue for creating a natural feel with the advantages of biomaterial implants to produce a readily available off-the-shelf product.

Bilayered bioactive scaffolds designed in Chapter 2 were shown to be successfully translated *in vivo* for ectopic tissue engineering. Although the scaffold design was able to induce cells to migrate into the scaffold and chondrogenically differentiate, the original collagen sponge material used in Chapter 2 was very soft and did not create a pronounced augmentation. Since implant shape is a critical factor for cosmetic applications, PLGA was selected as the implant material for subsequent *in vivo* experiments, because of its increased rigidity compared to collagen sponge. In addition to creating a pronounced augmentation, PLGA scaffolds promoted cell attachment and chondrogenic tissue formation, thus proving to be a successful alternative to collagen sponge. A major concern of current biomaterial-based implants for rhinoplasty augmentation is graft extrusion. When bioactive PLGA scaffolds were implanted above the native tip cartilage, scaffolds were able to integrate with the native tissue, reducing the chances for implant extrusion.

A major challenge in cell homing therapies for tissue engineering is recruiting the desired cell type and preventing unwanted cells from being recruited. Pilot studies incorporating SDF1β in the scaffold design resulted in engineered tissue containing many immune cells and blood cells in addition to chondrogenic tissue. Immune cells in the tissue might promote local inflammation, leading to decreased tissue volume over time. In an attempt to prevent the recruitment of immune cells and blood cells, new scaffold designs eliminated the delivery of SDF1β. Delivery of various concentrations of TGFβ3 alone was able to induce cell recruitment and chondrogenesis at a dose dependent concentration. Engineered tissue did not contain any blood cells and had a more homogeneous morphology, confirming that SDF1β was responsible for recruiting unwanted blood and immune cells.

Initially it was unknown if the high concentration of TGFβ3 locally released from Groups 9-11 would be toxic to surrounding cells and promote local tissue necrosis. However, after 10 weeks of implantation, visual inspection of the tissues surrounding the implant did not reveal any necrotic tissue. Furthermore, after the implants were removed, the underlying bone surface appeared healthy. Therefore, high concentrations of locally released TGFβ3 do not appear toxic to surrounding tissues.

Pilot experiments indicated that tissue engineered cartilage was heterogeneous and chondrogenesis was selectively present throughout the tissue. Cartilage scoring was added to subsequent groups in an attempt to mobilize local stem/progenitor cells present in the native cartilage tissue. The idea initially stemmed from current orthopedic treatments for cartilage tissue engineering, which use microfracture to promote limited tissue repair. It was unknown whether or not these results would be translated to the nasal cartilage, since a bone-marrow source is not present around the nasal cartilage. Gross-examination of harvested tissue displayed larger ectopic tissue formation amongst groups that received cartilage scoring

compared to groups that did not receive cartilage scoring. Histological analysis of harvested tissue revealed increased cartilage matrix as evident by Toluidine Blue staining amongst groups that received cartilage scoring. While these initial signs indicate that cartilage scoring had a positive impact on cartilage tissue engineering, additional experiments are necessary to confirm these results. Harvested tissue could be stained at early time points before chondrogenesis occurs for the presence of stem cell markers to confirm that cartilage scoring led to the recruitment of stem cells. Groups that did not receive cartilage scoring treatment contained scaffolds with different growth factor combinations than groups that received cartilage scoring treatment. Thus, a better evaluation of cartilage scoring effectiveness to be tested in future experiments would be to test identical scaffold conditions with and without cartilages scoring.

An important feature for rhinoplasty augmentation grafts is the ability to tailor the graft to the individual patient. Autologous grafts are stacked and sutured together in a bundle before implantation. The bioactive PLGA scaffolds can be easily modified to create larger augmentations by decreasing the mold diameter used to create the PLGA scaffold base. By keeping the PLGA liquid volume constant, using a smaller mold diameter would increase the thickness of the PLGA layer. For an off-the shelf product, three different scaffolds could be created with small, medium and large default sizes and easily trimmed for precise adjustments. Thus, the PLGA bioactive scaffold could potentially be used as a novel alternative implant design to current rhinoplasty augmentation treatment.

5.5 Future Studies

Bioactive scaffolds that slow-released TGFβ3 were able to successfully recruit local cells and induce chondrogenic differentiation of the recruited cells for cartilage tissue engineering.

However, the cell populations that were recruited in this tissue were unknown. In an attempt to better understand the cell types involved, three different primary cell populations were isolated from 12 week old male rats: septal cartilage cells, tip cartilage cells and bone marrow MSCs (**Figure 5.17**). Septal cartilage and tip cartilage were removed by dissection, minced and subjected to enzymatic digestion in a solution containing 3mg/mL Collagenase and 4mg/mL Dispase for 4 hours in a shaking water-bath. Large particles were filtered out of the solution and

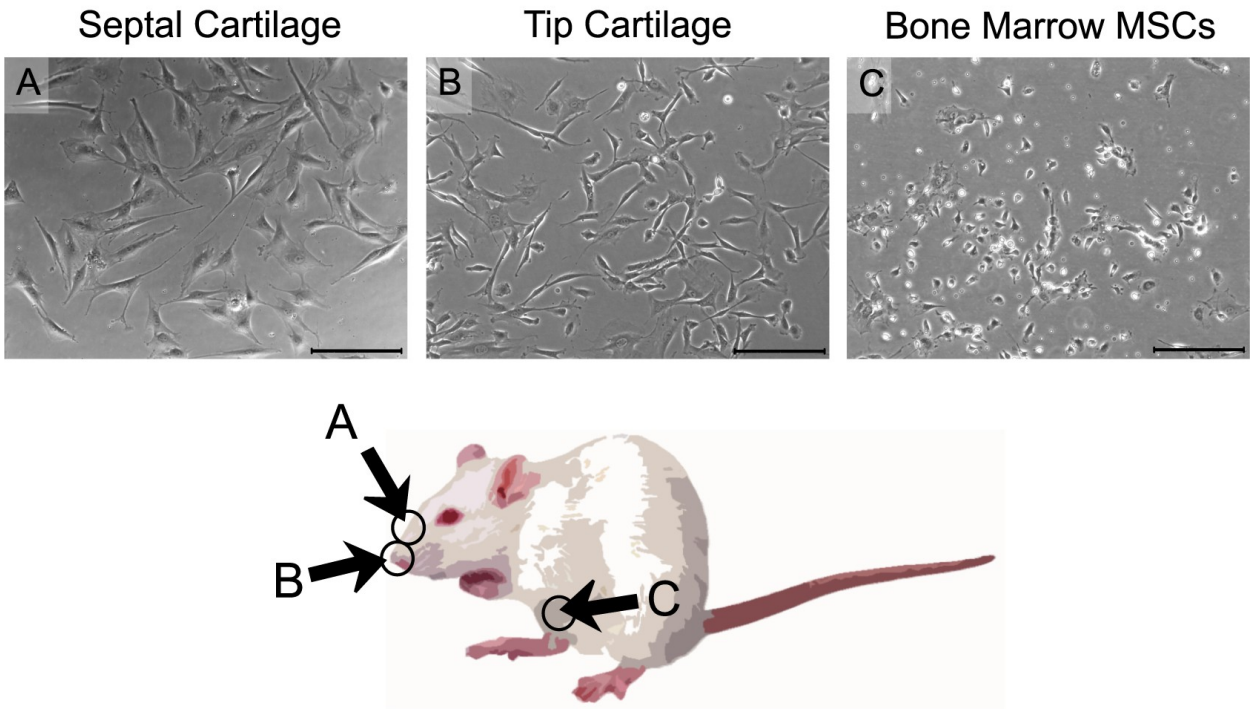

Figure 5.17. Cell Isolation to investigate potential stem/progenitor cell sources for rhinoplasty augmentation by cell homing. Cells were isolated for culture from (A) Nasal septal cartilage, (B) Nasal tip cartilage and (C) Bone Marrow. Scale = 200μm

cells were plated for culture. Bone marrow MSCs were isolated from the bone marrow of the tibia. Cells from three rats were pooled together to increase cell number. Culture medium consisted of DMEM containing 20% FBS, 1% AB/AM, 1% L-glutamine and 0.1% 2-

Mercaptoethanol. Distinct morphology variations could be seen amongst the three cell types. Septal cartilage cells (**Figure 5.17A**) and tip cartilage cells appeared spindle-like (**Figure 5.17C**) compared to the triangular shaped MSCs (**Figure 5.17C**). Size differences between the cells were also noted with the septal cells displaying the largest size, followed by the tip cartilage cells and MSCs.

Future experiments are planned to characterize the isolated cells for stem/progenitor cell properties. Flow cytometry will be used to investigate cell surface markers for the expression of CD90, CD45, CD105, CD73 and CD146. These values will be used to quantify the percentage of stem/progenitor cells among this population. Stem cell populations from all three cell types can then be sorted using FACS followed by the generation of cell clones for studies of differentiation and migration. Stem cell clones from these three cell types will be subjected to 3D pellet culture in the presence of chondrogenic medium. Pellets will be collected and stained with chemical stains for general cartilage matrix markers and immunohistochemistry for specific cartilage matrix markers (Col II/AGC/Sox 9). Additional pellets will be digested for PCR analysis for measuring cartilage specific genes (Col II/AGC/Sox 9). Migration studies will be conducted using the competition devices discussed in Chapter 4. Clonal progeny that are chondrogenic will be seeded on the peripheral wells of the migration device and simultaneously exposed to a single chemotactic factor. Cytokines with proven chemotactic effects amongst MSCs will be initially used for testing. Clones that are particularly chemotactic will be further studied to determine if cell surface receptors exist that are unique to these cells compared to clones that are not chemotactic. These cell surface receptors can be used when selecting cytokines for delivery from future bioactive scaffold designs for more specific recruitment of local chondrogenic and chemotactic cell populations.

Chapter 6. Conclusions and Discussion

6.1 Global Conclusions

1. ASCs, MSCs and SSCs can be chemotactically recruited into an acellular bioactive scaffold and chondrogenically differentiated *in vitro* by TGFβ3 and/or SDF1.

2. The microfluidic under agarose assay is a novel method of characterizing the process of stem cell homing in response to linear concentration gradients of single and competing cytokine signals.

3. TGFβ3 was the most potent factor at inducing the greatest MSC migration numbers and distances among 15 cytokines commonly present in patients with arthritis.

4. As shown in a rat rhinoplasty model, TGFβ3 slow-released from a predesigned bioscaffold can recruit native cells and chondrogenically differentiate them *in vivo.*

6.2 Accomplishment of Specific Aims

In aim 1 we sought to develop a system for the recruitment and chondrogenesis of ASCs, MSCs and SSCs, all of which are natively located adjacent to a full-thickness articular cartilage defect. We hypothesized that SDF1β would promote migration of ASCs, MSCs and SSCs into the scaffold and TGFβ3 would induce chondrogenic differentiation of the cells. To accomplish this goal, bilayered bioactive scaffold were created to slowly release TGFβ3 and/or SDF1β over time from gelatin microspheres. When scaffolds were placed on top of a monolayer of cultured ASCs, MSCs and SSCs, bioactive scaffolds were able to induce the recruitment and subsequent chondrogenic differentiation of all three cell types by TGFβ3 and/or SDF1β. After only 3 weeks of culture, a shiny white layer of tissue was formed in the scaffolds. After 6 weeks,

quantified cell numbers in the scaffolds revealed that TGFβ3 induced the greatest number of ASCs and MSCs to migrate into the scaffold, whereas combinatorial delivery of SDF1β and TGFβ3 induced the greatest number of migrated SSCs. Cartilage specific gene and protein expression were detected in the tissue using RT-PCR, immunohistochemistry and chemical staining. Thus, using our novel bioactive scaffold system, we were able to demonstrate three potential stem/progenitor cell sources that could be used for *in situ* cell recruitment and chondrogenesis.

For aim 2 our goal was to develop novel microfluidic devices to characterize the process of homing stem/progenitor cells. We hypothesized that cytokine concentration gradients would be formed in agarose filled microfluidic channels, which would induce migration of stem/progenitor cells towards cytokines that are chemotactic. To achieve this aim, microfluidic devices were designed and fabricated that enabled efficient migration assays to be conducted and monitored with time-lapse microscopy. These devices have distinct advantages over existing migration assays such as the Boyden chamber, scratch assay and traditional under-agarose assay. Advantages include the ability to form cytokine concentration gradients, the amenity to time-lapse imaging, the capacity to function on minimal amounts of reagents/cells, the precise control of spatial distance between the cytokine source and the cell source, the power to record the migratory patterns of individual cell populations and the capacity to determine the timing of migration without interrupting the assay. Devices were fabricated with both fixed and variable distances between the cell source and the cytokine source. Rigorous initial characterization of the devices was conducted to demonstrate that a diffusion profile could be created with cytokines of varying molecular weights and minimal agarose contractility occurred over time, ensuring uniform conditions between experiments. Fibronectin was found to be the most effective glass coating at promoting uniform cell attachment and morphology comparable to standard tissue culture plates. Serum-free culture conditions were found to inhibit

cell migration compared to serum-supplemented cultures and thus all subsequent experiments were performed using a low concentration of supplemental serum. To demonstrate the flexibility of our system to handle a variety of cell types and chemotactic agents, the chemotactic ability of equine bone marrow MSCs was observed in response to various biologic factors derived from whole blood. Additionally, the system was also amenable to human ASCs as observed by the migration towards an increasing concentration of SDF1β. To confirm that the device environment promoted physiological cell migration, cytoskeletal staining of MSCs after 24 hours of migration revealed that the cells were able to accurately polarize and orient themselves toward the direction of increasing cytokine concentration. An investigation into the effect of channel distance between the cell source and the cytokine source revealed that shorter distances between the MSC population and the PDGFBB source induced increasing migration numbers and migration distances compared to longer distances, likely an indication that higher PDGFBB concentrations are more effective at inducing MSC migration. Thus, the microfluidic migration device with varying channel lengths can be used as a novel method for optimizing cytokine concentrations for maximal cell migration. The novel migration devices developed in this aim have been demonstrated to successfully function with a variety of cell types and cytotactic factors and can serve as a new approach to efficiently determine optimal cytokine concentrations.

In aim 3 we investigated the homing behavior of stem/progenitor cells due to competing cytokine signals, mimicking *in vivo* microenvironments. We hypothesized that multiple cytokine concentration gradients could be separately formed, but simultaneously exposed to a single population of stem/progenitor cells and would promote selective cell migration towards cytokines that are chemotactic. To accomplish this goal, a novel microfluidic chemotaxis assay system was developed that enabled one population of MSCs to be simultaneously exposed to six different cytokines, mimicking *in vivo* microenvironments. In addition to the advantages

discussed above for Aim 2, this device has unique advantages over current migration devices; it has the ability to assay the effects of competing cytokines on a single cell source or, conversely, to test the effects of a single cytokine on multiple cell sources. Rigorous characterization of the device using fluorescently tagged dextrans revealed that cytokines were able to uniformly diffuse from the peripheral wells to the center well (or the reverse), indicating a fair competition among cytokines. The utility of this device was demonstrated by testing the chemotactic effects of 15 cytokines on MSCs. Cytokines were selected based on their presence in the synovial joint in health or arthritis. Quantification of cell migration number, migration distance, migration indices and motility over time revealed MIP1α, PDGFBB, TNFα, TGFβ3 and Lymphotactin to be the most potent chemotactic factors among the first 3 groups of tested cytokines. Testing these potent factors together revealed TGFβ3 to be the best at inducing the highest cell migration number and farthest migration distance, confirming our previous *in vivo* study data [85]. Migration distance values were stratified into categories of <100 μm, 100-200 μm and >200 μm, representing a unique ability of this system to obtain detailed information about migration distance. Migration effects due to PDGFBB yielded varying results when tested in a competition setting compared to individual testing, further demonstrating the importance of testing factors in a competition setting. Thus, this microfluidic under agarose assay is a novel method of characterizing the process of stem cell homing in the presence of competing cytokine signals.

To extend our results to an *in vivo* application, in aim 4 we sought to apply the knowledge gained in aims 1-3 to develop a bioactive cell homing scaffold to promote chondrogenesis for rhinoplasty augmentation. We hypothesized that PLGA would provide a rigid substrate for cell attachment, SDF1β would promote migration of local stem cells around the nasal dorsum into the scaffold and TGFβ3 would induce chondrogenic differentiation of the cells. To accomplish this aim, we developed a new scaffold by modifying the bilayered scaffold used in Aim 1 to contain a PLGA base instead of a collagen sponge. Characterization of various

PLGA formulations *in vitro* revealed an increasing mechanical strength with increasing PLGA concentration, but a decrease in degradation time with increasing PLGA concentration. To test the principle of *in situ* chondrogenesis by cell homing, scaffolds made from 10% w/v, 20% w/v and 40% w/v PLGA that slowly released SDF1β + TGFβ3, SDF1β + TGFβ3 + IGF1 + PDGFBB or TGFβ3 alone were implanted in the subcutaneous nasal dorsum of Sprague Dawley rats with cytokine-free scaffolds and defect alone scaffolds serving as controls. Selected groups also received scoring of the native tip cartilage to induce local progenitor cell migration. Analysis at 6 weeks revealed large ectopic tissue formation compared to a 10 week time point, suggesting a potential challenge in maintaining tissue volume over time, which is a topic for future investigations. Groups containing SDF1β induced significant inflammatory cell infiltration into the scaffold. TGFβ3 alone was successful at inducing both cell homing and chondrogenesis with a dose dependent effect as indicated by immunohistochemical and chemical staining. Scaffolds made from 10% w/v and 40% w/v PLGA yielded fewer voids in tissue formation compared to 20% w/v PLGA. However, for rhinoplasty augmentation, the material must possess rigid structural properties, indicating that 40% w/v PLGA would be advantageous over 10% w/v PLGA. Thus, as shown in a rat model, cells can be recruited into a predesigned bioscaffold and chondrogenically differentiated *in vivo,* representing a potential alternative therapy for rhinoplasty augmentation procedures.

Chapter 6.3 Future Directions

The work described in this thesis helped to answer important questions pertaining to cell sources for cartilage regeneration and chemotactic cues that are effective at recruiting these cells into a bioactive scaffold both *in vitro* and *in vivo*. Additionally, novel cell homing assay devices were developed that efficiently tested the chemotactic effects of either individual cytokines or multiple cytokines, observable under real-time microscopy. However, because the area of tissue regeneration by cell homing is relatively new, many aspects have yet to be fully investigated, leaving room for future investigation.

In Chapter 2, we discovered that synovium derived stem cells, adipose derived stem cells and bone marrow derived mesenchymal stem cells have both chemotactic and chondrogenic potential. Additional stem/progenitor cell types natively residing near a cartilage defect in the knee could possibly be recruited and chondrogenically differentiated for improved tissue regeneration. Future experiments include isolating various local tissues such as the periosteum, perichondrium, meniscus and ligament and digesting the tissues into a cell suspension for culture. With single-cell clonal analysis, we plan to uncover stem cell subsets that display properties of being cytotactic and chondrogenic, and investigate signature cell surface markers for this cell group. Corresponding cytokines that specifically bind to these cell surface markers could then be selected and investigated for their chemotactic potential. Using this approach, novel bioactive scaffolds could be designed to more actively target and recruit specific native local stem/progenitor cell sources for tissue regeneration. Similar experiments could be conducted with the tissues surrounding the subcutaneous nasal dorsum to uncover stem/progenitor cell sources and chemotactic cues specific for recruiting these cells. These cues could then be incorporated into a bioactive scaffold to engineer more homogeneous ectopic cartilage tissue by cell homing for rhinoplasty augmentation.

In our current *in vivo* study, we analyzed the regenerated tissue for the presence of cartilage specific matrix proteins using immunohistochemistry and chemical stains. To obtain a more in-depth analysis of the regenerated tissue and cell sources involved in the regeneration, future experiments could be conducted to digest the regenerated tissue into a cell suspension, and subsequently characterize the cell populations involved using FACS analysis of cell surface markers. By understanding the cell types that were actively recruited, we could determine if undesired cells such as monocytes, leukocytes and fibroblasts were also recruited. In such a case, we could investigate if cell surface receptors exist on the stem cell population that are absent on the nonspecific cells and select cytokines accordingly that bind to only the stem cell specific surface markers for more precise cytotactic targeting.

In this work, we tested the chemotactic effects of simultaneously exposing a single cell population to multiple cytokines with our novel microfluidic device. In future experiments, we plan to reverse the configuration in the device and test a single cytokine against multiple cell types. Local stem/progenitor cells isolated from tissues surrounding a cartilage defect will be simultaneously tested. In addition to determining if a particular cell population amongst a group of cells is more prone to migration in response to a particular cytokine of interest, we could also help to delineate critical information regarding the timing of the migration. For example, we could determine if one cell type begins migrating within 3 hours of cytokine exposure as compared to another cell type which begins migrating within 10 hours of exposure. This information would be critical to design novel bioactive scaffolds that control-release cytokines at predesigned rates to actively recruit targeted cell types at different times. This type of scaffold would be useful for bone tissue engineering, to initially recruit endothelial cells for blood vessel formation, followed by MSCs for osteogenic differentiation, resulting in vascularized bone.

Using our novel microfluidic cell migration platforms, we determined cell migration numbers, distances, migration indices and motility patterns over time as a proof-of-concept

study to demonstrate the device functionality. However, these devices have the potential to test a wide variety of additional migration parameters. Further migration experiments that can be conducted with this microfluidic system include tests to determine the speed of cell migration to delineate if a cytokine is chemokinetic. It is predicted that a chemokinetic factor would promote an increase in cell speed as the cell approaches an increasing cytokine concentration. The percent of cells that change direction in response to various cytokine signals could also be tested. A cell would likely change directions if the factor inhibited chemotaxis. Additionally, because the microfluidic platform is amenable to live cell imaging, the cell density at which a population prefers to migrate could be determined, providing insight into whether the cell population relies on cell-cell contact for migration or whether it is able to migrate in solitude.

6.4 Impact to the Field

Scaffolds for Cell Homing

The bilayered scaffold used in Chapters 2 and 5 for cell homing and chondrogenesis consisted of a base material (collagen sponge or PLGA) that is amenable to cell attachment and tissue formation and a top hydrogel layer encapsulating gelatin microspheres that slowly release cytokines over time. Because this design can easily be modified, the scaffold has wide implications to the field of tissue regeneration and could be applied to most tissue types including bone, meniscus, fat, liver, skin and blood vessel (**Table 6.1**).

Table 6.1 Bioactive scaffold design for tissue regeneration by cell homing. Native tissue elastic moduli were used to select scaffold materials that could be fabricated with mechanical properties in this range. Scaffold cytokines were selected based on potential migration or differentiation effects on the native cell sources.

	Cortical Bone	Meniscus	Fat	Skin	Blood vessel
Native Elastic Modulus	167MPa	0.42Mpa	3.2kPa	69kPa	300kPa
Native Cells	Osteoblasts	Fibrochondrocytes	Adipocytes	Keratinocytes	Endothelial Cells/ Smooth Muscle Cells
Bulk Scaffold Material	HA-TCP	Polyurethane	PLGA	Collagen Sponge	Elastin/Collagen
Scaffold Cytokines	BMP2	CTGF/TGFβ3	bFGF	EGF, bFGF, PDGF, TGFβ1	EC: VEGF/IGF/bFGF SMC: PDGF
Scaffold Shape	Cylinder	Horseshoe Disc	Disc	Sheet	Tube

For this scaffold system to be effective, the tissue type must have direct access to a local stem/progenitor cell source. Once the scaffold is placed in the tissue regeneration site, the local stem/progenitor cells will become the source for targeted cell recruitment. Systemically

recruiting cells from the bone marrow has been shown to occur after injury. However, it has never been confirmed that a bioactive scaffold alone has the ability to recruit systemic cells, although speculations have been made [85].

The initial step in designing a bioactive scaffold for tissue regeneration by cell homing is identifying the cell types that make up the native tissue and their corresponding progenitor cell type. For example, a bioactive scaffold designed for bone tissue engineering would focus on osteoblast precursor cells such as MSCs (**Table 6.1**). Subsequently, chemotactic cytokines are selected to recruit stem or progenitor cells that can differentiate into the mature cell types. Since MSCs have been shown to be actively recruited by PDGFBB, this cytokine could be incorporated into a bioactive scaffold for bone regeneration. Additional cytokines are selected that promote the differentiation of stem/progenitor cells into the mature cells natively found in the tissue. For bone regeneration, BMP2 has been shown to have potent effects on MSC differentiation into osteoblasts and could be incorporated into the scaffold (**Table 6.1**).

The next step in the scaffold design process is tailoring the microspheres to release the selected cytokines. Cytokines specific for regenerating any tissue can be incorporated into the tissue. This is possible because the gelatin microspheres are negatively charged and will electrostatically bind to any positively charged cytokine when rehydrated at pH 7.4. Thus, cytokines that are particularly chemotactic for a certain cell type can be loaded into gelatin microspheres provided their charge is positive. Likewise, cytokines specific for differentiating stem/progenitor cells for any tissue type can be incorporated into these microspheres provided their charge is positive. For scaffolds in which the cell homing cytokines should be released first to recruit stem/progenitor cells into the scaffold followed by the cell differentiation cues, microspheres could be tailored to have varying release times. By altering the microsphere cross-linking density with lower or higher glutaraldehyde concentrations, the microsphere

degradation time would vary. Lower glutaraldehyde concentrations would allow for faster microsphere degradation and a faster cytokine release profile whereas higher glutaraldehyde concentrations would yield the opposite effect. Thus the release times could be individually controlled for different cytokines in the scaffold.

An important component of the scaffold design is selecting an appropriate bulk material. The material should degrade at a similar rate to the rate of new tissue formation and should contain mechanical properties similar to the native tissue (**Table 6.1**). Thus, the bulk material in the original bilayered scaffold design would have to be replaced to match the mechanical properties of the native tissue. For example, softer tissues such as adipose or skin, would require a material with a lower elastic modulus compared to bone. Furthermore, local microenvironments such as extracellular matrices and spatial organization are thought to effect cell behavior and maintain cell phenotype [142-145]. In our current scaffold design, we chose a base of collagen sponge to mimic the native collagen-rich extracellular matrix of cartilage. For tooth regeneration on the other hand, a harder scaffold material might be more suitable. Incorporation of ameliogenin protein, a precursor for enamel formation, into the material structure might help to promote physiological microenvironments similar to native teeth [146]. Thus, materials for the base of the bilayered scaffold should be individually selected to mimic the native tissue microenvironment to promote physiological cell conditions.

Traditional tissue engineering approaches of creating scaffolds with shapes that mimic native tissue structures could easily be incorporated into the current cubic scaffold design. For example, the bulk scaffold material could be shaped into a tube for blood vessel regeneration. Cytokine releasing microspheres could be directly incorporated within the pores of the bulk scaffold material to eliminate the need for a double layered design for better maintenance of anatomic shape. With this design, varying differentiation cues could be incorporated into

disparate regions of the bulk scaffold to create diverse tissues within the same scaffold. For an osteochondral construct, microspheres containing PDGFBB could be incorporated throughout the bulk material for homogenous MSC recruitment. Microspheres containing TGFβ3 could be incorporated into half of the material for chondrogenic differentiation whereas the other half of the material could contain microspheres releasing BMP2 for osteogenic differentiation.

Additional considerations should be taken to ensure that the chosen material is amenable to cell attachment by the targeted cells. If the material chemistry does not contain a ligand or peptide to match receptors on the targeted cell type, the material must be modified and tethered with the appropriate ligand. Providing the appropriate ligand for cell attachment could potentially enhance the migration of the targeted cell type [147]. If the material chosen is not naturally amenable to cell attachment, such as polyethylene glycol, and modified to contain a ligand specific of the cell type of interest, this might help to prevent unintended cells that do not contain receptors for the tethered ligand, from attaching to the scaffold. Thus, more targeted cell homing approaches could be developed.

Microfluidic Cell Homing Assay Systems

Three novel microfluidic migration devices were fabricated with varying design characteristics: a device with individual uniform length channels, a device with varying length channels and a device with connected uniform length channels. These cell migration assay devices have potential broad applications in studying tissue development, cancer metastasis, infection, wound healing and tissue engineering. Additionally, the results from complex chemotactic studies could benefit the development of novel drug therapeutics.

Rigorous characterization with fluorescently tagged dextrans demonstrated the potential to create cytokine gradients with a wide range of molecular weights (3kDa-70kDa). Because the devices can accommodate a large range of molecular weights, most cytokines, growth factors or chemotactic agents can be tested. Since complex patterns of growth factor signaling are involved with the biological regulation of nearly all organ systems, these devices could be used to test the chemotactic effects of cytokines for regenerating any organ system.

The cell culture platform of a glass substrate coated with fibronectin was amenable to the culture of multiple cell types, including ASCs, MSCs, and SSCs from both human and equine donors. Virtually any cell type that can attach and thrive on a fibronectin coated substrate could be used in this system. Therefore, these devices have wide applications to test cell motility properties of a variety of cell types including primary cells, immortalized cell lines, clonally derived cells, stem/progenitor cells, cancer cell lines and transgenic cell lines. Typical approaches for culturing embryonic stem cells and induced pluripotent stem cells involve the use of feeder cell layers. However, new methods have been discovered using chemically treated or UV treated substrates to promote pluripotent cell survival [148]. The glass substrates used as bases for these microfluidic devices could potentially be treated with these methods to enable our system to test the chemotactic effects of pluripotent cell types.

Cancer metastasis has been thought to occur due to the migration of cancer cells from the tumor to a remote location [149, 150]. These devices can be used to test various cytokines against different cancer cell lines to determine factors potent at inducing cell migration. Subsequently, novel cancer therapeutics could be developed that act to block metastasis by blocking the corresponding cytokine receptors responsible for inducing cancer cell migration. Additionally, tumors are thought to thrive due to a growing vascular network attached to the tumor [151]. One potential therapeutic approach for shrinking tumors is to destroy the vascular

supply to the tumor [151]. Endothelial cells are the primary cells involved in angiogenesis, which occurs by the directed migration of these cells to create new blood vessel sprouts [152]. Thus, testing the chemotactic effects of endothelial cells using our microfluidic chemotaxis devices could potentially lead to the development of new drugs to treat cancer.

References

1. Chung, C. and J.A. Burdick, *Engineering cartilage tissue.* Adv Drug Deliv Rev, 2008. **60**(2): p. 243-62.

2. Martin, I., et al., *Osteochondral tissue engineering.* J Biomech, 2007. **40**(4): p. 750-65.

3. Derubeis, A.R. and R. Cancedda, *Bone marrow stromal cells (BMSCs) in bone engineering: limitations and recent advances.* Ann Biomed Eng, 2004. **32**(1): p. 160-5.

4. Mano, J.F. and R.L. Reis, *Osteochondral defects: present situation and tissue engineering approaches.* J Tissue Eng Regen Med, 2007. **1**(4): p. 261-73.

5. Kinner, B., R.M. Capito, and M. Spector, *Regeneration of articular cartilage.* Adv Biochem Eng Biotechnol, 2005. **94**: p. 91-123.

6. Lu, L., et al., *In vitro and in vivo degradation of porous poly(DL-lactic-co-glycolic acid) foams.* Biomaterials, 2000. **21**(18): p. 1837-45.

7. Friedenstein, A.J., J.F. Gorskaja, and N.N. Kulagina, *Fibroblast precursors in normal and irradiated mouse hematopoietic organs.* Exp Hematol, 1976. **4**(5): p. 267-74.

8. Dowthwaite, G.P., et al., *The surface of articular cartilage contains a progenitor cell population.* J Cell Sci, 2004. **117**(Pt 6): p. 889-97.

9. Takahashi, K., et al., *Induction of pluripotent stem cells from adult human fibroblasts by defined factors.* Cell, 2007. **131**(5): p. 861-72.

10. Yu, J., et al., *Induced pluripotent stem cell lines derived from human somatic cells.* Science, 2007. **318**(5858): p. 1917-20.

11. Tuli, R., et al., *Human mesenchymal progenitor cell-based tissue engineering of a single-unit osteochondral construct.* Tissue Eng, 2004. **10**(7-8): p. 1169-79.

12. Guo, X., et al., *Repair of osteochondral defects with autologous chondrocytes seeded onto bioceramic scaffold in sheep.* Tissue Eng, 2004. **10**(11-12): p. 1830-40.

13. Xu, J.W., et al., *Tissue-engineered cartilage composite with expanded polytetrafluoroethylene membrane.* Ann Plast Surg, 2001. **46**(5): p. 527-32.

14. Shao, X.X., et al., *Evaluation of a hybrid scaffold/cell construct in repair of high-load-bearing osteochondral defects in rabbits.* Biomaterials, 2006. **27**(7): p. 1071-80.

15. Mason, J.M., et al., *Cartilage and bone regeneration using gene-enhanced tissue engineering.* Clin Orthop Relat Res, 2000(379 Suppl): p. S171-8.

16. Park, K., et al., *Scaffold-free, engineered porcine cartilage construct for cartilage defect repair--in vitro and in vivo study.* Artif Organs, 2006. **30**(8): p. 586-96.

17. Choumerianou, D.M., H. Dimitriou, and M. Kalmanti, *Stem cells: promises versus limitations.* Tissue Eng Part B Rev, 2008. **14**(1): p. 53-60.

18. Mao, J.J., *Stem-cell-driven regeneration of synovial joints.* Biol Cell, 2005. **97**(5): p. 289-301.

19. Darling, E.M. and K.A. Athanasiou, *Biomechanical strategies for articular cartilage regeneration.* Ann Biomed Eng, 2003. **31**(9): p. 1114-24.

20. Gao, J., et al., *Repair of osteochondral defect with tissue-engineered two-phase composite material of injectable calcium phosphate and hyaluronan sponge.* Tissue Eng, 2002. **8**(5): p. 827-37.

21. Jiang, C.C., et al., *Repair of porcine articular cartilage defect with a biphasic osteochondral composite.* J Orthop Res, 2007. **25**(10): p. 1277-90.

22. Lee, C.R., et al., *Effects of a cultured autologous chondrocyte-seeded type II collagen scaffold on the healing of a chondral defect in a canine model.* J Orthop Res, 2003. **21**(2): p. 272-81.

23. Schaefer, D., et al., *Tissue-engineered composites for the repair of large osteochondral defects.* Arthritis Rheum, 2002. **46**(9): p. 2524-34.

24. Wood, J.J., et al., *Autologous cultured chondrocytes: adverse events reported to the United States Food and Drug Administration.* J Bone Joint Surg Am, 2006. **88**(3): p. 503-7.

25. Scanzello, C.R., A. Plaas, and M.K. Crow, *Innate immune system activation in osteoarthritis: is osteoarthritis a chronic wound?* Curr Opin Rheumatol, 2008. **20**(5): p. 565-72.

26. Buckwalter, J.A. and J.A. Martin, *Osteoarthritis.* Adv Drug Deliv Rev, 2006. **58**(2): p. 150-67.

27. Caplan, A.I. and V.M. Goldberg, *Principles of tissue engineered regeneration of skeletal tissues.* Clin Orthop Relat Res, 1999(367 Suppl): p. S12-6.

28. Karp, J.M. and G.S. Leng Teo, *Mesenchymal stem cell homing: the devil is in the details.* Cell Stem Cell, 2009. **4**(3): p. 206-16.

29. Sackstein, R., et al., *Ex vivo glycan engineering of CD44 programs human multipotent mesenchymal stromal cell trafficking to bone.* Nat Med, 2008. **14**(2): p. 181-7.

30. Rochefort, G.Y., et al., *Multipotential mesenchymal stem cells are mobilized into peripheral blood by hypoxia.* Stem Cells, 2006. **24**(10): p. 2202-8.

31. Wang, C.H., et al., *Late-outgrowth endothelial cells attenuate intimal hyperplasia contributed by mesenchymal stem cells after vascular injury.* Arterioscler Thromb Vasc Biol, 2008. **28**(1): p. 54-60.

32. Wynn, R.F., et al., *A small proportion of mesenchymal stem cells strongly expresses functionally active CXCR4 receptor capable of promoting migration to bone marrow.* Blood, 2004. **104**(9): p. 2643-5.

33. Weng, Y., et al., *Tissue-engineered composites of bone and cartilage for mandible condylar reconstruction.* J Oral Maxillofac Surg, 2001. **59**(2): p. 185-90.

34. Gotterbarm, T., et al., *An in vivo study of a growth-factor enhanced, cell free, two-layered collagen-tricalcium phosphate in deep osteochondral defects.* Biomaterials, 2006. **27**(18): p. 3387-95.

35. Tamai, N., et al., *A new biotechnology for articular cartilage repair: subchondral implantation of a composite of interconnected porous hydroxyapatite, synthetic polymer (PLA-PEG), and bone morphogenetic protein-2 (rhBMP-2).* Osteoarthritis Cartilage, 2005. **13**(5): p. 405-17.

36. Erggelet, C., et al., *Regeneration of ovine articular cartilage defects by cell-free polymer-based implants.* Biomaterials, 2007. **28**(36): p. 5570-80.

37. Chang, N.J., et al., *The combined effects of continuous passive motion treatment and acellular PLGA implants on osteochondral regeneration in the rabbit.* Biomaterials. **33**(11): p. 3153-63.

38. Smart, N. and P.R. Riley, *The stem cell movement.* Circ Res, 2008. **102**(10): p. 1155-68.

39. Aiuti, A., et al., *The chemokine SDF-1 is a chemoattractant for human CD34+ hematopoietic progenitor cells and provides a new mechanism to explain the mobilization of CD34+ progenitors to peripheral blood.* J Exp Med, 1997. **185**(1): p. 111-20.

40. Li, Y., et al., *Insulin-like growth factor 1 enhances the migratory capacity of mesenchymal stem cells.* Biochem Biophys Res Commun, 2007. **356**(3): p. 780-4.

41. Pelus, L.M. and S. Fukuda, *Chemokine-mobilized adult stem cells; defining a better hematopoietic graft.* Leukemia, 2008. **22**(3): p. 466-73.

42. Mohle, R., et al., *The chemokine receptor CXCR-4 is expressed on CD34+ hematopoietic progenitors and leukemic cells and mediates transendothelial migration induced by stromal cell-derived factor-1.* Blood, 1998. **91**(12): p. 4523-30.

43. Bleul, C.C., et al., *A highly efficacious lymphocyte chemoattractant, stromal cell-derived factor 1 (SDF-1).* J Exp Med, 1996. **184**(3): p. 1101-9.

44. Potapova, I.A., et al., *Culturing of human mesenchymal stem cells as three-dimensional aggregates induces functional expression of CXCR4 that regulates adhesion to endothelial cells.* J Biol Chem, 2008. **283**(19): p. 13100-7.

45. Voermans, C., et al., *Increased migration of cord blood-derived CD34+ cells, as compared to bone marrow and mobilized peripheral blood CD34+ cells across uncoated or fibronectin-coated filters.* Exp Hematol, 1999. **27**(12): p. 1806-14.

46. Chen, T., et al., *Stromal cell-derived factor-1/CXCR4 signaling modifies the capillary-like organization of human embryonic stem cell-derived endothelium in vitro.* Stem Cells, 2007. **25**(2): p. 392-401.

47. Thangarajah, H., et al., *IFATS collection: Adipose stromal cells adopt a proangiogenic phenotype under the influence of hypoxia.* Stem Cells, 2009. **27**(1): p. 266-74.

48. Burger, J.A., et al., *Fibroblast-like synoviocytes support B-cell pseudoemperipolesis via a stromal cell-derived factor-1- and CD106 (VCAM-1)-dependent mechanism.* J Clin Invest, 2001. **107**(3): p. 305-15.

49. Christopher, M.J., et al., *Suppression of CXCL12 production by bone marrow osteoblasts is a common and critical pathway for cytokine-induced mobilization.* Blood, 2009. **114**(7): p. 1331-9.

50. Yong, K., et al., *Cord blood progenitor cells have greater transendothelial migratory activity and increased responses to SDF-1 and MIP-3beta compared with mobilized adult progenitor cells.* Br J Haematol, 1999. **107**(2): p. 441-9.

51. Shi, M., et al., *Regulation of CXCR4 expression in human mesenchymal stem cells by cytokine treatment: role in homing efficiency in NOD/SCID mice.* Haematologica, 2007. **92**(7): p. 897-904.

52. Cristino, S., et al., *Expression of CXC chemokines and their receptors is modulated during chondrogenic differentiation of human mesenchymal stem cells grown in three-dimensional scaffold: evidence in native cartilage.* Tissue Eng Part A, 2008. **14**(1): p. 97-105.

53. Wu, Q., et al., *Extracellular calcium increases CXCR4 expression on bone marrow-derived cells and enhances pro-angiogenesis therapy.* J Cell Mol Med, 2009. **13**(9B): p. 3764-73.

54. Schantz, J.T., H. Chim, and M. Whiteman, *Cell guidance in tissue engineering: SDF-1 mediates site-directed homing of mesenchymal stem cells within three-dimensional polycaprolactone scaffolds.* Tissue Eng, 2007. **13**(11): p. 2615-24.

55. Thieme, S., et al., *Stromal cell-derived factor-1alpha-directed chemoattraction of transiently CXCR4-overexpressing bone marrow stromal cells into functionalized three-dimensional biomimetic scaffolds.* Tissue Eng Part C Methods, 2009. **15**(4): p. 687-96.

56. Sukegawa, A., et al., *Repair of Rabbit Osteochondral Defects by an Acellular Technique with an Ultrapurified Alginate Gel Containing Stromal Cell-Derived Factor-1.* Tissue Eng Part A.

57. Mahmud, G., et al., *Directing cell motions on micropatterned ratchets.* Nat Phys, 2009. **5**(8): p. 606-612.

58. Horwitz, A.R. and J.T. Parsons, *Cell migration--movin' on.* Science, 1999. **286**(5442): p. 1102-3.

59. Boyden, S., *The chemotactic effect of mixtures of antibody and antigen on polymorphonuclear leucocytes.* J Exp Med, 1962. **115**: p. 453-66.

60. Heit, B. and P. Kubes, *Measuring chemotaxis and chemokinesis: the under-agarose cell migration assay.* Sci STKE, 2003. **2003**(170): p. PL5.

61. Liang, C.C., A.Y. Park, and J.L. Guan, *In vitro scratch assay: a convenient and inexpensive method for analysis of cell migration in vitro.* Nat Protoc, 2007. **2**(2): p. 329-33.

62. Hara-Chikuma, M. and A.S. Verkman, *Aquaporin-1 facilitates epithelial cell migration in kidney proximal tubule.* J Am Soc Nephrol, 2006. **17**(1): p. 39-45.

63. Zicha, D., G.A. Dunn, and A.F. Brown, *A new direct-viewing chemotaxis chamber.* J Cell Sci, 1991. **99 (Pt 4)**: p. 769-75.

64. Zigmond, S.H., *Ability of polymorphonuclear leukocytes to orient in gradients of chemotactic factors.* J Cell Biol, 1977. **75**(2 Pt 1): p. 606-16.

65. Daniel Zicha, G.D.a.G.J., *Analyzing Chemotaxis Using the Dunn Direct-Viewing Chamber* Methods in Molecular Biology, 1997. **290**: p. 449-457.

66. Kim, B.J. and M. Wu, *Microfluidics for Mammalian Cell Chemotaxis.* Ann Biomed Eng.

67. Nelson, R.D., P.G. Quie, and R.L. Simmons, *Chemotaxis under agarose: a new and simple method for measuring chemotaxis and spontaneous migration of human polymorphonuclear leukocytes and monocytes.* J Immunol, 1975. **115**(6): p. 1650-6.

68. Englert, D.L., M.D. Manson, and A. Jayaraman, *Flow-based microfluidic device for quantifying bacterial chemotaxis in stable, competing gradients.* Appl Environ Microbiol, 2009. **75**(13): p. 4557-64.

69. Chung, S., et al., *Cell migration into scaffolds under co-culture conditions in a microfluidic platform.* Lab Chip, 2009. **9**(2): p. 269-75.

70. Cheng, S.Y., et al., *A hydrogel-based microfluidic device for the studies of directed cell migration.* Lab Chip, 2007. **7**(6): p. 763-9.

71. Chu, C.R., M. Szczodry, and S. Bruno, *Animal models for cartilage regeneration and repair.* Tissue Eng Part B Rev. **16**(1): p. 105-15.

72. Oseni, A., et al., *Advancing nasal reconstructive surgery: the application of tissue engineering technology.* J Tissue Eng Regen Med.

73. Jang, Y.J., et al., *Combined use of crushed cartilage and processed fascia lata for dorsal augmentation in rhinoplasty for Asians.* Laryngoscope, 2009. **119**(6): p. 1088-92.

74. Quatela, V.C. and J.M. Pearson, *Management of the aging nose.* Facial Plast Surg, 2009. **25**(4): p. 215-21.

75. Sajjadian, A., N. Naghshineh, and R. Rubinstein, *Current status of grafts and implants in rhinoplasty: Part II. Homologous grafts and allogenic implants.* Plast Reconstr Surg. **125**(3): p. 99e-109e.

76. Stryker. *Nasal Products*. Medpor Implants 2011 [cited.

77. Ahn, J., C. Honrado, and C. Horn, *Combined silicone and cartilage implants: augmentation rhinoplasty in Asian patients.* Arch Facial Plast Surg, 2004. **6**(2): p. 120-3.

78. Raghunath, J., et al., *Advancing cartilage tissue engineering: the application of stem cell technology.* Curr Opin Biotechnol, 2005. **16**(5): p. 503-9.

79. Fodor, W.L., *Tissue engineering and cell based therapies, from the bench to the clinic: the potential to replace, repair and regenerate.* Reprod Biol Endocrinol, 2003. **1**: p. 102.

80. Kim, J., et al., *Biological characterization of long-term cultured human mesenchymal stem cells.* Arch Pharm Res, 2009. **32**(1): p. 117-26.

81. Lepperdinger, G., et al., *Controversial issue: is it safe to employ mesenchymal stem cells in cell-based therapies?* Exp Gerontol, 2008. **43**(11): p. 1018-23.

82. Rubio, D., et al., *Spontaneous human adult stem cell transformation.* Cancer Res, 2005. **65**(8): p. 3035-9.

83. Bladergroen, B.A., et al., *In vivo recruitment of hematopoietic cells using stromal cell-derived factor 1 alpha-loaded heparinized three-dimensional collagen scaffolds.* Tissue Eng Part A, 2009. **15**(7): p. 1591-9.

84. Benya, P.D. and J.D. Shaffer, *Dedifferentiated chondrocytes reexpress the differentiated collagen phenotype when cultured in agarose gels.* Cell, 1982. **30**(1): p. 215-24.

85. Lee, C.H., et al., *Regeneration of the articular surface of the rabbit synovial joint by cell homing: a proof of concept study.* Lancet. **376**(9739): p. 440-8.

86. Jones, E.A., et al., *Enumeration and phenotypic characterization of synovial fluid multipotential mesenchymal progenitor cells in inflammatory and degenerative arthritis.* Arthritis Rheum, 2004. **50**(3): p. 817-27.

87. Son, B.R., et al., *Migration of bone marrow and cord blood mesenchymal stem cells in vitro is regulated by stromal-derived factor-1-CXCR4 and hepatocyte growth factor-c-met axes and involves matrix metalloproteinases.* Stem Cells, 2006. **24**(5): p. 1254-64.

88. Mazzetti, I., et al., *A role for chemokines in the induction of chondrocyte phenotype modulation.* Arthritis Rheum, 2004. **50**(1): p. 112-22.

89. Gao, J., J.Q. Yao, and A.I. Caplan, *Stem cells for tissue engineering of articular cartilage.* Proc Inst Mech Eng H, 2007. **221**(5): p. 441-50.

90. Fan, H., et al., *Porous gelatin-chondroitin-hyaluronate tri-copolymer scaffold containing microspheres loaded with TGF-beta1 induces differentiation of mesenchymal stem cells in vivo for enhancing cartilage repair.* J Biomed Mater Res A, 2006. **77**(4): p. 785-94.

91. Kimura, Y., et al., *Adipose tissue engineering based on human preadipocytes combined with gelatin microspheres containing basic fibroblast growth factor.* Biomaterials, 2003. **24**(14): p. 2513-21.

92. Yun, K. and H.T. Moon, *Inducing chondrogenic differentiation in injectable hydrogels embedded with rabbit chondrocytes and growth factor for neocartilage formation.* J Biosci Bioeng, 2008. **105**(2): p. 122-6.

93. Lutolf, M.P., et al., *Repair of bone defects using synthetic mimetics of collagenous extracellular matrices.* Nat Biotechnol, 2003. **21**(5): p. 513-8.

94. Marion, N.W. and J.J. Mao, *Mesenchymal stem cells and tissue engineering.* Methods Enzymol, 2006. **420**: p. 339-61.

95. Karystinou, A., et al., *Distinct mesenchymal progenitor cell subsets in the adult human synovium.* Rheumatology (Oxford), 2009. **48**(9): p. 1057-64.

96. Alhadlaq, A., et al., *Adult stem cell driven genesis of human-shaped articular condyle.* Ann Biomed Eng, 2004. **32**(7): p. 911-23.

97. Awad, H.A., et al., *Chondrogenic differentiation of adipose-derived adult stem cells in agarose, alginate, and gelatin scaffolds.* Biomaterials, 2004. **25**(16): p. 3211-22.

98. De Bari, C., et al., *Multipotent mesenchymal stem cells from adult human synovial membrane.* Arthritis Rheum, 2001. **44**(8): p. 1928-42.

99. De Bari, C., et al., *A biomarker-based mathematical model to predict bone-forming potency of human synovial and periosteal mesenchymal stem cells.* Arthritis Rheum, 2008. **58**(1): p. 240-50.

100. Jones, E., et al., *Mesenchymal stem cells in rheumatoid synovium: enumeration and functional assessment in relation to synovial inflammation level.* Ann Rheum Dis. **69**(2): p. 450-7.

101. Moioli, E.K., et al., *Hybrid Adipogenic Implants from Adipose Stem Cells for Soft Tissue Reconstruction In Vivo.* Tissue Eng Part A.

102. Lee, C.H., et al., *Tissue formation and vascularization in anatomically shaped human joint condyle ectopically in vivo.* Tissue Eng Part A, 2009. **15**(12): p. 3923-30.

103. Thorpe, S.D., et al., *The response of bone marrow-derived mesenchymal stem cells to dynamic compression following TGF-beta3 induced chondrogenic differentiation.* Ann Biomed Eng. **38**(9): p. 2896-909.

104. Hildner, F., et al., *FGF-2 abolishes the chondrogenic effect of combined BMP-6 and TGF-beta in human adipose derived stem cells.* J Biomed Mater Res A. **94**(3): p. 978-87.

105. Varshney, R.R., et al., *Chondrogenesis of synovium-derived mesenchymal stem cells in gene-transferred co-culture system.* Biomaterials. **31**(26): p. 6876-91.

106. Knudson, C.B. and W. Knudson, *Cartilage proteoglycans.* Semin Cell Dev Biol, 2001. **12**(2): p. 69-78.

107. Shen, W., et al., *The effect of incorporation of exogenous stromal cell-derived factor-1 alpha within a knitted silk-collagen sponge scaffold on tendon regeneration.* Biomaterials. **31**(28): p. 7239-49.

108. He, X., J. Ma, and E. Jabbari, *Migration of marrow stromal cells in response to sustained release of stromal-derived factor-1alpha from poly(lactide ethylene oxide fumarate) hydrogels.* Int J Pharm. **390**(2): p. 107-16.

109. Kim, J.Y., et al., *Regeneration of Dental-Pulp-like Tissue by Chemotaxis-Induced Cell Homing.* Tissue Eng Part A.

110. Agrawal, V., et al., *Epimorphic regeneration approach to tissue replacement in adult mammals.* Proc Natl Acad Sci U S A. **107**(8): p. 3351-5.

111. Kumar, A., P.B. Gates, and J.P. Brockes, *Positional identity of adult stem cells in salamander limb regeneration.* C R Biol, 2007. **330**(6-7): p. 485-90.

112. Lee, C.H., et al., *CTGF directs fibroblast differentiation from human mesenchymal stem/stromal cells and defines connective tissue healing in a rodent injury model.* J Clin Invest. **120**(9): p. 3340-9.

113. Nie, H., et al., *Delivery of bioactive cues for in situ tissue regeneration.* Pharm Res, 2010. **In Press**.

114. Zheng, Z., et al., *Delayed Wound Closure in Fibromodulin-Deficient Mice Is Associated with Increased TGF-beta3 Signaling.* J Invest Dermatol. **131**(3): p. 769-78.

115. Mendelson, A., et al., *Chondrogenesis by chemotactic homing of synovium, bone marrow, and adipose stem cells in vitro.* Faseb J. **25**(10): p. 3496-504.

116. Prockop, D.J., *Repair of tissues by adult stem/progenitor cells (MSCs): controversies, myths, and changing paradigms.* Mol Ther, 2009. **17**(6): p. 939-46.

117. Prasad A, L.C., Hurt S, Venne MH and Parent S *Cytokine Detection In Culture Media Containing 10% FBS –A Comparison Of Two Commonly Used Homogeneous High Throughput Assay Technologies*. 2009, PerkinElmer: Waltham.

118. Doorn, J., et al., *Therapeutic Applications of Mesenchymal Stromal Cells: Paracrine Effects and Potential Improvements.* Tissue Eng Part B Rev.

119. Laird, D.J., U.H. von Andrian, and A.J. Wagers, *Stem cell trafficking in tissue development, growth, and disease.* Cell, 2008. **132**(4): p. 612-30.

120. Iwamoto, T., et al., *Molecular aspects of rheumatoid arthritis: chemokines in the joints of patients.* Febs J, 2008. **275**(18): p. 4448-55.

121. Hannoush, E.J., et al., *Impact of enhanced mobilization of bone marrow derived cells to site of injury.* J Trauma. **71**(2): p. 283-9; discussion 289-91.

122. Singer, N.G. and A.I. Caplan, *Mesenchymal stem cells: mechanisms of inflammation.* Annu Rev Pathol. **6**: p. 457-78.

123. Shah, S., et al., *Mobilization of bone marrow cells to the site of injury is necessary for wound healing.* J Trauma, 2009. **67**(2): p. 315-21; discussion 321-2.

124. Fox, J.M., *Recent advances into the understanding of mesenchymal stem cell trafficking.* British Journal of Haematology, 2007. **137**(6): p. 491-502.

125. Prockop, D.J. and J. Youn Oh, *Mesenchymal Stem/Stromal Cells (MSCs): Role as Guardians of Inflammation.* Mol Ther.

126. Lauffenburger, D., C. Rothman, and S.H. Zigmond, *Measurement of leukocyte motility and chemotaxis parameters with a linear under-agarose migration assay.* J Immunol, 1983. **131**(2): p. 940-7.

127. Todaro, G.J., G.K. Lazar, and H. Green, *The initiation of cell division in a contact-inhibited mammalian cell line.* J Cell Physiol, 1965. **66**(3): p. 325-33.

128. Yelin E, C.M., Foreman A, Pasta D, Murphy L, Helmick C, *National and state medical expenditures and lost earnings attribute to arthritis and other rheumatic conditions - United States, 2003.* MMWR, 2007. **56**(1): p. 4-7.

129. Rohner, E., et al., *Inflammatory synovial fluid microenvironment drives primary human chondrocytes to actively take part in inflammatory joint diseases.* Immunol Res.

130. Cuellar, J.M., et al., *Diagnostic utility of cytokine biomarkers in the evaluation of acute knee pain.* J Bone Joint Surg Am, 2009. **91**(10): p. 2313-20.

131. Endres, M., et al., *Chemokine profile of synovial fluid from normal, osteoarthritis and rheumatoid arthritis patients: CCL25, CXCL10 and XCL1 recruit human subchondral mesenchymal progenitor cells.* Osteoarthritis Cartilage. **18**(11): p. 1458-66.

132. Ponte, A.L., et al., *The in vitro migration capacity of human bone marrow mesenchymal stem cells: comparison of chemokine and growth factor chemotactic activities.* Stem Cells, 2007. **25**(7): p. 1737-45.

133. Mishima, Y. and M. Lotz, *Chemotaxis of human articular chondrocytes and mesenchymal stem cells.* J Orthop Res, 2008. **26**(10): p. 1407-12.

134. Yoshioka, T., et al., *In vitro evaluation of biodegradation of poly(lactic-co-glycolic acid) sponges.* Biomaterials, 2008. **29**(24-25): p. 3438-43.

135. Jenniskens, Y.M., et al., *Biochemical and functional modulation of the cartilage collagen network by IGF1, TGFbeta2 and FGF2.* Osteoarthritis Cartilage, 2006. **14**(11): p. 1136-46.

136. Alexander, T.H., et al., *Insulin-like growth factor-I and growth differentiation factor-5 promote the formation of tissue-engineered human nasal septal cartilage.* Tissue Eng Part C Methods. **16**(5): p. 1213-21.

137. Cherla, R.P. and R.K. Ganju, *Stromal cell-derived factor 1 alpha-induced chemotaxis in T cells is mediated by nitric oxide signaling pathways.* J Immunol, 2001. **166**(5): p. 3067-74.

138. Pretzel, D., et al., *Relative percentage and zonal distribution of mesenchymal progenitor cells in human osteoarthritic and normal cartilage.* Arthritis Res Ther. **13**(2): p. R64.

139. Ghosh, S., et al., *In vitro model of mesenchymal condensation during chondrogenic development.* Biomaterials, 2009. **30**(33): p. 6530-40.

140. Hall, B.K. and T. Miyake, *Divide, accumulate, differentiate: cell condensation in skeletal development revisited.* Int J Dev Biol, 1995. **39**(6): p. 881-93.

141. Toh, W.S., et al., *Modulation of mesenchymal stem cell chondrogenesis in a tunable hyaluronic acid hydrogel microenvironment.* Biomaterials.

142. Toh, Y.C., et al., *Spatially organized in vitro models instruct asymmetric stem cell differentiation.* Integr Biol (Camb). **3**(12): p. 1179-87.

143. Engler, A.J., et al., *Matrix elasticity directs stem cell lineage specification.* Cell, 2006. **126**(4): p. 677-89.

144. Flaim, C.J., et al., *Combinatorial signaling microenvironments for studying stem cell fate.* Stem Cells Dev, 2008. **17**(1): p. 29-39.

145. McBeath, R., et al., *Cell shape, cytoskeletal tension, and RhoA regulate stem cell lineage commitment.* Dev Cell, 2004. **6**(4): p. 483-95.

146. Gibson, C.W., *The Amelogenin Proteins and Enamel Development in Humans and Mice.* J Oral Biosci. **53**(3): p. 248-256.

147. Guan, M., et al., *Directing mesenchymal stem cells to bone to augment bone formation and increase bone mass.* Nat Med.

148. Saha, K., et al., *Surface-engineered substrates for improved human pluripotent stem cell culture under fully defined conditions.* Proc Natl Acad Sci U S A. **108**(46): p. 18714-9.

149. Spano, D. and M. Zollo, *Tumor microenvironment: a main actor in the metastasis process.* Clin Exp Metastasis. **29**(4): p. 381-95.

150. Nguyen, D.X. and J. Massague, *Genetic determinants of cancer metastasis.* Nat Rev Genet, 2007. **8**(5): p. 341-52.

151. Linkous, A.G. and E.M. Yazlovitskaya, *Novel therapeutic approaches for targeting tumor angiogenesis.* Anticancer Res. **32**(1): p. 1-12.

152. Geudens, I. and H. Gerhardt, *Coordinating cell behaviour during blood vessel formation.* Development. **138**(21): p. 4569-83.

153. Schnabel, L.V., et al., *Platelet rich plasma (PRP) enhances anabolic gene expression patterns in flexor digitorum superficialis tendons.* J Orthop Res, 2007. **25**(2): p. 230-40.

154. Torricelli, P., et al., *Regenerative medicine for the treatment of musculoskeletal overuse injuries in competition horses.* Int Orthop. **35**(10): p. 1569-76.

155. Fortier, L.A., et al., *Concentrated bone marrow aspirate improves full-thickness cartilage repair compared with microfracture in the equine model.* J Bone Joint Surg Am. **92**(10): p. 1927-37.

156. McCarrel, T. and L. Fortier, *Temporal growth factor release from platelet-rich plasma, trehalose lyophilized platelets, and bone marrow aspirate and their effect on tendon and ligament gene expression.* J Orthop Res, 2009. **27**(8): p. 1033-42.

157. Fortier, L.A., et al., *Isolation and chondrocytic differentiation of equine bone marrow-derived mesenchymal stem cells.* Am J Vet Res, 1998. **59**(9): p. 1182-7.

158. Ortved, K.F., et al., *Treatment of subchondral cystic lesions of the medial femoral condyle of mature horses with growth factor enhanced chondrocyte grafts: A retrospective study of 49 cases.* Equine Vet J.

159. Schnabel, L.V., et al., *Effects of platelet rich plasma and acellular bone marrow on gene expression patterns and DNA content of equine suspensory ligament explant cultures.* Equine Vet J, 2008. **40**(3): p. 260-5.

Appendix

A.1 Equine Blood-Derived Biologics.

Biologics are medicinal products that are generated by a biologic process rather than being chemically synthesized. They are typically derived from whole blood or other blood components. Biologics are most commonly applied in an autogenous fashion thereby avoiding issues surrounding immune rejection and disease transmission. In horses, commonly used biologics for the treatment of musculoskeletal disorders include platelet rich plasma (PRP), bone marrow aspirate, bone marrow aspirate concentrate, and fibrinogen.

Bone marrow and bone marrow aspirate concentrate contain stem cells as well as platelets and therefore growth factors [153, 154]. They are both widely used biologic in treatment of equine tendon and ligament injuries and BMC has demonstrated efficacy in cartilage regeneration [154, 155]. The predominant chemotactic effects of platelet rich plasma (PRP) are due to the platelets, which are a reservoir of numerous anabolic growth factors. However, PRP also contains leukocytes which contain several catabolic cytokines [156]. The net effect of the platelet:leukocyte ratio is important for tissue function [156]. Cryoprecipitated fibrinogen [FIB] supports chondrocyte metabolism [157] and has been used as a vehicle for chondrocyte and MSC cartilage grafting procedures in equine patients [158].

These biologics have been used to augment tendon and cartilage regeneration in horses with the thought that it is primarily the milieu of growth factors that are responsible for improved clinical function [153, 154, 156, 159]. An added benefit of these biologics is their natural combination of growth factors that might be responsible for the recruitment of local tissue cells and regional stem cells to the site of injury. To evaluate the chemoattractant capacity of these biologics, cell migration assays can be performed.